SYNTHESIS OF THE POLARIZATION PROPERTIES OF CYGNUS A AT 8300 AND 9600 MEGAHERTZ

Thesis by

Ka Bing Winson Yip

In Partial Fulfillment of the Requirements

For the Degree of

Doctor of Philosophy

California Institute of Technology

Pasadena, California

1971

(Submitted June 9, 1971)

乾坤始奠　混沌初開

To Phyllis, Chee Foon

I am indebted to so many people that it is impossible to specifically thank every individual one here. However, I would like to thank G.A. Seielstad who initiated this project and studiously guided me through. I would also like to thank G.J. Stanley, the Director of Owens Valley Radio Observatory for generously providing me with the observing time and the members of the observatory staff, without whom I would not have been able to get on the air.

My sincere thanks to G.L. Berge whose constant and innumerable advices are greatly appreciated. It also gives me pleasure to thank K.W. Weiler and E.B. Fomalont for their numerous stimulating discussions.

I would like to thank Phyllis, my fiancee who patiently drafted and re-drafted the illustrations in this thesis.

Thanks are also due to Patti Melanson, who cheerfully completed the typing of this thesis in the shortest possible time.

The continued support of a Graduate Research Assistantship from the California Institute of Technology is gratefully acknowledged. This research at the Owens Valley Radio Observatory has been supported by the U.S. Office of Naval Research under Contract N00014-67-A-0094-0008.

ERRATUM

After this thesis has been written, a sign mistake in the reduction of the 9600 MHz polarized flux intensities was discovered. This altered the polarized map at 9600 MHz and the conclusions are thus greatly affected. The readers are referred to the publication of the corrected thesis for the proper results and conclusions. This thesis is published in the 'Preprint from the Owens Valley Radio Observatory of Caltech' in 1972 and in the Astrophysical Journal as well. A copy of the publication is attached at the end of this thesis.

ABSTRACT

Methods of polarized interferometry have been used in conjunction with the earth rotation aperture synthesis technique to study the polarized intensity distributions of Cygnus A at 8300 MHz and 9600 MHz. The total intensity distribution at 8300 MHz has also been obtained.

Although the resolutions obtained in these observations are about 20", it is still quite insufficient to reveal the structures in the components for a detailed comparison with the theoretical model proposed by Mills and Sturrock. The general feature of the ram pressure confinement mechanism, however, is consistent with this observation.

The polarized distributions yield a rather fast variation of large rotation measures across the east component. There is also a reversal of the longitudinal magnetic field in the direction of the west component. Correlations with the distribution of small hydrogen clouds deduced from HI absorption measurements have been discussed.

There seems to be little depolarization across this source except in the bridge, and this is believed to be occurring outside of the emitting region. However, no detailed models can be worked out without further information about the conditions of the intervening medium.

TABLE OF CONTENTS

CHAPTER I

INTRODUCTION

The discovery by Jansky (1) in 1932 of galactic noise at radio frequencies began a new era in astronomical investigation. With the detection of a variable source of radio frequency radiation at 5 meter wavelength by Hey, Parsons and Phillips (2) in the direction of the constellation of Cygnus, the existence of discrete sources of radio waves was unequivocably demonstrated. Detailed studies later by Bolton and Stanley (3) using a sea interferometer of higher resolving power confirmed that this source was less than 8' of arc. It is interesting to note that although this discrete source of intense radio radiation in Cygnus is the first one to be detected, it is only the second strongest source in the sky. The strongest radio source, which is located in the constellation of Cassiopeia, was not detected until 1948 when Ryle and Smith (4) accidentally came across it during an attempt to look for circular polarization in Cygnus.

Because it is the first radio object to be detected and because of its intense radiation, the earlier history of radio astronomical investigations is, to a large extent, the study of this radio source in Cygnus. During these first years after the discovery of the discrete sources, particularly before the reason for their intensity fluctuations was cleared up, the most popular idea was that the majority of the discrete sources were of stellar nature (5). The very low resolution of the then existing radio telescopes, however, was unable to determine the size of these 'radio stars'. The discovery of

the strong discrete source Taurus A and its identification with the Crab Nebula therefore pushed the question about the nature of these discrete sources to the forefront - Should Taurus A be identified with the stellar remnants of the supernova or with the Nebula itself, and what about the angular sizes of the most intense sources in Cygnus and Cassiopeia?

One of the reasons for the great concern about the dimensions of these discrete sources followed from the attempts in their optical identifications. Since so much more has been known about the theories and detection techniques of optical astronomy, the identifications of these sources could reveal much more about the structure and radiation mechanisms operating in these objects. This later aspect, in particular, fascinated the observers and theoreticians at that time. Because of the intensity of the radiations from Cygnus A and Cassiopiea A, they were at first thought to be quite close, even within the limits of our solar system (6)! Although measurements by Ryle (7) in 1949 and by Smith (8) in 1951 put the distance of Cygnus A at least 0.5 pc away, the lack of a sufficiently powerful radiation mechanism still left the observers with the impression of the proximity of these sources. The identification of Cygnus A with a pair of "colliding galaxies" (which has now been proved to be only a peculiar galaxy with a dark band in the middle by Baade and Minkowski (9) therefore stirred great excitement because this not only appeared to provide a very plausible source of energy, it also pointed out that Cygnus A is at a much greater distance than thought.

Of the several radio noise emitting sources first detected

(references 10 - 18) and later identified with optical objects (9), Cygnus A is undoubtedly the most well known and intensely studied. Although considerable work has been done since its discovery, much more remains. This classical object, which is so typical of the radio galaxies later detected in that it has two components approximately equidistant from a peculiar optical object, has the vintage position in the solution to many of the still unanswered radio astronomical puzzles.

As early as 1950, Alfven and Herlofson (19) suggested that the synchrotron mechanism is important in the generation of cosmic radio waves. This idea, however, was almost ignored except by a number of theoreticians in the Soviet Union, in particular Ginzburg and Shklovsky. It was only after the discovery of linear polarization in the optical continuum of the Crab Nebula (20,21) as predicted by Shklovsky (22), and the detection of linear polarization at centimeter wavelengths from the same source later (23) that this synchrotron radiation mechanism began to be generally accepted.

Although earlier attempts were made to detect linear polarization in the radio frequency radiation from intense extragalactic sources (4,24,25,26,27), Cygnus A is the first such source where linear polarization was detected (28). With this detection, a very powerful tool for the study of the magnetic structure of this source is provided.

As the investigation of the properties of Cygnus A becomes more and more intensive, observations with ever increasing resolution were sought. Moreover, the knowledge of the distribution of Cygnus A both in intensity and polarization as a function of frequency becomes

increasingly important for a more complete understanding of this and other radio sources.

After it was first shown by Jennison and Das Gupta (29) to be a double source, observations at different frequencies and resolutions (30,31,32,33,34) revealed essentially the same picture, with a bridge component apparent at some frequencies and resolutions but not at others. However, a detailed map of the brightness distribution at higher frequencies, especially of the fine structure in two dimensions of the outer edge of each component, may be important, among other things, in detecting synchrotron self absorption in the source (34).

Since linear polarization was first detected from the radiation of the extragalactic source Cygnus A (28), observations over a range of frequencies have been performed. These observations so far, however, have inadequate resolution to give even a rough description of the polarization distribution across the source. The greatest detail which has been observed to date consists of the integrated polarization for each of the two main components at wavelengths of 1.55 cm (35), 1.90 cm (36), 1.95 cm (37), 1.96 cm (36), 3.02 cm (38), 3.95 cm (39) and 6.40 cm (40). In spite of the relatively low resolutions, these observations have already revealed some very interesting properties relating to the structure of this source. Not only does the degree of polarization decrease rapidly from a maximum of about 8 percent at 3 cm (38) to about 1.3 percent at 5 cm (39), but its polarization angle, which shows exceptionally fast rotation, is also not linear with wavelength squared. This unusual behavior has been explained by several authors (Hollinger et al (41), Slysh (42) and

Soboleva (40)) by assuming that the two principle components of Cygnus A are polarized differently and have vastly different rotation measures. A more detailed picture of the polarization structures across the source is however very much in order.

The methods for the study of discrete sources of radiation by interferometry were first set forth by Michelson (43,44) who later applied these methods to the measurements of stellar diameters (45, 46). To attain higher resolutions in radio astronomical observations therefore, it is only logical to make use of these same principles. As a matter of fact, the use of interferometric techniques for higher resolutions in the study of structures of radio sources has been practised for quite some time. The most promising means to this end is the earth rotation synthesis technique. This was first applied by O'Brien (47) in an investigation of the sun and later developed in full by Ryle and his colleagues (48,49,50,51) for the study of source structures. Although polarization studies using interferometers have been made previously (52-58), the incorporation of this powerful aperture synthesis technique is just beginning to be exploited (59). The combination of aperture synthesis and the methods of interference polarimetry by Morris, Radhakrishnan and Seielstad (60) lay the framework of a very powerful tool for the investigation of the total intensity and polarization properties of cosmic radio sources.

This project employs the above mentioned combination of techniques for the study of the intensity and polarization of the radio source Cygnus A. Two frequencies are used for the deduction of the rotation measure pertaining to this source, and these frequencies are

close enough that there are no position-angle ambiguities of $n\pi$ radians between them. The synthesized beams have HPBW of about 22" at 8300 MHz and about 20" at 9600 MHz. Relatively detailed maps of the two components and the bridge have been obtained. From these maps, the spectral indices, rotation measure, intrinsic position angles and depolarization distributions for the components and the bridge are deduced. Attempts will be made to compare these results with a model proposed for Cygnus A.

CHAPTER TWO

MATHEMATICAL TECHNIQUES

Before going into the details of the actual observations and the results obtained, we review the methods of two dimensional synthesis and polarized interferometry with the Owens Valley interferometer.

Earth Rotation Synthesis

As shown by Moffet (61), the monochromatic pattern of a two-element, continuous-multiplication interferometer (62) is given by

$$R(x,y,t) = GA(x,y)\cos\left\{2\pi[u(x-\Omega t) + vy] + \psi\right\} \qquad (1)$$

where x and y are the cartesian coordinates centered at α_0, δ_0, an appropriate origin in terms of right ascension and declination on the sky; G is the gain of the receiver; A(x,y) is the effective area of either antenna if they are identical; ψ is the phase error of the instrument; Ω is the sidereal rate; t is the sidereal time and u,v are the x,y projections of the antenna separation on the celestial sphere given by

$$\begin{aligned} u &= s\cos\theta\sin p \\ v &= s\cos\theta\cos p \end{aligned} \qquad (2)$$

with s the spacing in wavelengths, θ the angle between the source direction and the median plane and p the position angle specifying the orientation of the interferometer fringes on the sky.

The rotation of the earth varies the projection length and orientation of the interferometer baseline to provide different resolutions at various position angles for the source under observation.

The parameters θ and p giving the values of these projections in equation (2) are of course not the most convenient or physical choices. However, one can also express u and v in terms of the source parameters (h,δ) and the parameters of the baseline (H,D). (For east-west baseline, hour angle of interferometer pole = H = 6^h and declination of pole = D = 0° and for north-south baseline, H = 0^h and D = -52°46' 06.2"). Starting with equations (2) and (5) in Moffet's paper (61), one can obtain easily the following expressions:

EW :
$$\begin{aligned} u &= s\cos h \\ v &= s \sin\delta \sin h \end{aligned} \tag{3}$$

NS :
$$\begin{aligned} u &= -s \sin\Phi \sin h \\ v &= \cos\Phi \cos\delta + \sin\Phi \sin\delta \cos h \end{aligned} \tag{4}$$

where Φ is the geographic latitude of the observatory.

Introducing the concept of the normalized complex visibility function $\beta(u,v) = V(u,v)e^{i\phi(u,v)}$, where V is the normalized visibility amplitude and ϕ the visibility phase, the response of a tracking interferometer to a discrete radio source of brightness temperature distribution T(x,y) is

$$R(t) = GAS'V(u,v)\cos[\phi(u,v) - 2\pi u\Omega t + \psi] \tag{5}$$

where $S' = \frac{2k}{\lambda^2}\int\int A(x,y)T(x,y)\,dxdy$ (k = Boltzmann's constant, λ = wavelength) is the total flux and

$$\beta(u,v)=Ve^{i\phi} = \frac{\int_{\infty}^{\infty}\int A(x,y)T(x,y)e^{i2\pi(ux+vy)}dxdy}{\int_{\infty}^{\infty}\int A(x,y)T(x,y)dxdy} \tag{6}$$

Since S'V, ϕ are the observed quantities and T(x,y) is the desired result, we invert this transform and obtain

$$A(x,y)T(x,y) = \frac{\lambda^2}{2k}\int_{-\infty}^{\infty}\int S'V(u,v)e^{i\pi(u,v)}e^{-i2\pi(ux+vy)}dudv \qquad (7)$$

As Bracewell (63) has shown, it is sufficient to observe the points on one half of the UV plane. Moreover, because of the physical construction of the antennas (the $\pm 4^h$ in hour angle limit), a continuous integration of the visibility function on the UV plane is not possible. In this project, this has been divided into two sets of observations, a set using the EW spacings and another using the NS ones. The coverage on the UV plane, therefore, is not the smooth ellipses one would expect ideally, but the two broken segments of ellipses as shown in figure (1). It should be noticed also that the gap between these two sets of spacings is smaller than the Bracewell unit cell (~1264λEW and ~3680λNS for Cygnus A at 9600 MHz) and therefore does not cause any extraneous sidelobes. These unit cells are derived using the model of Ryle, Elsmore and Neville for Cygnus A at 21 cm (32) and the assumption that the intensity of the components is zero three half widths away from the maxima.

Polarized Interferometry

To describe partially polarized quasi-monochromatic radiation, four parameters are required. These parameters give the intensity, the degree of polarization, the plane of polarization and the ellipticity of the radiation at each point and in any given direction. A very convenient representation of these properties of polarized light are the four Stokes parameters, named after Sir George Stokes

in 1852. They are defined as (64):

$$
\begin{aligned}
I &= \langle E_x^2 \rangle + \langle E_y^2 \rangle = I_0 + I_{90} = I_{R.H.} + I_{L.H.} \\
Q &= \langle E_x^2 \rangle - \langle E_y^2 \rangle = I_0 - I_{90} = I_e \cos 2\beta \cos 2\chi = I_p \cos 2\chi \\
U &= \langle 2E_x E_y \rangle \cos\delta = I_{45} - I_{135} = I_e \cos 2\beta \sin 2\chi = I_p \sin 2\chi \\
V &= \langle 2E_x E_y \rangle \sin\delta = I_{R.H.} - I_{L.H.} = I_e \sin 2\beta
\end{aligned}
\tag{8}
$$

where E_x, E_y are the transverse electric field in two orthogonal directions, δ is their phase difference, χ is the inclination of the major axis of the polarization ellipse to the x-axis and β is its axial ratio, I_e is the intensity of the polarized part of the wave and I_p that of the linearly polarized component, I_θ is the intensity at an angle θ to the x-axis and $I_{R.H.}$ and $I_{L.H.}$ are the intensities of the right- and left-handed circularly polarized components. The parameter I is the total intensity and is the sum of two orthogonal intensities whereas Q and U specify the linear polarization. The circular polarization is given by V.

We now try to relate these four parameters of a polarized distribution to the response of a two element interferometer. It has been shown by Morris, Radhakrishnan and Seielstad (60) that this response is given by

$$
\begin{aligned}
\underline{R}(t) = \frac{k(t)}{2} \Big[& \bar{\underline{I}} \left\{ \cos(\phi_1 - \phi_2)\cos(\theta_1 - \theta_2) + i\sin(\phi_1 - \phi_2)\sin(\theta_1 + \theta_2) \right\} \\
& + \bar{\underline{Q}} \left\{ \cos(\phi_1 + \phi_2)\cos(\theta_1 + \theta_2) + i\sin(\phi_1 + \phi_2)\sin(\theta_1 - \theta_2) \right\} \\
& + \bar{\underline{U}} \left\{ \sin(\phi_1 + \phi_2)\cos(\theta_1 + \theta_2) - i\cos(\phi_1 + \phi_2)\sin(\theta_1 - \theta_2) \right\} \\
& + \bar{\underline{V}} \left\{ \cos(\phi_1 - \phi_2)\sin(\theta_1 + \theta_2) + i\sin(\phi_1 + \phi_2)\cos(\theta_1 - \theta_2) \right\} \Big]
\end{aligned}
\tag{9}
$$

where $\underline{\bar{I}},\underline{\bar{Q}},\underline{\bar{U}},\underline{\bar{V}}$ are the unnormalized Fourier transforms of the respective distributions I, Q, U and V over the source, e.g.

$$\underline{\bar{I}} = \underline{\bar{I}}(u,v) = \iint_{\infty}^{\infty} I(x,y)e^{i2\pi(ux+vy)}dxdy$$

$k(t) = GAe^{-i(2\pi u\Omega t + \psi)}$ describes the characteristic pattern of the interference fringes and ϕ_1, ϕ_2, θ_1, θ_2 are the position angles and ellipticities of the respective receiving horns of the two antennas. Let us now relate these transforms $\underline{\bar{I}}$, $\underline{\bar{Q}}$, $\underline{\bar{U}}$, and $\underline{\bar{V}}$ to the actual position angles of the horns used during the observations.

Before going into this, we would first look into the Stokes parameter $\underline{\bar{V}}$ in a little more detail. It has been theoretically predicted that circular polarization is negligibly small (65,66) and is only likely to be observed at low radio frequencies (67). Moreover, an upper limit of 2 percent has actually been measured at 3.15 cm for Cygnus A (68). Although detections have been claimed in recent searches for circular polarization in compact objects (69,70,71), the magnitudes involved are only a couple of percent or less. The Stokes parameter $\underline{\bar{V}}$ has therefore been assumed to be zero.

Some simplifying assumptions can now be made with equation (9). The values of θ_1, θ_2, the ellipticities of the horns and thus responsible for the instrumental circular polarization have been found to be very small (see DATA ANALYSIS). The assumptions of $\cos(\theta_1 \pm \theta_2) \approx 1$ and $\sin(\theta_1 \pm \theta_2) \approx \theta_1 \pm \theta_2 \equiv \theta^{\pm}$ are therefore valid. With these and the assumption that $\underline{\bar{V}} = 0$, equation (9) becomes

$$R(t) = \frac{k(t)}{2}\Big\{ \underline{\bar{I}}[\cos(\phi_1-\phi_2)+i\theta^{+}\sinh(\phi_1-\phi_2)]$$

$$+ \underline{\bar{Q}}[\cos(\phi_1+\phi_2)+i\theta^{-}\sin(\phi_1+\phi_2)] \qquad (10)$$

$$+ \underline{\bar{U}}[\sin(\phi_1+\phi_2)-i\theta^{-}\cos(\phi_1+\phi_2)]\Big\}$$

During the observations, horn positions of $\phi_1/\phi_2 = 0^{\circ}/0^{\circ}$, $0^{\circ}/90^{\circ}$ and 45°/135° are used. Allowing for the possibility of a horn setting error ε and utilizing the information that θ and ε are small, the responses of the interferometer to polarized radiation for the different configurations are

$$\phi_1=0,\ \phi_2=\varepsilon_0.$$

$$\underline{R}_0(t) = \frac{1}{2}k(t)\Big\{\underline{I}+\underline{Q}+\underline{U}[\varepsilon_0-i\theta_0^{-}]\Big\} \qquad (11)$$

$$\phi_1=0,\ \phi_2=90^{\circ}+\varepsilon_{90}$$

$$\underline{R}_{90}(t) = -\frac{1}{2}k(t)\Big\{\underline{I}[\varepsilon_{90}+i\theta_{90}^{+}] + \underline{Q}[\varepsilon_{90}-i\theta_{90}^{-}]-\underline{U}\Big\} \qquad (12)$$

$$\phi_1=45^{\circ},\ \phi_2=135^{\circ}+\varepsilon_{135}$$

$$\underline{R}_{135}(t) = -\frac{1}{2}k(t)\Big\{\underline{I}[\varepsilon_{135}+i\theta_{135}^{+}] + \underline{Q} + \underline{U}[\varepsilon_{135}-i\theta_{135}^{-}]\Big\} \qquad (13)$$

Since for Cygnus A at 3 cm, $\sqrt{Q^2 + U^2} < 0.3I$ and θ's and ε's are small (see Tables IV and V), $U[\varepsilon-i\theta^{-}]$ and $Q[\varepsilon-i\theta^{-}]$ can be neglected.

We now introduce the definitions

$$\eta_{90} = \varepsilon_{90} + i\theta_{90}^{+}$$

$$\eta_{135} = \varepsilon_{135} + i\theta_{135}^{+}$$

Writing the response of the interferometer and the desired Stokes parameters $\underline{I}$, $\underline{Q}$, $\underline{U}$ in terms of their respective amplitudes and phases, i.e.

$$\underline{R}_0(t) = \frac{1}{2} k(t) V_0 e^{i\phi_0}$$

$$\underline{R}_{90}(t) = \frac{1}{2} k(t) V_{90} e^{i\phi_{90}} \tag{14}$$

$$\underline{R}_{135}(t) = \frac{1}{2} k(t) V_{135} e^{i\phi_{135}}$$

$$\underline{I} = V_I e^{i\phi_I}$$

$$\underline{U} = V_U e^{i\phi_U}$$

$$\underline{Q} = V_Q e^{i\phi_Q}$$

the quantities of interest can be written in terms of the measured quantities as

$$V_I e^{i\phi_I} = \left\{ V_0 e^{i\phi_0} + V_{135} e^{i\phi_{135}} \right\} / (1-\eta_{135})$$

$$V_U e^{i\phi_U} = V_{90} e^{i\phi_{90}} + \frac{\eta_{90}}{(1-\eta_{135})} \left\{ V_0 e^{i\phi_0} + V_{135} e^{i\phi_{135}} \right\} \tag{15}$$

$$V_Q e^{i\phi_Q} = -\frac{1}{(1-\eta_{135})} \left\{ V_{135} e^{i\phi_{135}} + \eta_{135} V_0 e^{i\phi_0} \right\}$$

The desired intensity and polarization distributions can then be obtained from these equations by the use of equation (7). The beam shape A(x,y) in that equation can be measured experimentally and an appropriate correction applied.

Horn Calibrations

The parameters θ^+ and ε characteristic of the antennas have to be determined before the brightness distributions across the source can

be deduced from equation (15). Two approaches, both employing unresolved and unpolarized sources, have been used. The first approach consists of measurements of a parallel and an approximate orthogonal horn configuration, while the second one consists of two approximate orthogonal horn configurations only.

Since approximate orthogonal horns are used, it is appropriate at this point to separate ε, the horn setting error, into two parts, Δ_e and Δ_d. Δ_e is the error inherent in the horn mounting system while Δ_d is the non-orthogonality of the horns as shown in the display (i.e., Δ_d is set by the observer and is a guess at the true horn orthogonal positions due to the lack of this information at the time of observation). Equations (11) and (12) can now be written, for an unresolved and unpolarized source, as

$$\phi_1 = 0,\ \phi_2 = \Delta_d^0 - \Delta_e^0$$
$$\underline{R}_0(t) = \frac{k(t)}{2}\,\underline{I} \tag{16}$$

$$\phi_1 = 0,\ \phi_2 = 90^\circ + \Delta_d^{90} - \Delta_e^{90}$$
$$\underline{R}_{90}(t) = -\frac{k(t)}{2}\,\underline{I}\,[\Delta_d^{90} - \Delta_e^{90} + i\theta_{90}^+] \tag{17}$$

Solving these two equations,

$$\Delta_e^{90} = \frac{V_{90}}{V_0}\cos(\phi_{90}-\phi_0) + \Delta_d^{90}$$
$$\theta_{90}^+ = -\frac{V_{90}}{V_0}\sin(\phi_{90}-\phi_0) \tag{18}$$

Similar relations can be derived for Δ_e^{135} and θ_{135}^+ from equations (11) and (13).

For the second method, we start with the real and imaginary parts of equation (17),

$$V_{90}\cos\phi_{90} = -\frac{k(t)}{2}\underline{I}[\Delta_d^{90}-\Delta_e^{90}]$$

$$V_{90}\sin\phi_{90} = -\frac{k(t)}{2}\underline{I}\,\theta_{90}^{+}$$

Therefore, with two approximate orthogonal measurements, $\Delta_{d_1}^{90}$ and $\Delta_{d_2}^{90}$,

$$\frac{V_{90}^{(1)}\cos\phi_{90}^{(1)}}{V_{90}^{(2)}\cos\phi_{90}^{(2)}} = \frac{\Delta_{d_1}^{90} - \Delta_e^{90}}{\Delta_{d_2}^{90} - \Delta_e^{90}}$$

and thus

$$\Delta_e^{90} = \frac{\Delta_{d_2}^{90} V_{90}^{(1)}\cos\phi_{90}^{(1)} - \Delta_{d_1}^{90} V_{90}^{(2)}\cos\phi_{90}^{(2)}}{V_{90}^{(1)}\cos\phi_{90}^{(1)} - V_{90}^{(2)}\cos\phi_{90}^{(2)}} \tag{20}$$

The ratio of equation (19) gives the value of θ^{+},

$$\tan\phi_{90} = \frac{\theta_{90}^{+}}{(\Delta_d^{90}-\Delta_e^{90})}$$

The two values of θ^{+} resulting from the two approximate orthogonal measurements can then be averaged. Identical approach applies to the 45/135 horn configuration. These corrections are listed in Tables IV and V.

CHAPTER THREE

OBSERVATIONS

Instruments

The observations for this thesis have been carried out with the two ninety foot equatorially mounted parabolic antennas at the Caltech Owens Valley Radio Observatory. Excellent descriptions of the instruments and their operation have been given by Read (72) and Berge (73). Basically, the receiver is of the superheterodyne type with the local oscillator frequencies at 8300 MHz in one instance and 9600 MHz in the other. The IF frequency is 10 MHz, and the bandwidth is about 5 MHz. Because of the need of having the horns of the antennas at different orientations, they are mounted on rotary joints and rotated by remote control from the observing room. An accuracy of 0.01 in the display horn position has been obtained. The two antennas can be moved on wide gauge railway tracks with discrete stations every 100 feet both in the east-west and north-south directions out to a maximum spacing of 1600 feet. These observations extend to 800 feet east-west and 400 feet north-south, and the coverage in the UV plane is as shown in figure (1). Figure (2) shows the synthesized beams for the two frequencies obtained with these spacings.

Calibrators

There are two kinds of calibrators used in these observations. One is for the calibration of the instrumental corrections θ^+ and Δ_e, and the other for the calibration of the gain and phase of the interferometer system. The instrumental calibrators are to be discussed

Figure 1

The coverage of the Fourier (u,v) plane for Cygnus A (3C405) at 9600 MHz with the interferometer of the Owens Valley Radio Observatory.

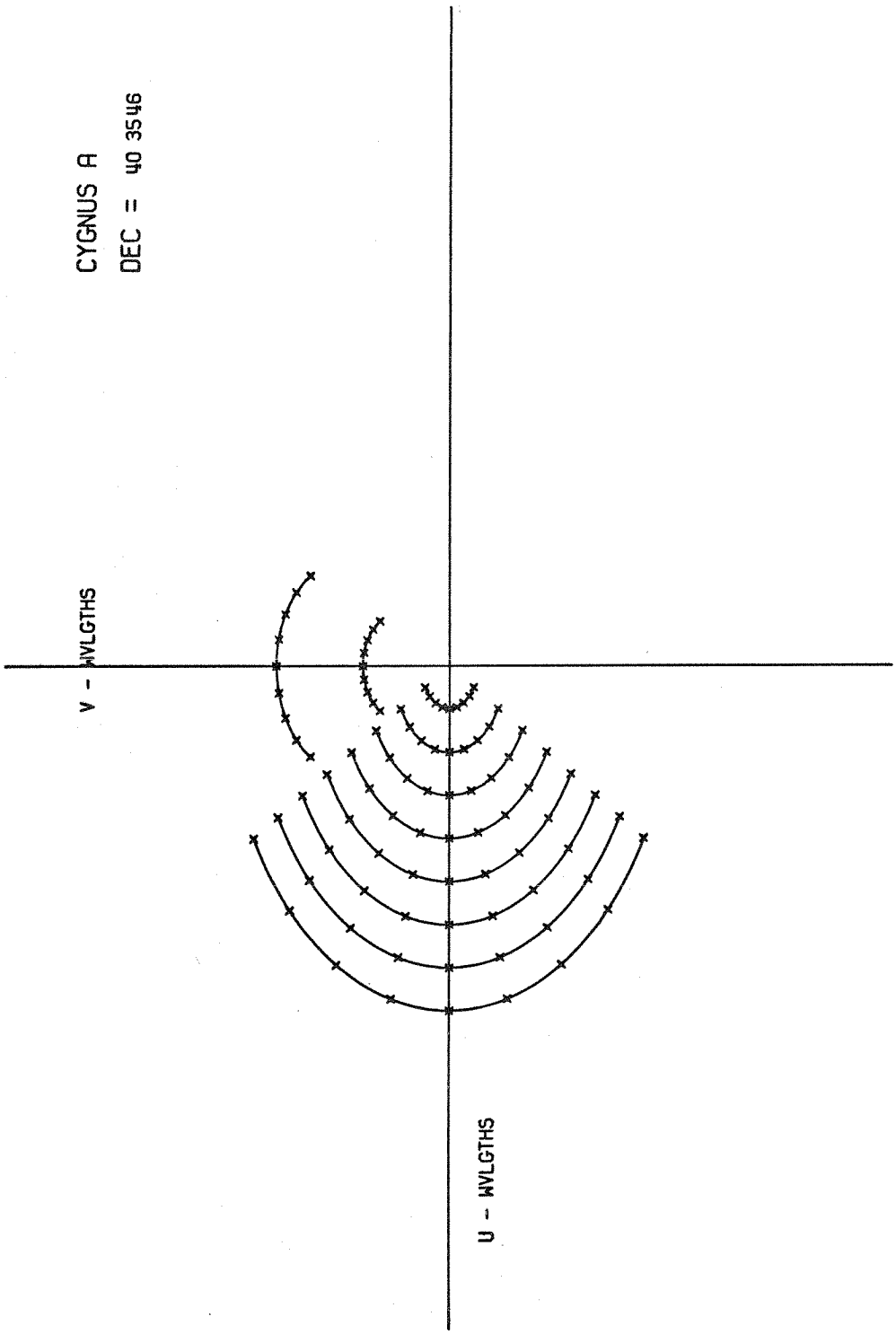
CYGNUS A
DEC = 40 35 46
V - WVLGTHS
U - WVLGTHS

Figure 2

Synthesized beam derived from a point source at (a) 8300 MHz and (b) 9600 MHz at the declination of Cygnus A with the (u,v) plane coverage as in Fig. 1.

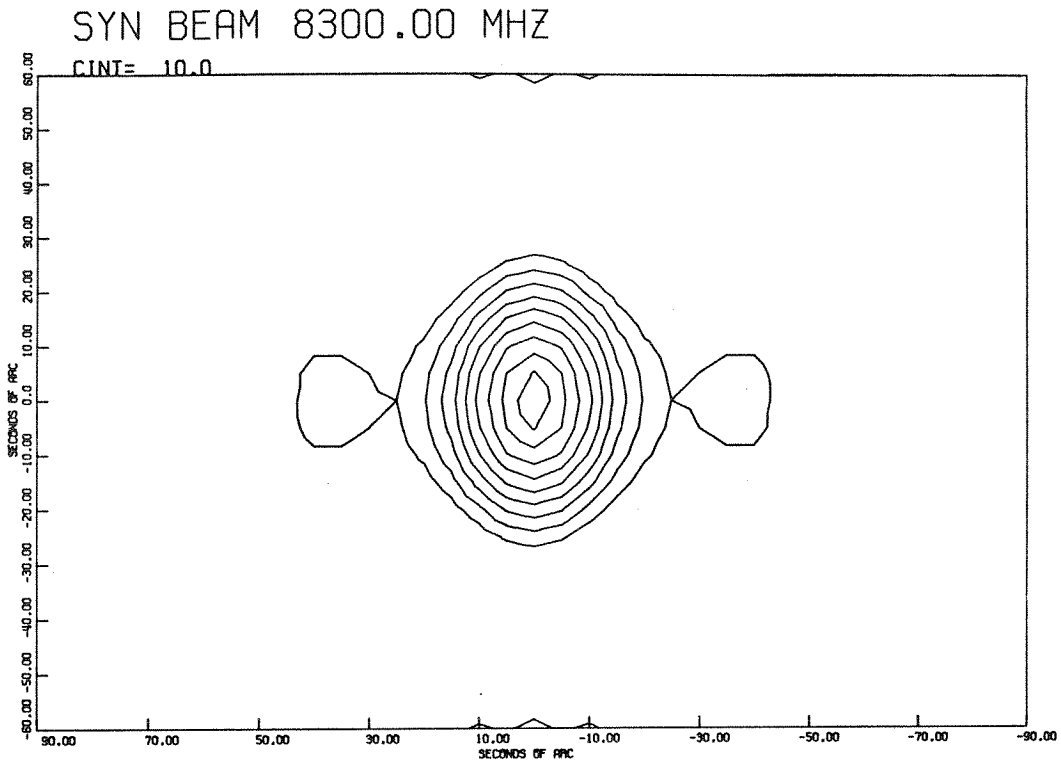
SYN BEAM 8300.00 MHZ
CINT= 10.0
SECONDS OF ARC
90.00
70.00
50.00
30.00
10.00
-10.00
-30.00
-50.00
-70.00
-90.00

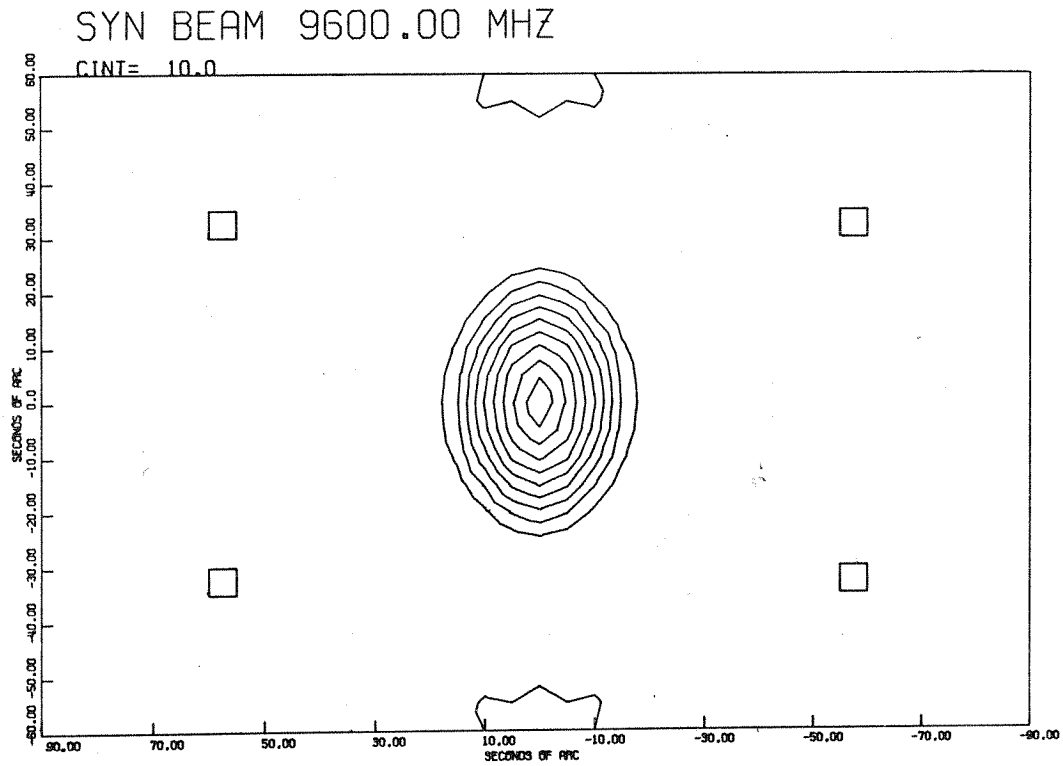
SYN BEAM 9600.00 MHZ
CINT= 10.0
SECONDS OF ARC
90.00
70.00
50.00
30.00
10.00
-10.00
-30.00
-50.00
-70.00
-90.00

first.

As mentioned, the choice of an unpolarized source simplifies this calibration a great deal. The two calibrators used are NGC 7027 and 3C 84. Both of these sources are unresolved at the interferometer spacings ($\lesssim$ 3000 wavelengths) employed for these instrumental calibrations (74,75). There were some doubts in the beginning of the project about the polarization variability of 3C 84 as pointed out by Aller (76) and NGC 7027 was therefore used exclusively in the beginning in 1968. After some discussions with Dr. G. A. Seielstad and Mr. E. T. Olsen (private communication), it was concluded that 3C 84 was unpolarized in 1969 and 1970. In fact, the average polarization for 3C 84 in the relevant period in 1969 was less than 0.1 percent and in 1970 less than 0.25 percent, as found by Olsen.

Since the measured flux density of 3C 84 during these calibrations was six or seven times that of NGC 7027 (77), the advantage of using the former as calibrator is apparent. Typical results of the horn and instrumental calibrations shown in figures (3-6) illustrate this point.

The calibrators for the gain and phase of the interferometer system will now be discussed. In general, these calibrators have to be unresolved at the largest spacing used and at the same time, rather strong in flux density. At 3 cm, however, sources that have flat or inverted spectra and small angular sizes are very likely to be variables (78,79,80).

The values of the intensities of the flux calibrators for these measurements are extrapolated from those given at 8000 MHz by Dent

Figure 3

Sample data for the instrumental polarization calibrations at the 0°/90° horn configuration and 8300 MHz with (a) NGC 7027 and (b) 3C84 as calibrators.

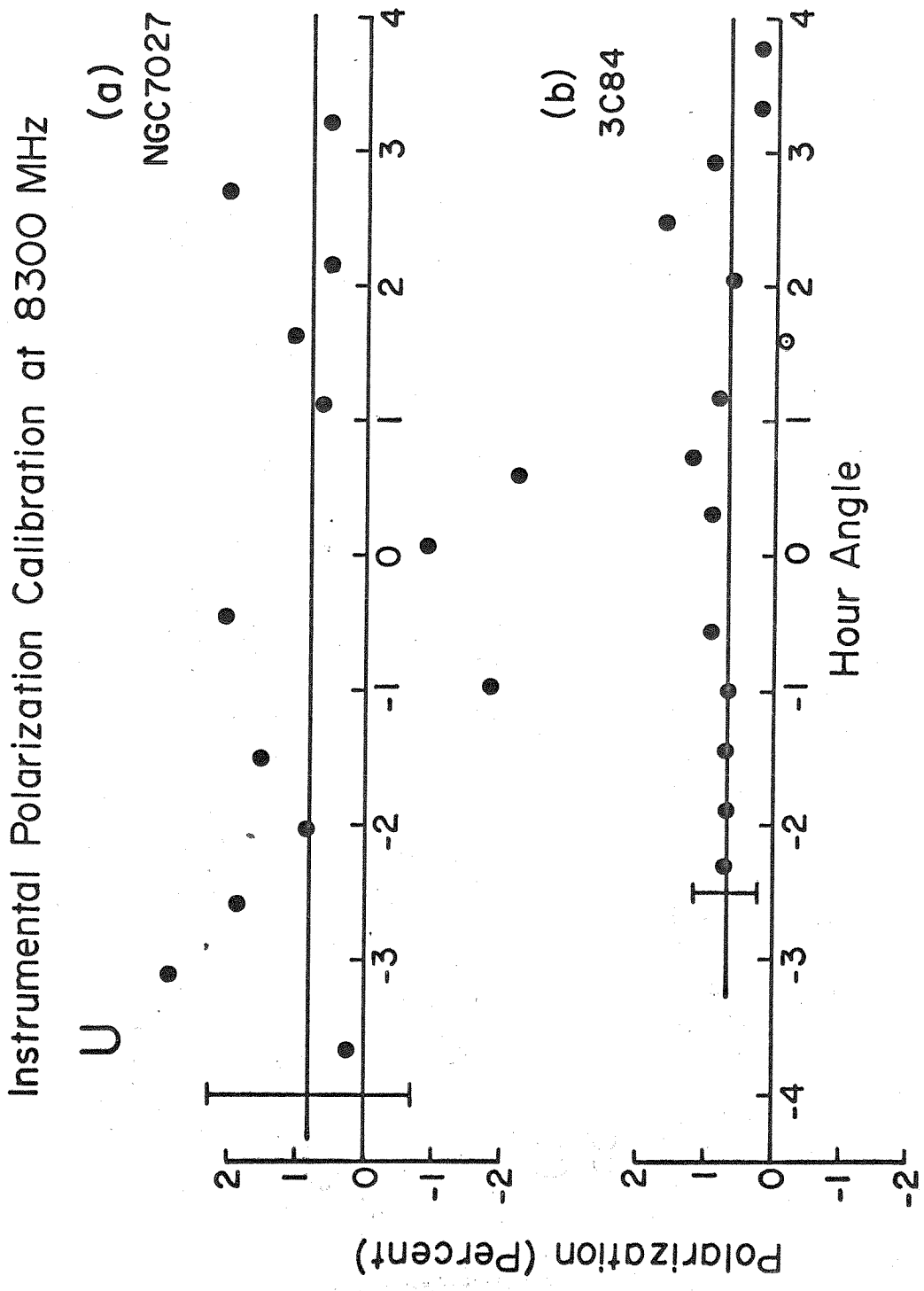
Instrumental Polarization Calibration at 8300 MHz
U
(a)
NGC7027
(b)
3C84
Polarization (Percent)
Hour Angle
2
1
0
-1
-2
-3
-4
3
4

Figure 4

Sample data for the horn null calibrations at the 0°/90° horn configuration and 8300 MHz with (a) NGC 7027 and (b) 3C84 as calibrators.

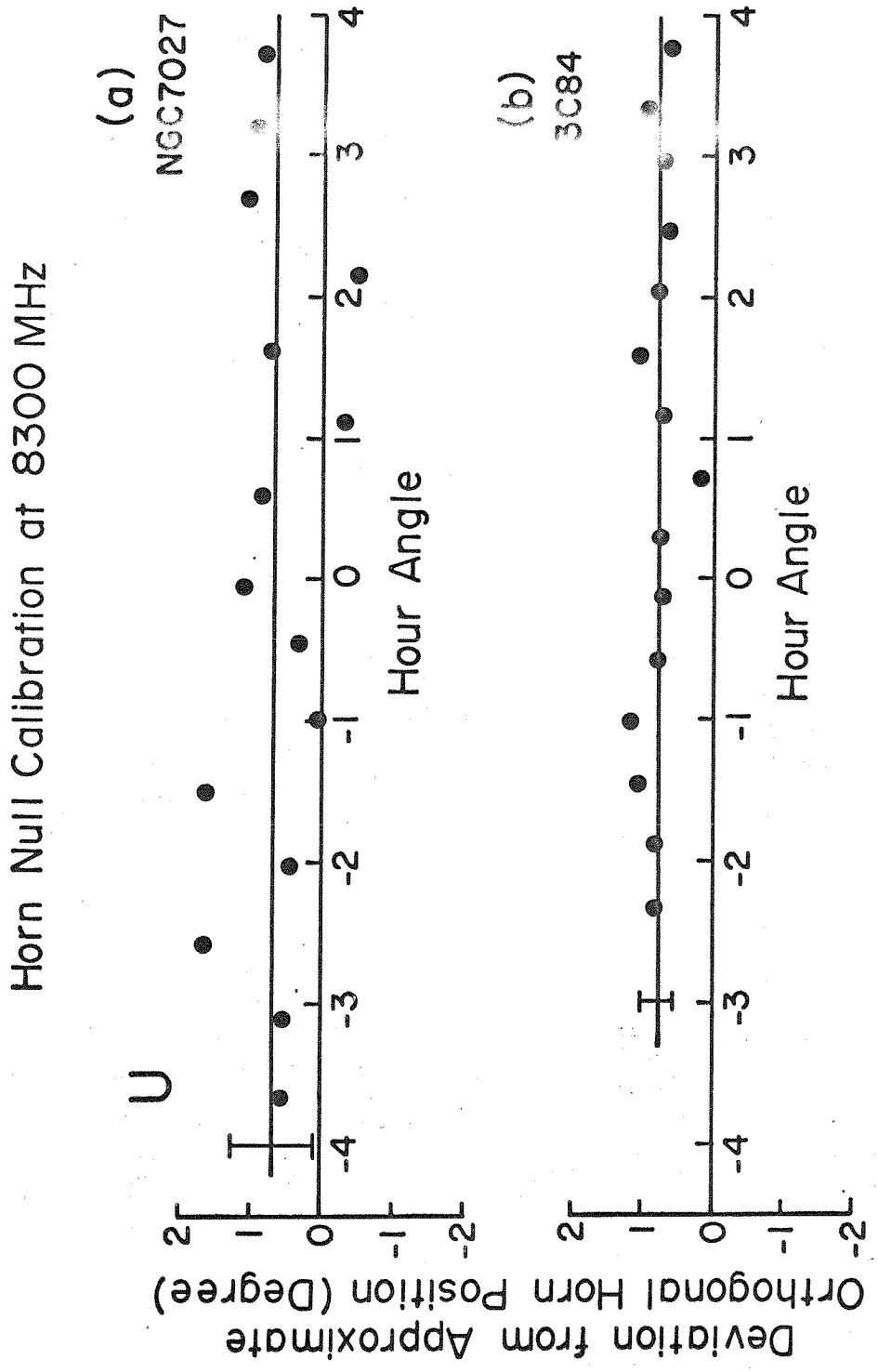
Horn Null Calibration at 8300 MHz
(a)
NGC7027
U
(b)
3C84
Hour Angle
Hour Angle
Deviation from Approximate
Orthogonal Horn Position (Degree)

Figure 5

Sample data for the instrumental polarization calibrations at the 0°/90° horn configuration and 9600 MHz with (a) NGC 7027 and (b) 3C84 as calibrators.

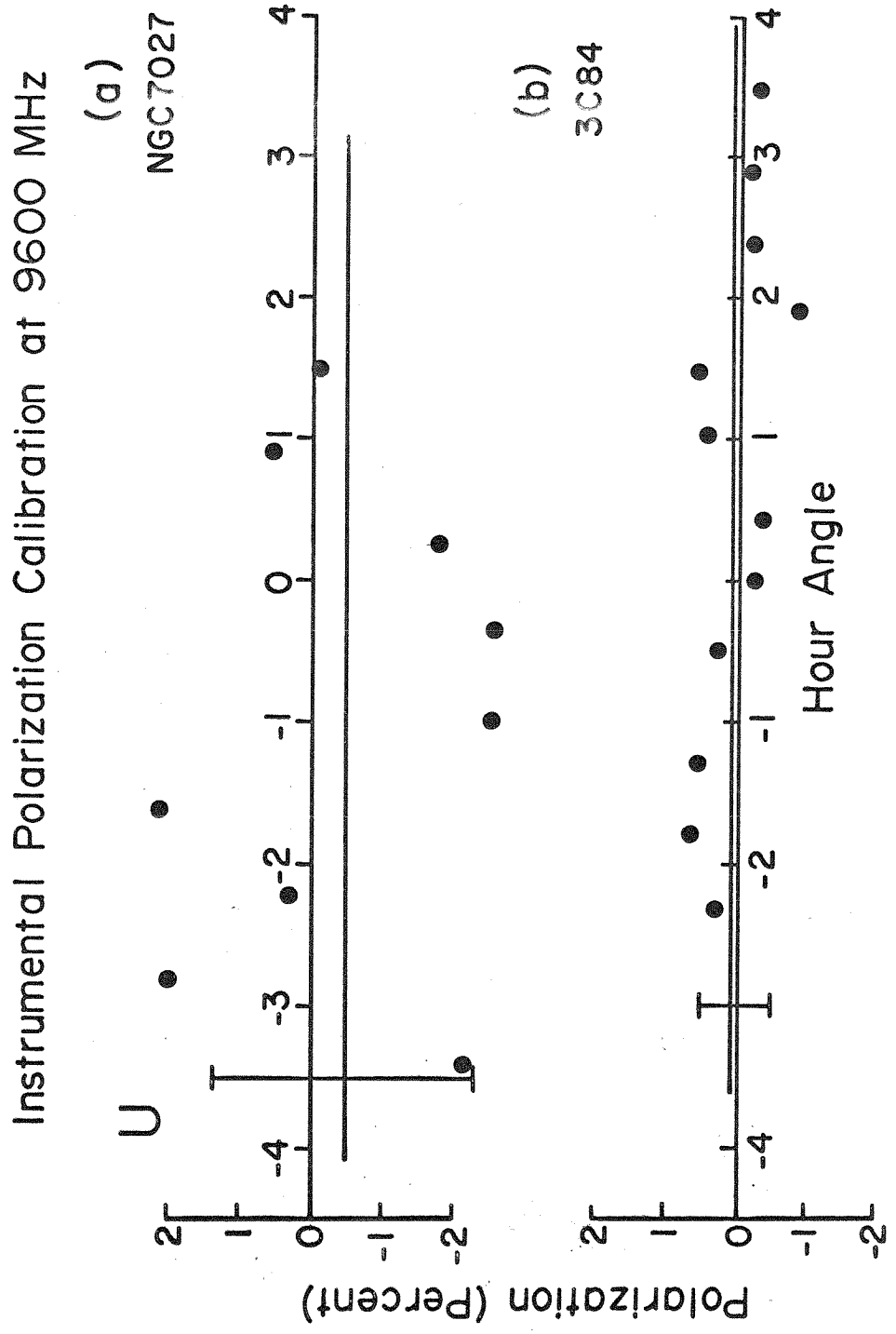
Instrumental Polarization Calibration at 9600 MHz
(a)
NGC7027
U
(b)
3C84
Polarization (Percent)
Hour Angle
2
1
0
-1
-2
-3
-4
3
4

Figure 6

Sample data for the horn null calibrations at the 0°/90° horn configuration and 9600 MHz with (a) NGC 7027 and (b) 3C84 as calibrators.

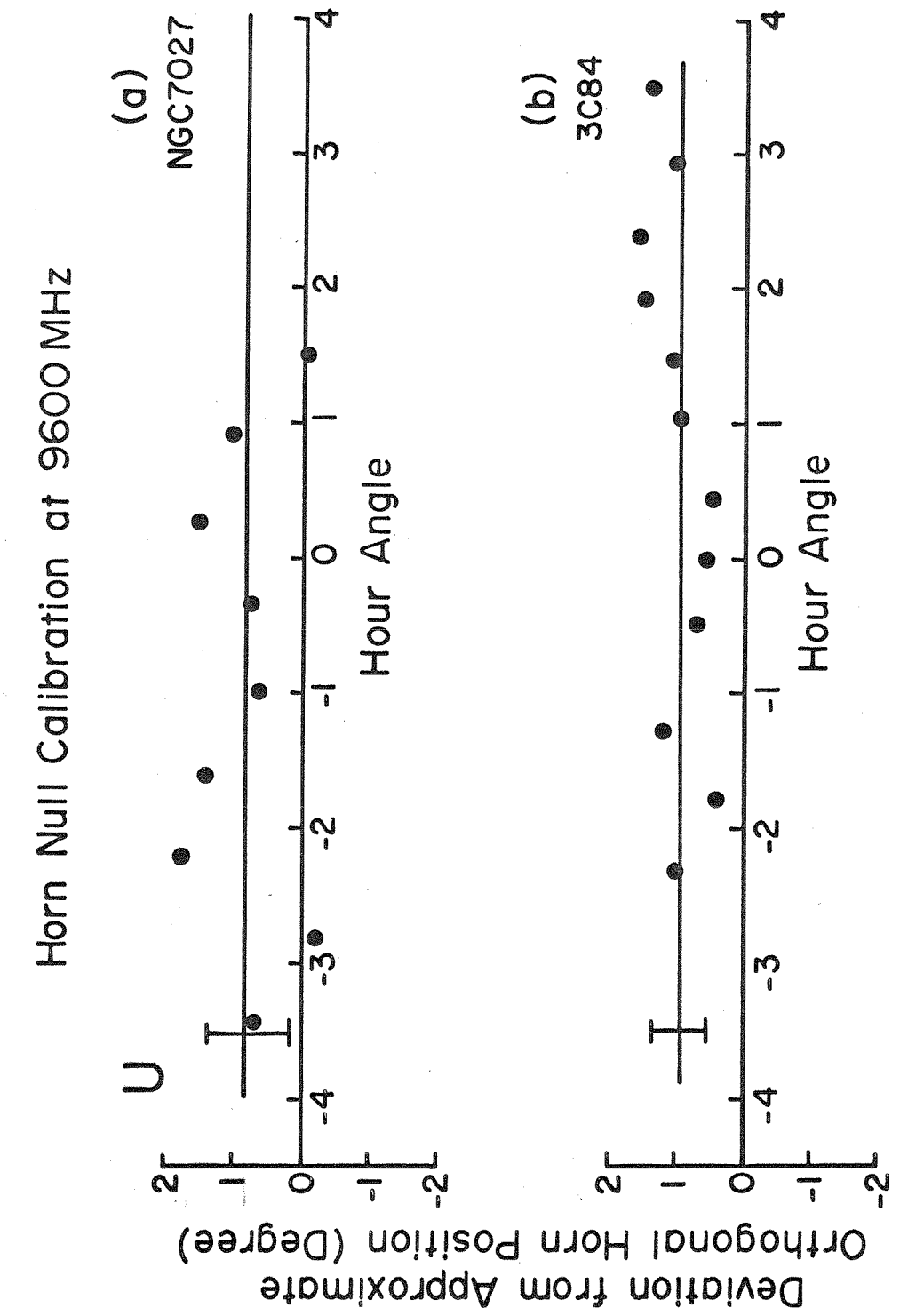
Horn Null Calibration at 9600 MHz
(a)
NGC7027
U
(b)
3C84
Hour Angle
Hour Angle
Deviation from Approximate
Orthogonal Horn Position (Degree)

and Haddock (81), and the spectral index used for these extrapolations are the ones given in the same paper. These 8000 MHz values have later to be revised because they are found to be a bit too low (82). The corrections are about 7 percent at 8300 MHz and 10.2 percent at 9600 MHz (82). Table I gives a list of the flux calibrators used, with the original values extrapolated from these two author's paper and the corrected values which are adopted in the calculations. The phase calibrators are listed in Table II. The right ascension values are taken from Fomalont (83) and the declinations are from the Observer's Handbook of the Owens Valley Radio Observatory.

Observing Program

A summary of the observations in this thesis is given in Table III. Usually ten minute records are allowed for U and Q observations and six mirutes for the parameter I. For horn calibrations, NGC 7027 requires ten minutes while 3C 84 requires only six or seven. Along each elliptical track on the UV plane, special efforts are made so that the gaps between observations in hour angle for each Stokes parameter do not exceed the Bracewell criterion.

It should be noticed that the horn-receiver system has been changed in the middle of 1969. This new transistorized system gives a much better phase stability. The rms scatter in phase (as derived from the non-zeroness of the phases from all the relevant phase calibrations) for the new system is 26 millilobes at 8300 MHz and 21 millilobes at 9600 MHz, while they are 43 millilobes and 72 millilobes for the old system. More details of these will be given in the DATA ANALYSIS section. It should also be noted that 3C 84 became the main

TABLE Ia

Source	Extrapolated Flux	Corrected Flux
3C 48	3.14 f.u.	3.36 f.u.(1)
3C 147	4.85	5.19
3C 196	2.46	2.63
3C 286	5.34	5.71
3C 295	3.43	3.67
NGC 7027*	6.07	6.49

Flux calibrators at 8300 MHz. Extrapolated fluxes are from the original paper of Dent and Haddock while corrected fluxes are these fluxes scaled up by 7%.

TABLE Ib

Source	Extrapolated Flux	Corrected Flux
3C 48	2.70 f.u.	2.97 f.u.
3C 147	4.40	4.84
3C 196	2.12	2.33
3C 286	4.90	5.39
3C 295	2.85	3.14
NGC 7027*	6.61	7.27

Flux calibrators at 9600 MHz. The scale factor is 10.2% in this case.

(1) $1\,\text{f.u.} = 10^{-26}$ watts $m^{-2}Hz^{-1}$

* From ref. (77).

TABLE II

Phase Calibrators

Source	Right Ascension			Declination		
3C 48	01^h	34^m	$49^s.81$	32	54'	20".2
3C 84	03	16	29.60	41	19	52.0
3C 147	05	38	43.58	49	49	43.1
3C 196	08	09	59.43	48	22	08.0
3C 286	13	28	49.67	30	45	59.3
3C 295	14	09	33.75	52	26	13.6
3C 345	16	41	17.67	39	54	11.1
3C 380	18	28	13.41	48	42	39.3
NGC 7027*	21	05	09.4	42	02	03.1

All positions are for the epoch 1950.0.

*From optical position given in ref. (74).

TABLE III

Sequence of Observations

Spacing	Frequency	Date Start	Date End	
200' EW	9600 MHz.	3/ 6/68	3/13/68	Horn Calib.
"	8300	3/14/68	3/16/68	"
400' EW	8300	5/21/68	5/23/68	Synthesis
"	9600	5/23/68	5/24/68	"
800' EW	9600	5/25/68	5/26/68	"
"	8300	5/27/68	5/30/68	"
600' EW	8300	5/30/68	6/ 2/68	"
"	9600	6/ 2/68	6/ 3/68	"
700' EW	9600	6/ 4/68	6/ 7/68	"
"	8300	6/ 7/68	6/10/68	"
400' NS	9600	9/12/68	9/15/68	"
"	8300	9/16/68	9/19/68	"
New 3 cm. receivers installed in this period.				
200' NS	9600	7/ 8/69	7/ 9/69	Horn Calib.
"	"	7/ 9/69	7/10/69	Synthesis
"	8300	7/10/69	7/11/69	"
"	"	7/11/69	7/11/69	Horn Calib.
600' NS	8300	7/12/69	7/13/69	Synthesis
"	"	7/13/69	7/13/69	Horn Calib.
"	"	7/13/69	7/14/69	Synthesis
"	9600	7/15/69	7/15/69	Horn Calib.
"	"	7/15/69	7/16/69	Synthesis
"	"	7/16/69	7/16/69	Horn Calib.
"	"	7/16/69	7/17/69	Synthesis
300' EW*	9600	7/19/69	7/21/69	"
"	8300	7/21/69	7/23/69	"
200' EW*	9600	10/22/69	10/23/69	"
"	8300	10/23/69	10/24/69	"
100' EW	9600	10/25/69	10/26/69	"
"	8300	10/26/69	10/27/69	"
300' EW	9600	6/ 3/70	6/ 3/70	Horn Calib.
"	"	6/ 3/70	6/ 5/70	Synthesis
"	8300	6/ 5/70	6/ 5/70	Horn Calib.
"	"	6/ 5/70	6/ 6/70	Synthesis
"	"	6/ 6/70	6/ 7/70	Horn Calib.
"	"	6/ 7/70	6/ 8/70	Synthesis
500' EW	9600	8/29/70	8/31/70	"
"	8300	8/31/70	9/ 3/70	"

*Data discarded and replaced by later observations.

horn and instrumental calibrator after this new system came into operation.

The two methods of horn calibration discussed in the MATHEMATICAL TECHNIQUES section have been used for the observations. Essentially, the emphasis is on the second one during the first part of the observing schedule and on the first one during the later part. Tables IV and V give typical horn calibrations and instrumental polarizations of the two horn receiver systems relevant to the determination of the three Stokes parameters in equation (15).

The 1950.0 position of Cygnus A used is $19^h\ 57^m\ 44.^s5$ and $40°35'46.''0$. The right ascension and declination are taken from Fomalont (83,84).

CHAPTER FOUR

DATA ANALYSIS

Figures (3-6) illustrate the scatter in the horn and instrumental calibrations. It can also be seen that the stronger source 3C 84 is significantly better than NGC 7027.

Figure (7) is a typical plot of the visibility amplitude and phase as a function of hour angle. For close spacings (up to three or four hundred feet), these experimental data agree quite well with the corresponding visibilities of a double gaussian model.

Interpolation

Bracewell's fan-beam inversion scheme (85), which is one of the schemes used, requires the values of the visibility functions along certain position angle 'rays' on the UV plane. These numbers, therefore, have to be interpolated from the adjacent measured values. The interpolations include points within $0^h.2$ to $0^h.5$ of the desired hour angle, weighted exponentially as in Weiler (59). Smooth curves through the measured points are produced separately for the real and imaginary parts. Comparisons are then made between the points plotted this way and plotted in the manner of figure (7), and points which do not fall along the smooth curve to within the errors accepted (see ERROR ANALYSIS) are discarded. The real and imaginary parts of the remaining points are again plotted up and a smooth curve is then drawn by hand through these points. The visibilities at the desired hour angles are then read off from these plots.

The corrections due to the non-orthogonality of the horns during observation and the instrumental polarization as listed in Tables IV

Figure 7

Plots of (a) observed visibility phase and (b) observed visibility amplitudes as a function of hour angle at 8300 MHz and 500' EW.

Observed Cygnus A Visibilities at 8300 MHz 500'EW

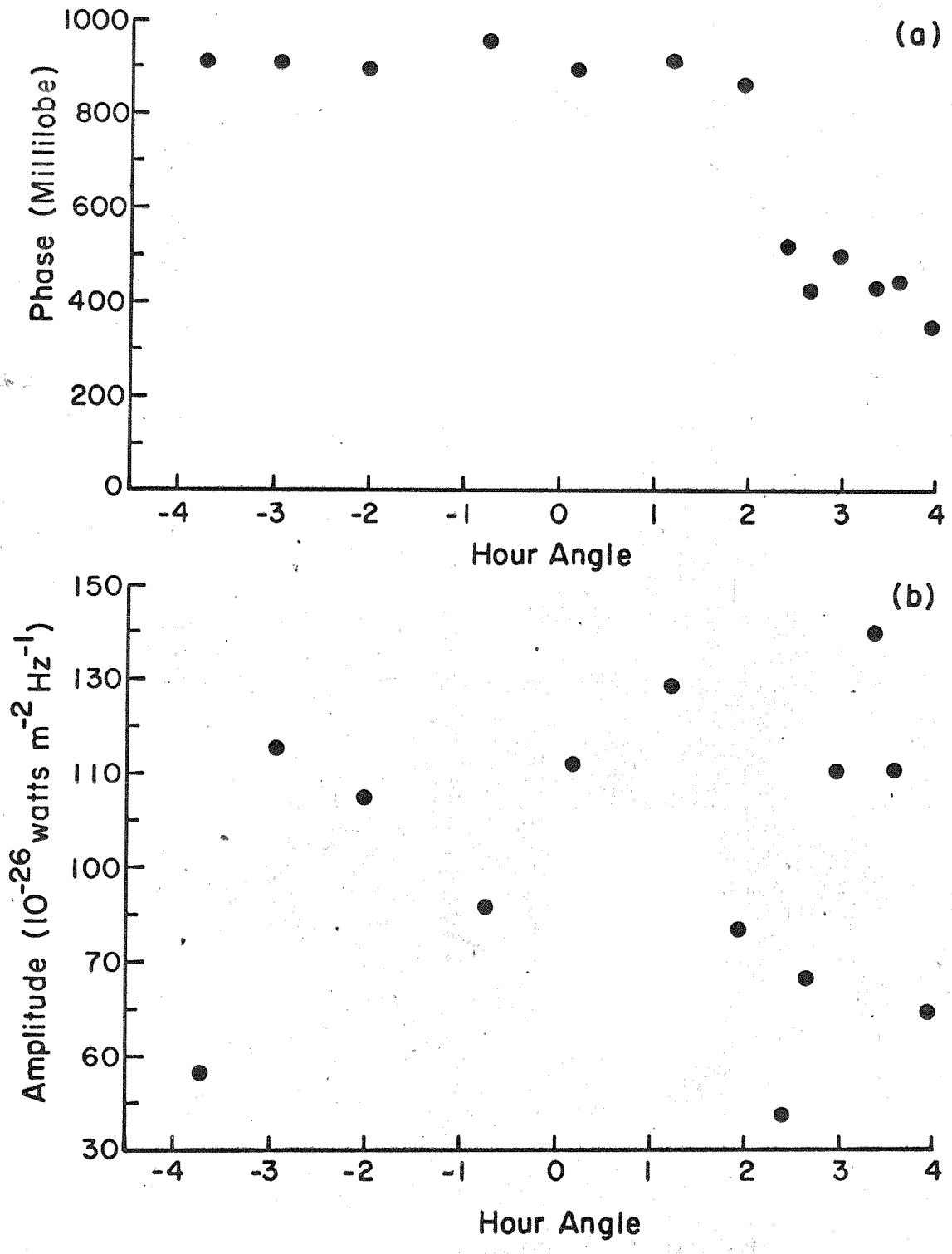

and V are applied as in equation (15). The correction factors to the flux calibrators are also included in all these interpolated visibilities. These scaling factors are 1.07 at 8300 MHz and 1.10 at 9600 MHz to the values given by Dent and Haddock (81).

Inversion

In order to determine accurately the D.C. level of the brightness temperature transform, the total flux density integrated over all of Cygnus A, is necessary. This flux density has been deduced from the papers by Baars, Mezger and Wendker (86) and by Parker (87). With an 8000 MHz flux density of 217 f.u. and a spectral index of -1.19 (86), the 8300 MHz and 9600 MHz values are 207.8 f.u. and 174.7 f.u., respectively. These numbers agree nearly exactly with those obtained by interpolation from a detailed plot (figure 8) of the data gathered in Table IV(b) in Parker's paper.

Because the Stokes parameters U and Q are inverted separately before they are combined point by point according to the relations

$$I_p = U^2 + Q^2$$

and (22)

$$X = (1/2)\tan^{-1}(U/Q) \quad ,$$

their zero spacing fluxes have to be deduced as well. Figure (9) is a plot of the integrated percentage polarization and position angle as a function of wavelength squared from the values given by Schraml and Turlo (37) with the point from Hollinger and Hobbs at 3.6 cm (88) included. The best curve is then drawn through these points and the values at 8300 MHz (3.61 cm) and 9600 MHz (3.12 cm) read off. They are 6.3 percent at a position angle of 138° and 7.9 percent at

TABLE IV

Instrumental Corrections for Old Receiver System

Freq (MHz)	Horn Position (ϕ_1/ϕ_2)	Δ_d (rad)	Δ_e (rad)	$\varepsilon=\Delta_d-\Delta_e$	θ^+ (rad)
8300	0/90.72	$1.26*10^{-2}$	$1.19*10^{-2}$	$6.98*10^{-4}$	$-3.0*10^{-3}$
	45/135.68	$1.19*10^{-2}$	$1.26*10^{-2}$	$-6.98*10^{-4}$	$5.0*10^{-3}$
9600	9/90.21	$3.67*10^{-3}$	$5.24*10^{-3}$	$-1.57*10^{-3}$	$0.0*10^{-3}$
	45/134.91	$-1.57*10^{-3}$	$1.40*10^{-3}$	$-2.97*10^{-3}$	$-5.0*10^{-3}$

TABLE V

Instrumental Corrections for New Receiver System

Freq (MHz)	Horn Position (ϕ_1/ϕ_2)	Δ_d (rad)	Δ_e (rad)	$\varepsilon=\Delta_d-\Delta_e$ (rad)	θ^+ (rad)
8300	0/89.90	$-1.75*10^{-3}$	$2.27*10^{-2}$	$-2.44*10^{-2}$	$-7.78*10^{-3}$
	45/134.80	$-3.50*10^{-3}$	$1.87*10^{-2}$	$-2.22*10^{-2}$	$-4.52*10^{-3}$
9600	0/89.90	$-1.75*10^{-3}$	$2.43*10^{-2}$	$-2.60x10^{-2}$	$-5.40*10^{-4}$
	45/134.80	$-3.50*10^{-3}$	$1.74*10^{-2}$	$-2.09*10^{-2}$	$-5.01*10^{-3}$

Figure 8

Spectral flux densities of Cygnus A.

Flux Densities of Cygnus A (Parker, 1968)

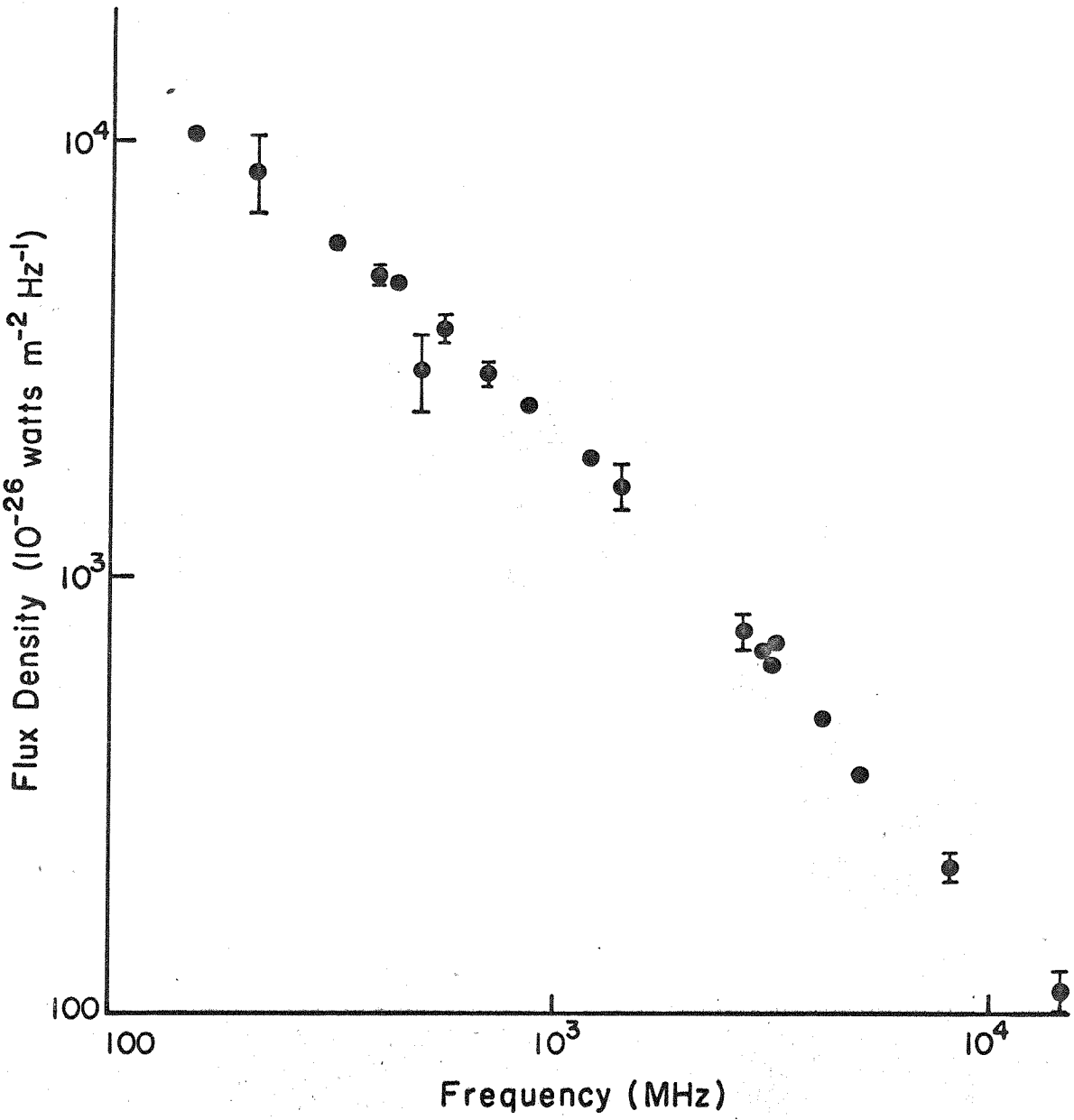

Figure 9

(a) Integrated position angle of Cygnus A.

(b) Integrated percentage polarization of Cygnus A.

Intergrated Polarization of Cygnus A

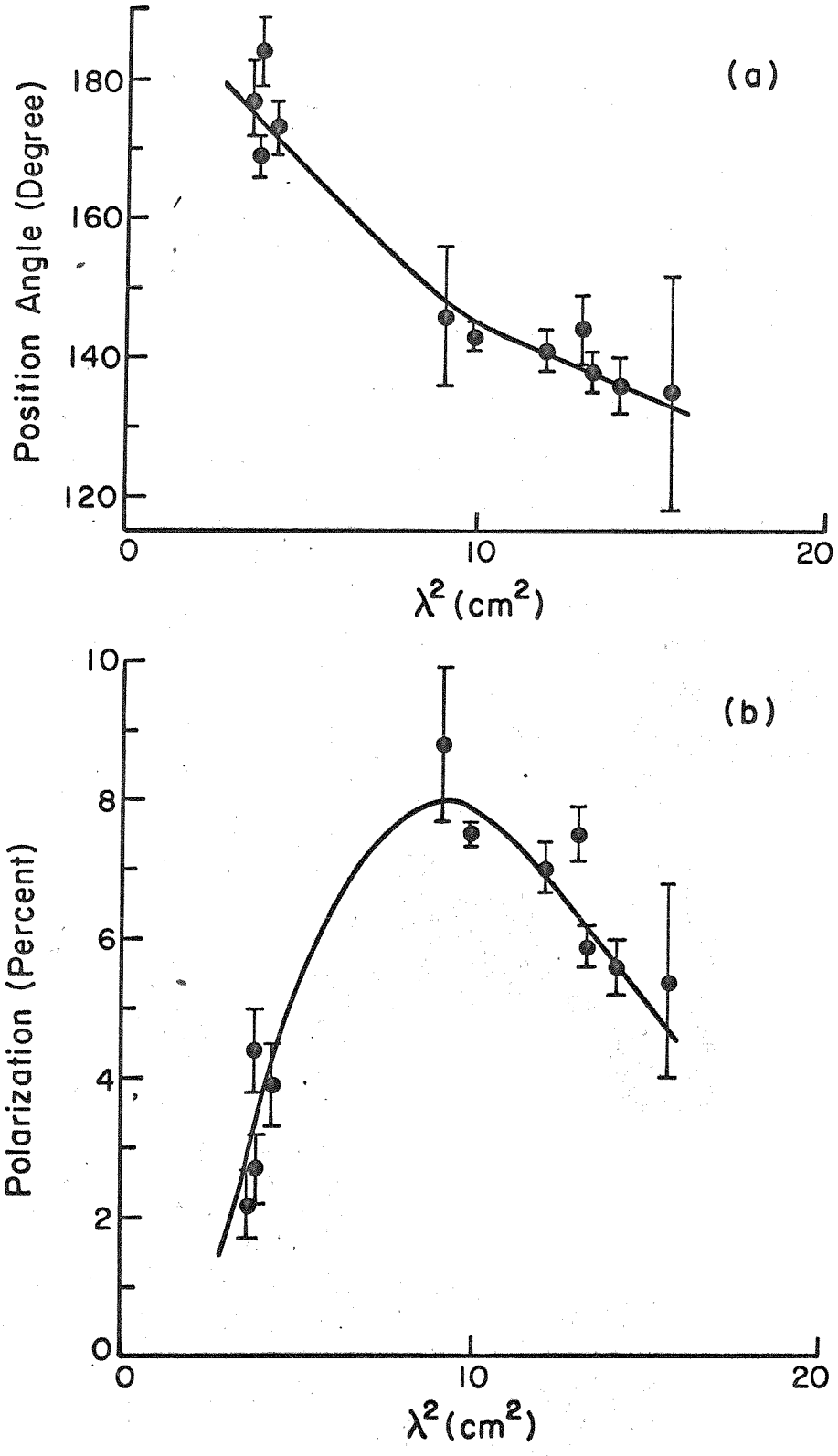

145°, respectively. Substituting into equation (22), the values are found to be -13.02 f.u. for U, 1.37 f.u. for Q at 8300 MHz and -13.12 f.u. for U, 4.78 f.u. for Q at 9600 MHz. The sign convention is shown in Table VI.

Having obtained these zero spacing fluxes, we can now proceed with the inversions. For the intensity map, due to the rather low density of observed points on the UV plane, the 8300 MHz and 9600 MHz data have been combined before inversion. Because of the closeness in frequencies, a scaling factor of $(8.3/9.6)^{-1.19} = 1.19$ has to be applied between the two sets of visibility amplitudes. The 9600 MHz data have been scaled to 8300 MHz and the combined visibilities inverted. It should be noted that the error introduced, if any, by any expected differences in the spectral index is less than the errors between two such nearby frequencies in the two separate intensity maps. Now, the Bracewell fan beam inversion scheme cannot be conveniently used in this case because the observation points are not equally spaced along each position angle ray. Rather, an inversion program developed by Dr. D. Rogstad and modified by Mr. S. Shostak has been used. This program makes use of gaussian weighting functions and smooths the available observed points onto a set of grid points on the UV plane. The visibility amplitudes are tapered to one-third of their original values at the largest spacing.

The polarized distribution maps have been inverted with the Bracewell fan beam technique. This inversion technique has the advantage that it allows one to select out to some extent the bad data points. It first inverts along a position angle ray and then

TABLE VI

Sign Conventions for the Stokes Parameters U and Q

Horns	Response
0/90	U
45/135	-Q

Plane of Polarization	Q	U
0°-45°	Q>0	U>0
45°-90°	Q<0	U>0
90°-135°	Q<0	U<0
135°-180°	Q>0	U<0

integrates these one dimensional brightness temperatures over the UV plane. Studying these one dimensional profiles, one can pick out the 'bad' ones, those with negative side lobes greater than 40 percent, for example, and discard them. In practice, however, it is not always true that the profiles with large side lobes are bad because in integrating these profiles for the two dimensional map, cancellation of positive and negative side lobes occur. These profiles, however, give clues as to what one may try to discard. Of course, one has to be careful that the Bracewell criteria is still satisfied after the removal of some of these strips. The same standard convolution is applied to these U and Q maps which are then combined point by point to yield the polarization maps at the two frequencies.

Error Analysis

The errors in the final maps come, to a considerable extent, from the instabilities in the electronics of the observing instruments and from the phase fluctuations caused by the atmosphere. These atmospheric effects will be discussed later. The deviations of the calibrated values of the flux and phase calibrators from their given values therefore are indications of the magnitudes of the errors involved. Of course, it should be noted that inaccuracies of the flux values given for the flux calibrators and the positions given for the phase calibrators cause inaccurate calibrated D.C. levels, but considerable care has been exercised and these inaccuracies should be small. Figures (10) and (11) show the kind of scatter in flux and phase obtained in this project. Both data from the old and new receiver systems have been included.

Figure 10

Histograms showing deviations of the measured flux values of the calibrators from their true values at (a) 8300 MHz and (b) 9600 MHz.

Comparison Between True and Measured Flux Valves

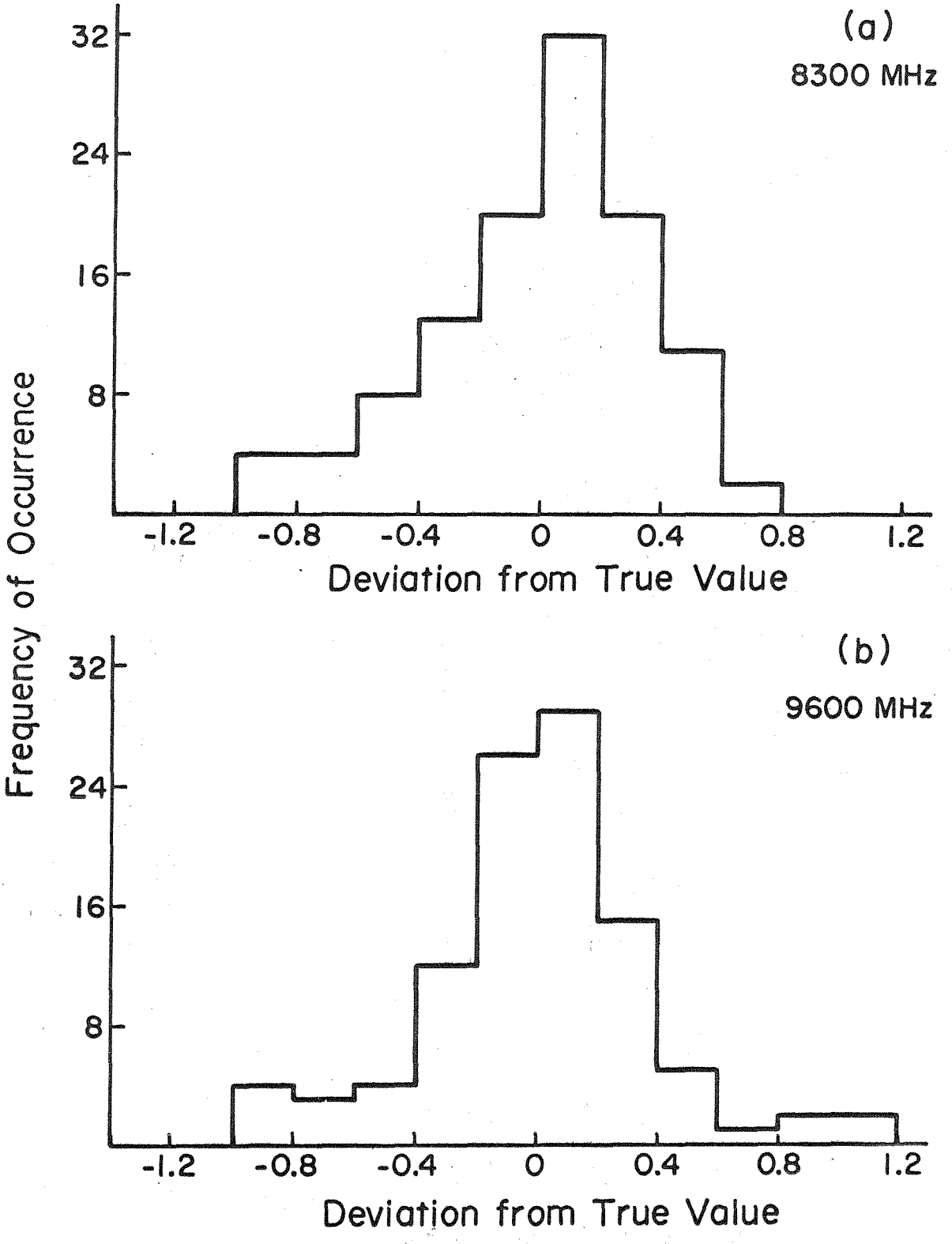

Figure 11

Histograms showing deviations of the measured phase values of the calibrators from their expected value (zero) at (a) 8300 MHz and (b) 9600 MHz.

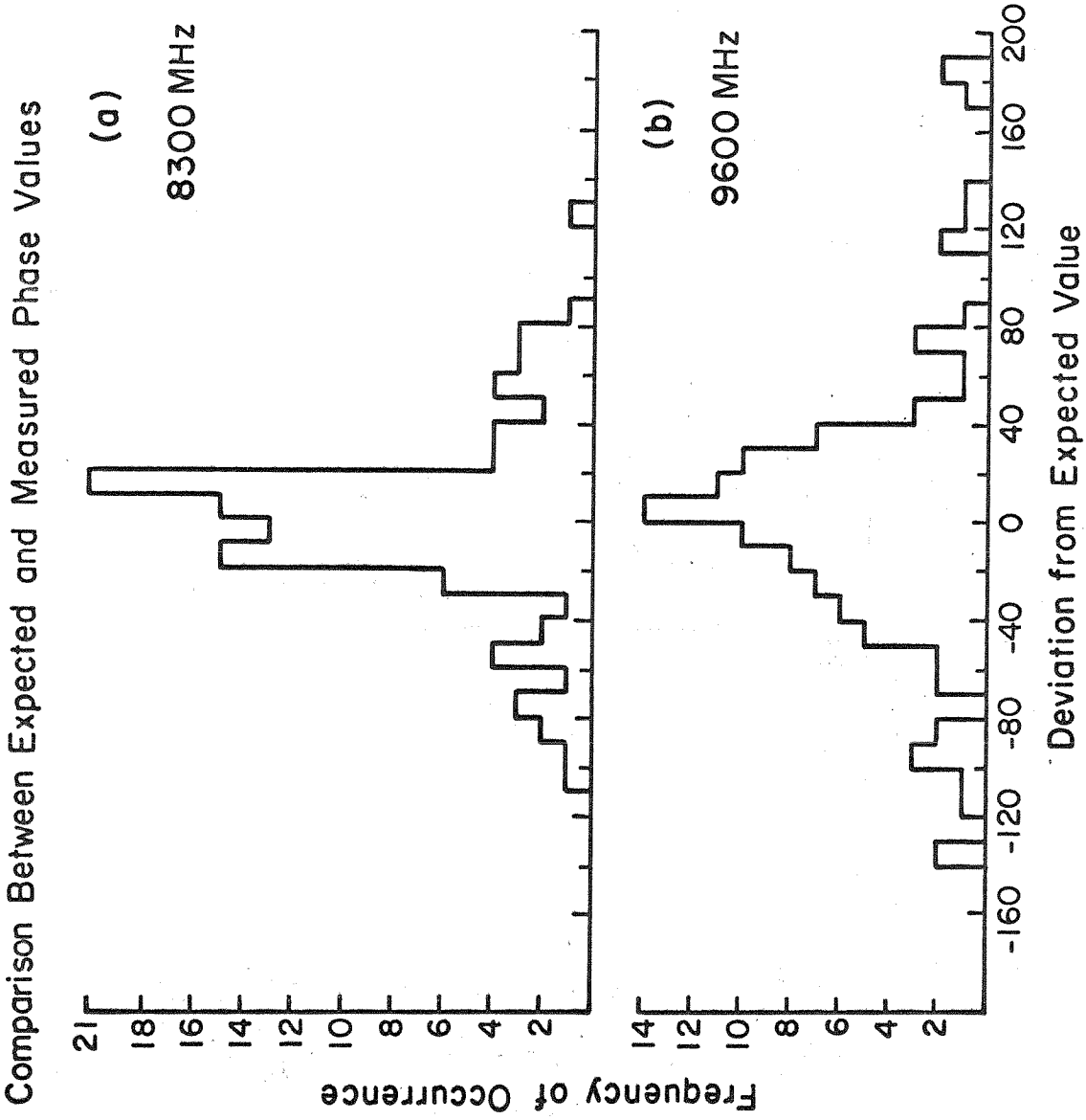
Comparison Between Expected and Measured Phase Values
(a)
8300 MHz
(b)
9600 MHz
Frequency of Occurrence
Deviation from Expected Value
21
18
16
14
12
10
8
6
4
2
-160
-120
-80
-40
0
40
80
120
160
200

The r.m.s. deviations for both the 8300 MHz and 9600 MHz flux calibrators for all the spacings are about 0.38 f.u. The typical variations for a single eight hour observating run after calibration is shown in figure (12). For the phase calibrators, the calibration programs force their expected phase values to be zero. The departure from zero, therefore, is an indication of the errors incurred. As an illustration of the improved phase stability of the new transistorized receiver system for the latter part of the observations, histograms showing the deviations from zero of the phase calibrators for the two receiver systems at the two frequencies are shown in figure (13) and (14). The r.m.s. deviation at 8300 MHz is 36 millilobes and is 51 millilobes at 9600 MHz for the whole observations. Figure (15) illustrates the variations in a typical eight hour run.

Besides the instrumental instabilities mentioned above, the other major source of error comes from the calibrations of the horns. In particular, for the calibrations when the weaker source NGC 7027 was used in the beginning, the standard deviations involved in the average instrumental circular polarizations are considerable. Tables IV and V show the results of the horn calibrations and their errors and the data have been corrected for these calibrations before the visibilities were Fourier inverted.

The possible effects of the bandwidth of the radio receivers are now considered. As shown by Weiler (59), if the receiving bandwidth is finite and symmetric, no error is introduced in the position angle measurements. This position angle, PA_ν, of a linearly polarized

Figure 12

Typical fluctuations of the measured flux values of the calibrators from their true values at (a) 8300 MHz and (b) 9600 MHz.

Typical Fluctuation of Measured Flux Calibrator Values

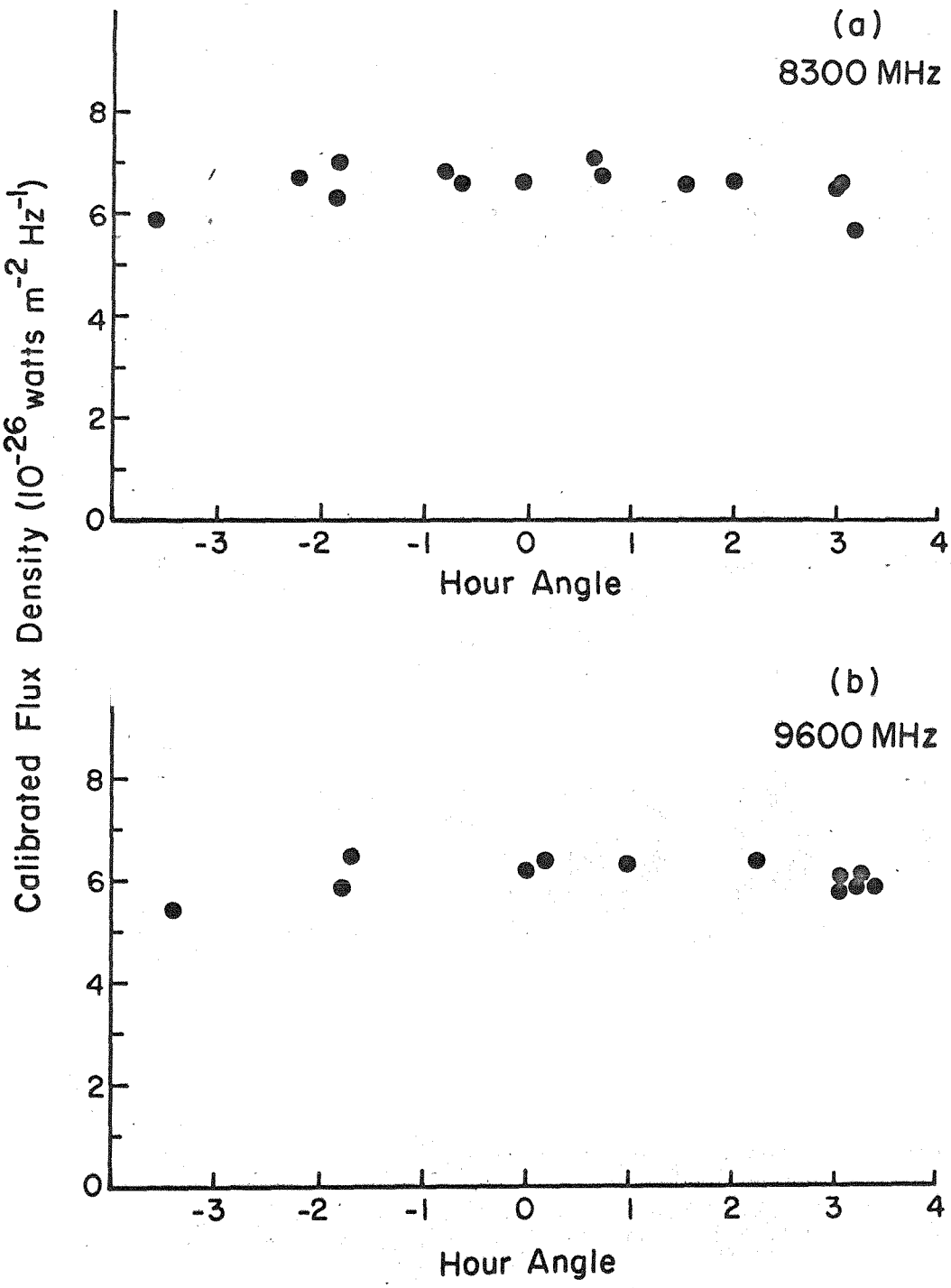

Figure 13

Comparison between the phase stabilities of the old and new receiver systems at 8300 MHz. Abscissa gives the deviations from the expected zero value for these phase calibrators.

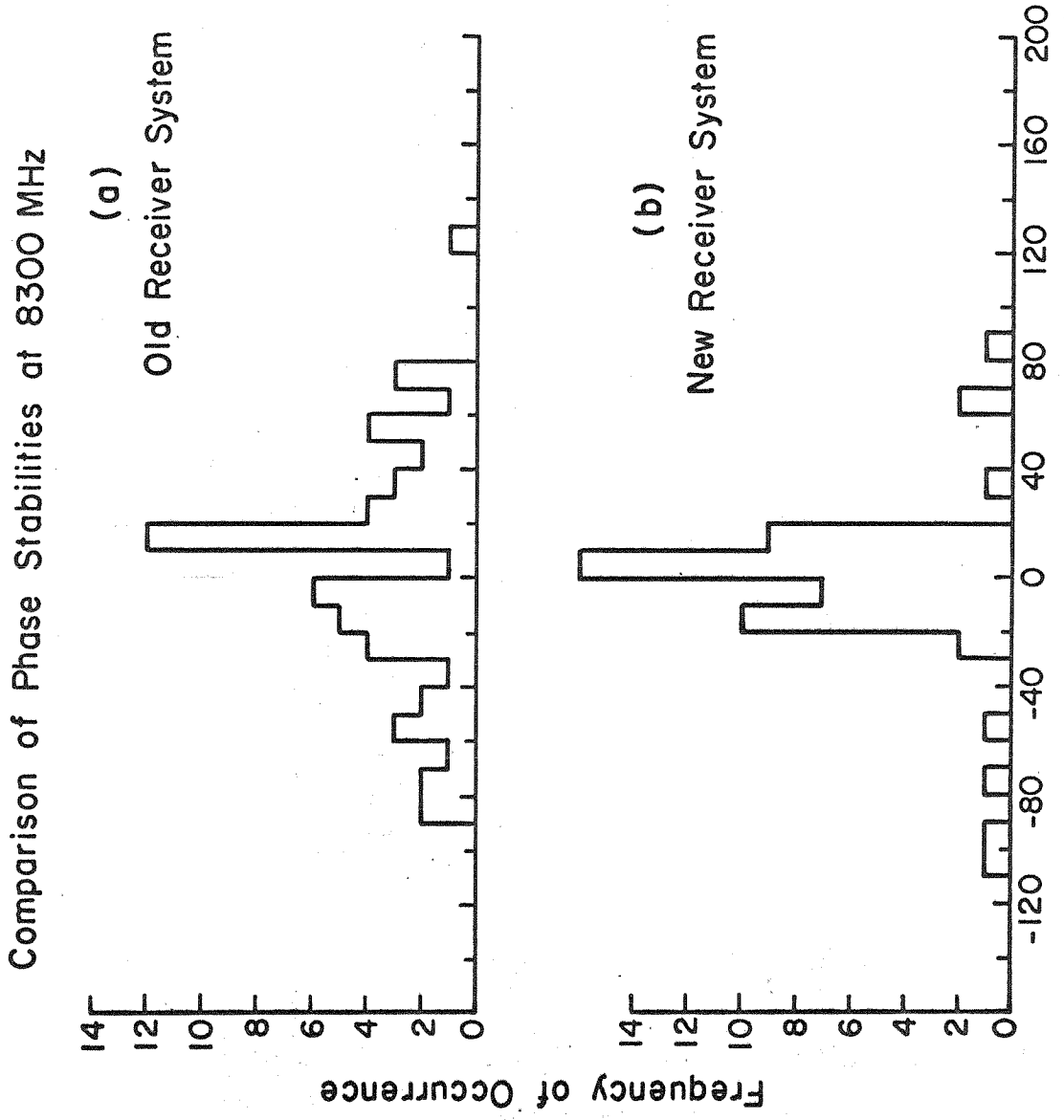
Comparison of Phase Stabilities at 8300 MHz
(a)
Old Receiver System
(b)
New Receiver System
Frequency of Occurrence
Deviation from Expected Value
0
2
4
6
8
10
12
14
-120
-80
-40
0
40
80
120
160
200

Figure 14

Comparison between the phase stabilities of the old and new receiver systems at 9600 MHz.

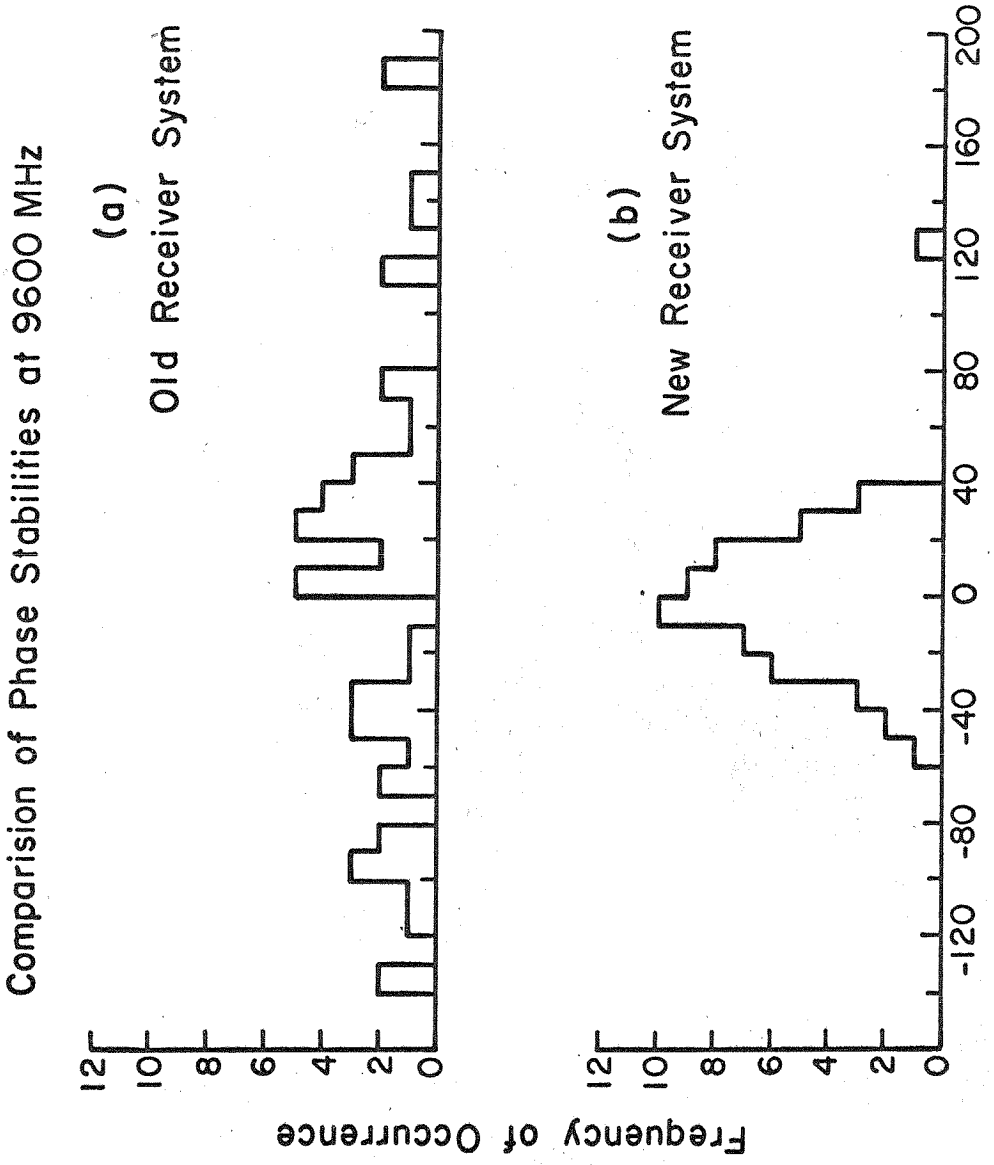
Comparision of Phase Stabilities at 9600 MHz
(a)
Old Receiver System
(b)
New Receiver System
Frequency of Occurrence
Deviation from Expected Value
0
2
4
6
8
10
12
-120
-80
-40
0
40
80
120
160
200

Figure 15

Typical fluctuations of the measured phase values of the calibrators from their expected zero values at 8300 MHz and 9600 MHz.

Typical Fluctuation of Measured Phase Calibrator Values

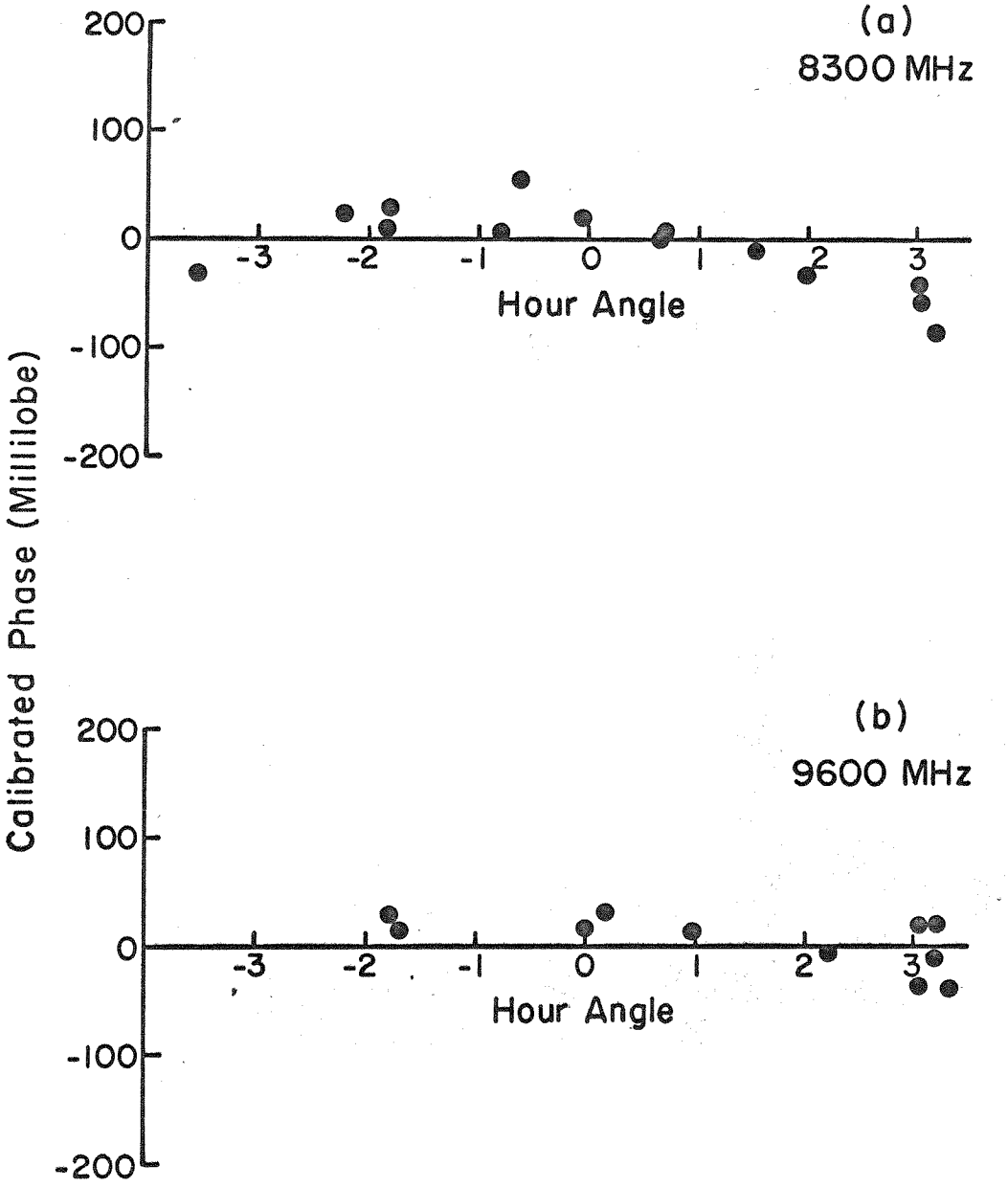

cosmic radio wave has a wavelength dependence of

$$PA_\nu = PA_0 + R_m \lambda^2 \tag{23}$$

where PA_0 and R_m are the "intrinsic position angle" and "rotation measure" respectively. Although the position angle measurements are not affected, the rotation across the bandwidth reduces the observed polarization (P) below the true value (p). Since the receiver bandpass function R_ν in this project can also be represented by two equal gaussians symmetrically placed about the observing frequency ν_0 and separated from it by a frequency interval ν_1 with each gaussian having a full width at half maximum of ν_2, the following expression derived by Weiler is still valid.

$$P=p \cos\{(4R_m c^2 \nu_1)/\nu_0{}^3\} \exp\{-(4R_m^2 c^4 \nu_2{}^2)/(2.77\nu_0{}^6)\} \tag{24}$$

where c is the velocity of light in vacuum. The relevant values for this project are $\nu_0 = 8.3 \times 10^9$ or 9.6×19^9 Hz, $\nu_1 = 10^7$ Hz and $\nu_2 = 5 \times 10^6$ Hz. As can be seen, the factor of bandwidth depolarization for the range of R_m encountered is unity.

The fluctuations in the refractivity of the atmosphere cause fluctuations in the phase between two points separated by some distance and receiving the same wave-front. Baars (89) worked out the expression for the r.m.s. phase fluctuation for an interferometer separation of ρ as

$$\overline{\Delta S} = 1.7k\sqrt{L}C_n\rho^{5/6} \tag{25}$$

where $k = 2\pi/\lambda$ is the wave number, L is the 'thickness' of atmosphere effective for turbulence and C_n is the refractive index. Taking L

to be 3000 meters as Baars did in his paper and the range of C_n as $2 \times 10^{-8} \leq C_n \leq 4 \times 10^{-7}$ $m^{-1/3}$, the r.m.s. fluctuations in phase for the largest spacing of 800 feet used are between 6 and 116 millilobes at 9600 MHz and between 5 and 100 millilobes at 8300 MHz. Of course, the large spread comes from the correspondingly large range in C_n.

From the observational results recently obtained by Hinder (90) using the Cambridge one mile telescope at 5 GHz, a phase fluctuation of about 16 millilobes due to atmospheric effects can be deduced for a separation of about 1000 feet. However, the results directly applicable to this project have been obtained by Seielstad (private communication) at 9600 MHz and a baseline of 3500 feet at the Owens Valley Radio Observatory. The fluctuation found by Seielstad is 60 millilobes. Using the $\rho^{5/6}$ dependence in equation (25), the phase fluctuation at 800 feet and 9600 MHz due to atmospheric effects becomes 18 millilobes. Thus, it can be seen that these atmospheric turbulences contribute significantly to the errors in the phases measured.

All these above mentioned errors will manifest themselves as departures from zero in the inversion range where there is thought to be no emission. Following the methods of Fomalont (83), the errors in the resultant maps of I, U, Q and $\sqrt{U^2+Q^2}$ are given as the r.m.s. average brightness external to the area of the source considered significant. These are given in Table VII.

TABLE VII

Estimated Error in Brightness Temperature Maps

	Freq (MHz)	Error (Percent)
I	8300	8.3
U	8300	11.1
	9600	8.8
Q	8300	11.0
	9600	16.2
$\sqrt{U^2+Q^2}$	8300	10.0
	9600	9.6

CHAPTER 5

OBSERVATIONAL RESULTS

The map of the total radiation I from the combined 8300 MHz and 9600 MHz data is shown in figure (16). The contours are ten percent intervals and the lowest one drawn is also ten percent. The superposition of these radio contours on the optical photograph is shown in figure (17). The area of the map is 3' by 2' with the center corresponding to a position of $\alpha(1950.0)=19^h57^m44.5^s$ and $\delta(1950.0)=40°35'46.''0$. The peak intensity for the I map is 420.5 f.u./(arcmin)^2. The bridge component, the extension of the west component in the eastward direction as seen by Mitton and Ryle in their 2.7 GHz and 5 GHz (34) observations is still clearly seen at 8.3 GHz. Moreover, the steepness of the outer edges in both components and the slight northward tilt of the bridge as noted by these authors are also visible. The east component is more intense and the ratio of the peak intensities of these two components is about 1.1:1. The major axis of these components is at a position angle of about 107°, measuring from north through east, and the separation of the peaks of these components is about 124". For comparison with the 1.4, 2.7 and 5.0 GHz maps of Mitton and Ryle (34), these data have been convolved to yield the same resolution as that of the 1.4 GHz map by Cambridge. The profile along the major axis of the source at these four frequencies are shown in figure (18). It is apparent from these profiles that the spectrum of the bridge is steeper than that of the outer edges, as have been noted before (34). Figure (19) gives the detailed normalized numbers (each number is separated by 3" from the adjacent

Figure 16

Total intensity map of Cygnus A (3C405) at 8300 MHz. Area of map is 3'x2' and the center cross is at $\alpha(1950.0) = 19^h57^m44.5^s$ and $\delta(1950.0) = 40°35'46.0''$. The contours are 10 percent and the lowest one drawn is also 10 percent.

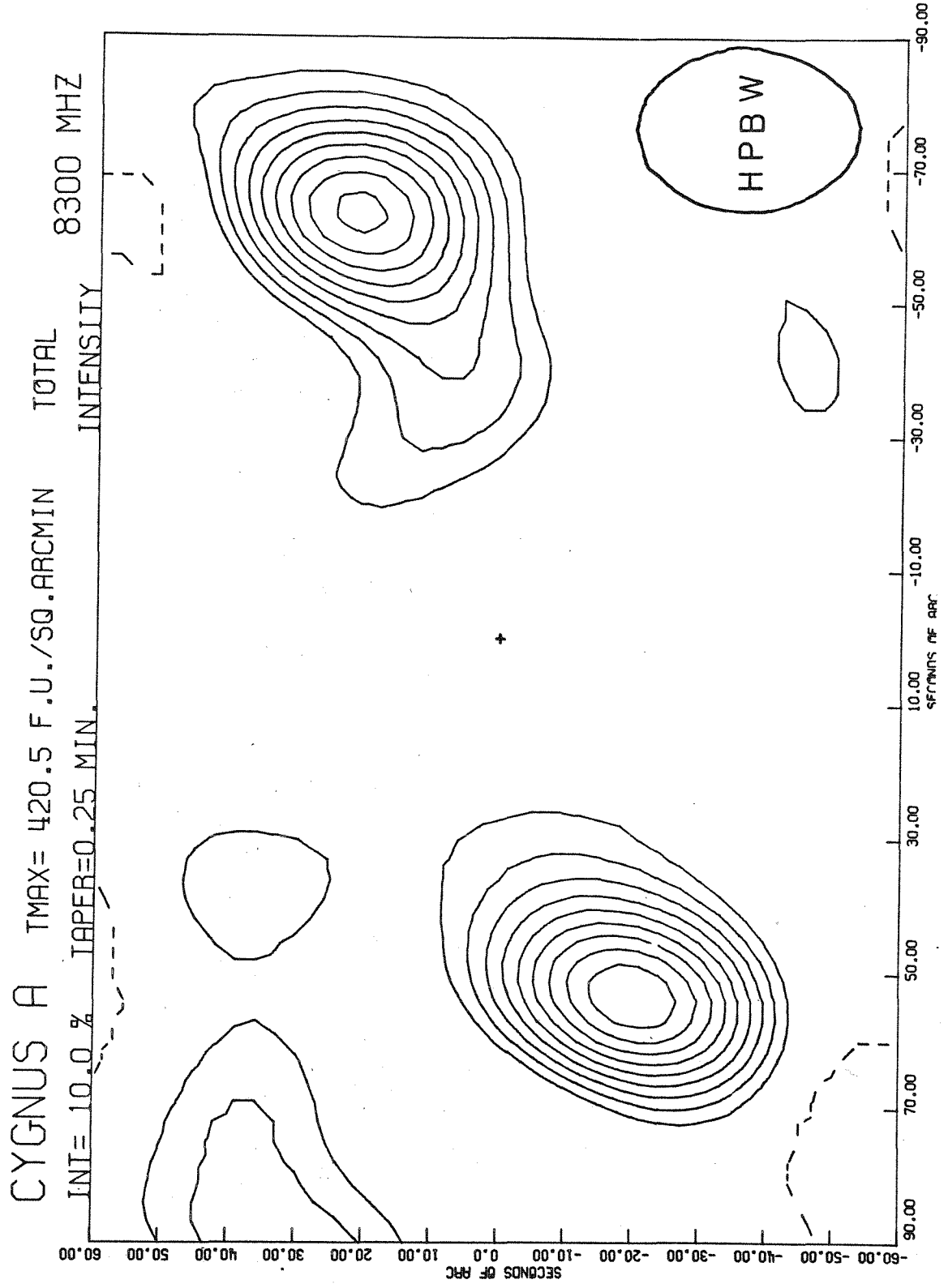
CYGNUS A
TMAX= 420.5 F.U./SQ.ARCMIN
INI= 10.0 %
TAPER=0.25 MIN.
TOTAL
INTENSITY
8300 MHZ
HPBW
SECONDS OF ARC
60.00
50.00
40.00
30.00
20.00
10.00
0.0
-10.00
-20.00
-30.00
-40.00
-50.00
-60.00
90.00
70.00
50.00
30.00
10.00
-10.00
-30.00
-50.00
-70.00
-90.00

Figure 17

Superposition of the total intensity contours at 8300 MHz on the optical picture from the 48" Mount Palomar Sky Survey.

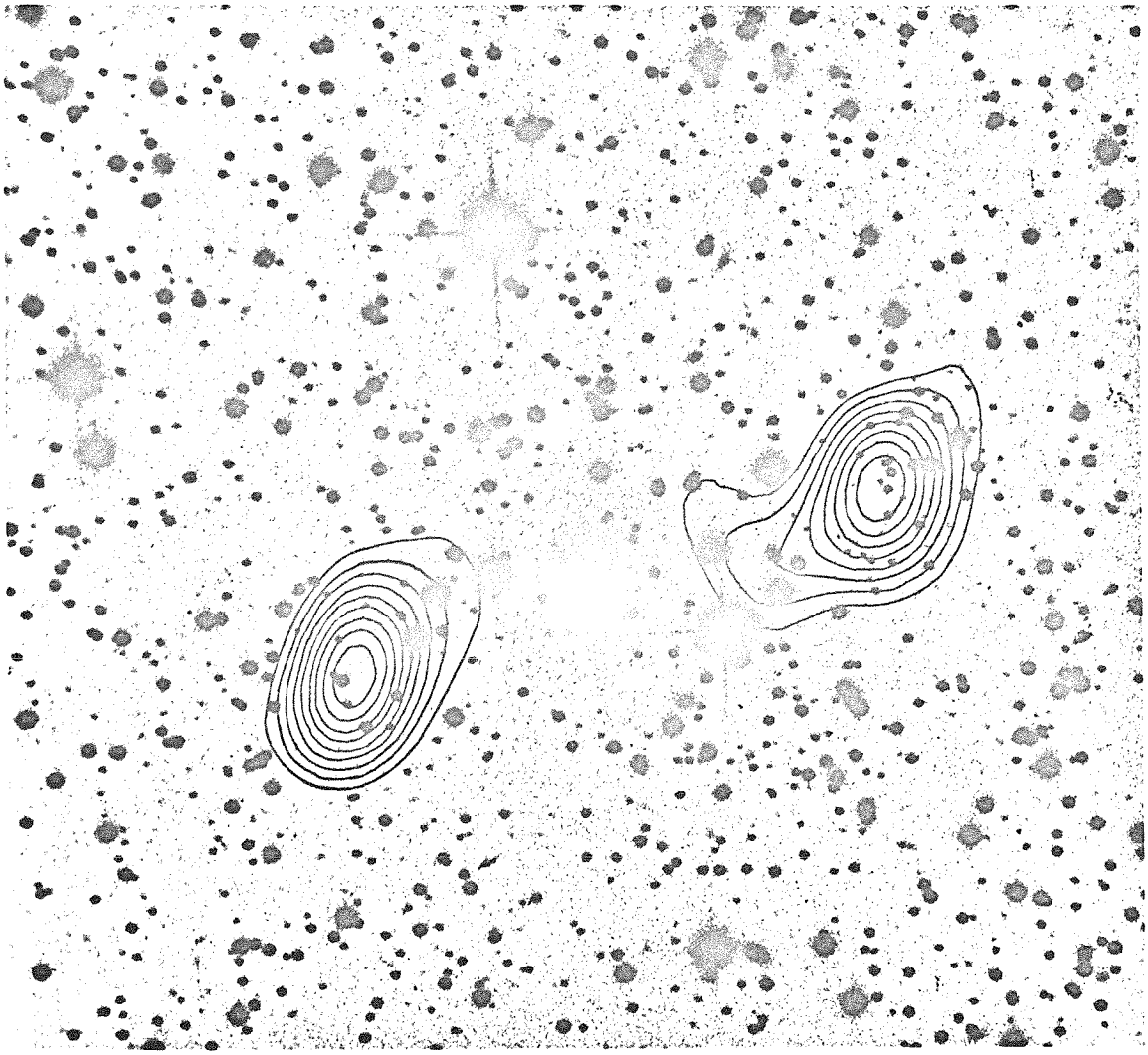

Figure 18

Brightness temperature profiles along the major axis of Cygnus A at 1.4, 2.7, 5.0 and 8.3 GHz. All profiles are convolved to the resolution of the 1.4 GHz map.

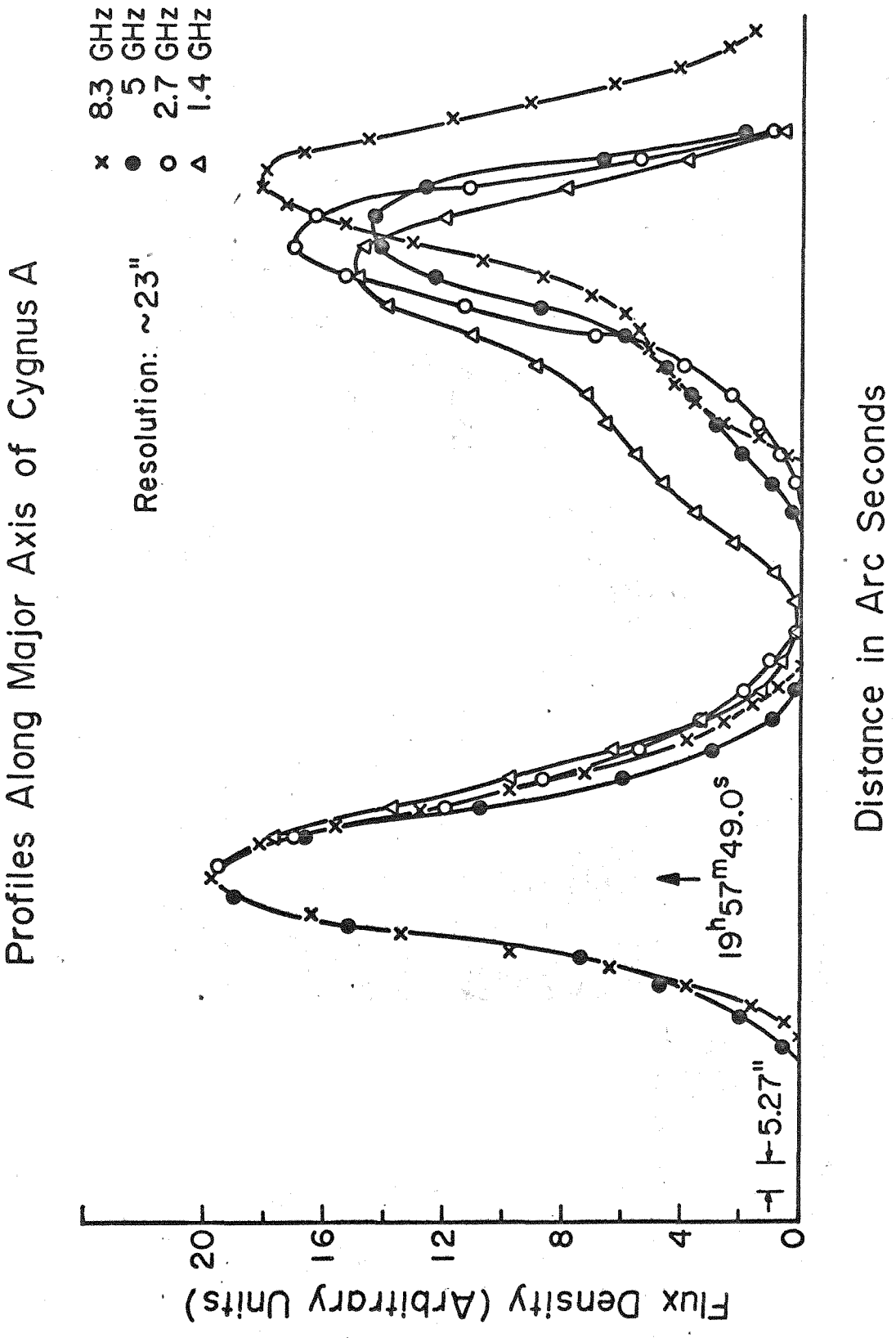
Profiles Along Major Axis of Cygnus A
× 8.3 GHz
● 5 GHz
○ 2.7 GHz
△ 1.4 GHz
Resolution: ~23"
19h57m49.0s
5.27"
Flux Density (Arbitrary Units)
0
4
8
12
16
20
Distance in Arc Seconds

Figure 19

Distribution of total intensity on Cygnus A at 8300 MHz. The numbers have been normalized to a maximum of 100, corresponding to a value of 420.5 f.u./(arcmin)^2. Separation between adjacent numbers is 3".

CYGNUS A 8300 MHz

TOTAL INTENSITY

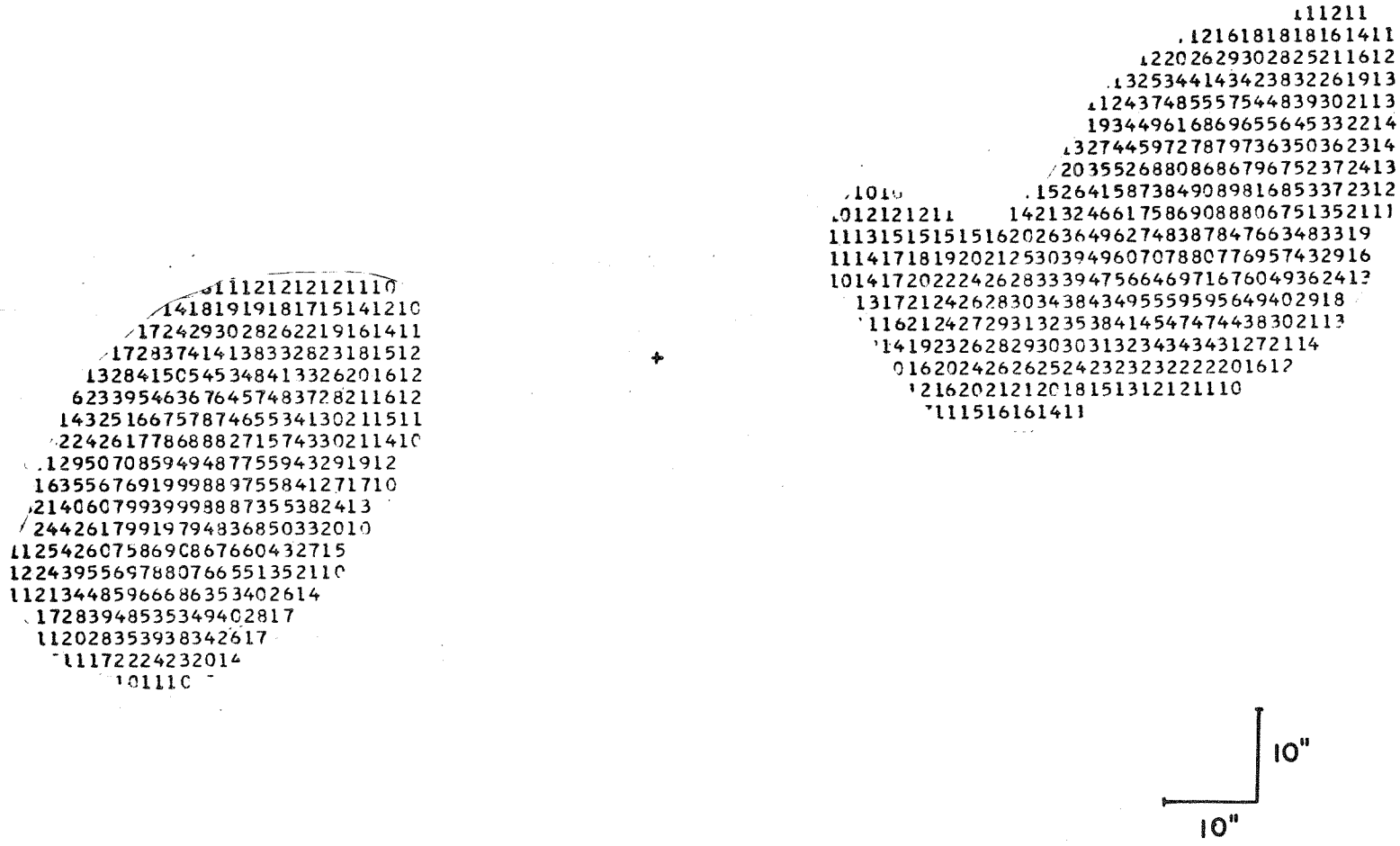

ones in both directions) from which this total intensity map has been plotted. These numbers have been normalized to a maximum value of 100.

Figures (20) and (21) are the maps of the linear polarized radiation of Cygnus A at 8300 MHz and 9600 MHz. The contours for the observed polarized intensities $\sqrt{U^2+Q^2}$ are plotted in parts (a) while the percentage polarization and position angles are in parts (b). The lengths of these vectors are proportional to the observed polarization percentages $100\sqrt{U^2+Q^2}/I$, while the orientations indicate the position angles. Each vector covers an area of 9"x9" and only the vectors whose magnitudes exceed 15 percent of the maximum polarized flux intensity in the corresponding maps are drawn. Moreover, in order to avoid unusually large percentages, no percentage vectors are drawn if the total intensity at the point under consideration is less than 15 percent of the maximum total intensity. These vectors show a slight concentration towards the inner regions of the components whose areas are delineated by the 10 and 50 percent contours from the total intensity map. The dimensions and positions of these maps are identical to those of the intensity map and a line whose length corresponds to ten percent polarization is also drawn at the upper right corner for reference. The values for the polarized intensities and percentages for these plots are shown in figures (22) through (25).

A comparison of the polarization of the components at the two frequencies reveals some very interesting results. The gradual increase in position angles from the east edge of the east component to the west edge is barely noticeable at 8300 MHz but becomes quite

Figure 20

Polarization map of Cygnus A (3C405) at 8300 MHz.

(a) The polarized intensity $\sqrt{U^2+Q^2}$ plotted in 10 percent contours.

(b) The percentages and position angles of polarization. The length of each vector gives the percentage polarization and the orientation gives the observed position angle.

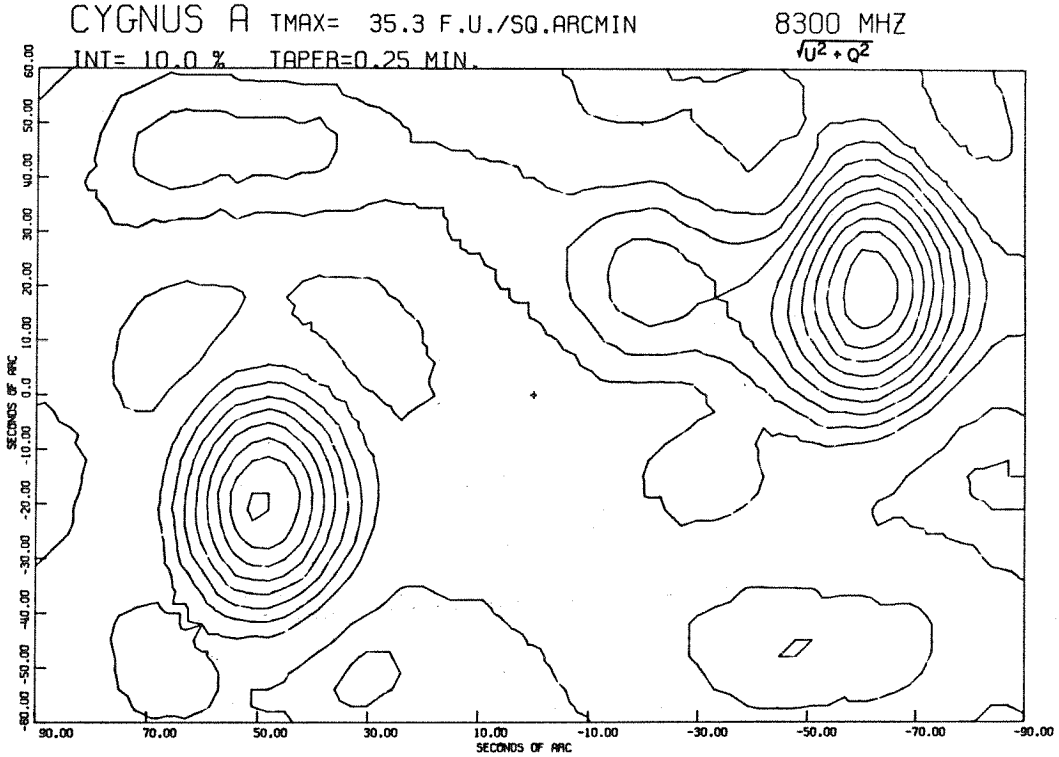
CYGNUS A TMAX= 35.3 F.U./SQ.ARCMIN
8300 MHZ
√U² + Q²
INT= 10.0 %
TAPER=0.25 MIN.
SECONDS OF ARC
60.00
50.00
40.00
30.00
20.00
10.00
0.0
-10.00
-20.00
-30.00
-40.00
-50.00
-60.00
90.00
70.00
50.00
30.00
10.00
-10.00
-30.00
-50.00
-70.00
-90.00
SECONDS OF ARC

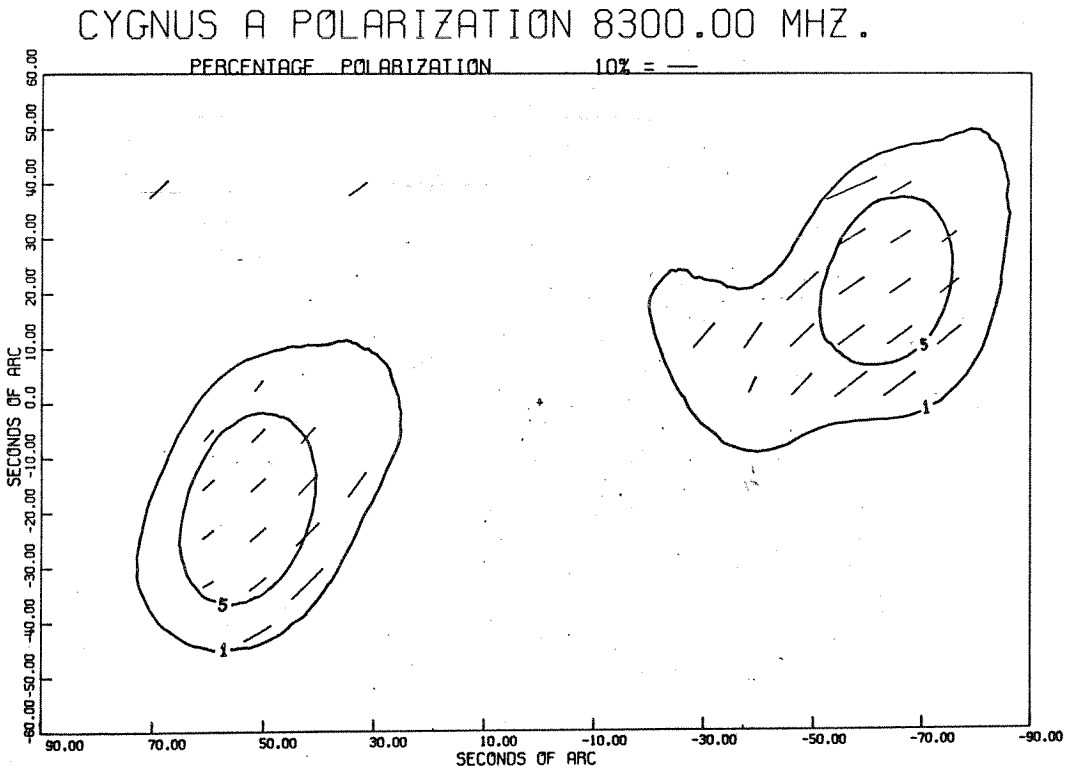
CYGNUS A POLARIZATION 8300.00 MHZ.
PERCENTAGE POLARIZATION
10% = ——
SECONDS OF ARC
60.00
50.00
40.00
30.00
20.00
10.00
0.0
-10.00
-20.00
-30.00
-40.00
-50.00
-60.00
5
1
5
1
90.00
70.00
50.00
30.00
10.00
-10.00
-30.00
-50.00
-70.00
-90.00
SECONDS OF ARC

Figure 21

Polarization map of Cygnus A (3C405) at 9600 MHz.

(a) The polarized intensity $\sqrt{U^2+Q^2}$ plotted in 10 percent contours.

(b) The percentages and position angles of polarization. The length of each vector gives the percentages polarization and the orientation gives the observed position angle.

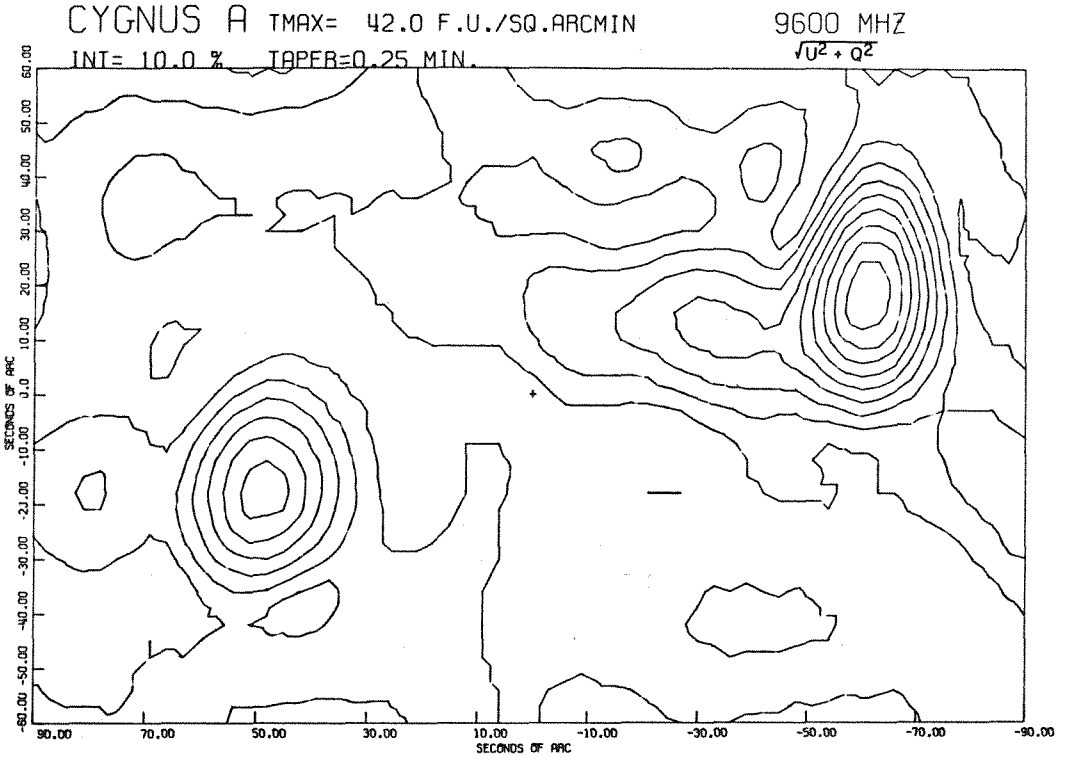
CYGNUS A TMAX= 42.0 F.U./SQ.ARCMIN 9600 MHZ
√U² + Q²
INI= 10.0 % TAPER=0.25 MIN.
SECONDS OF ARC
60.00 50.00 40.00 30.00 20.00 10.00 0.0 -10.00 -21.00 -30.00 -40.00 -50.00 -60.00
90.00 70.00 50.00 30.00 10.00 -10.00 -30.00 -50.00 -70.00 -90.00
SECONDS OF ARC

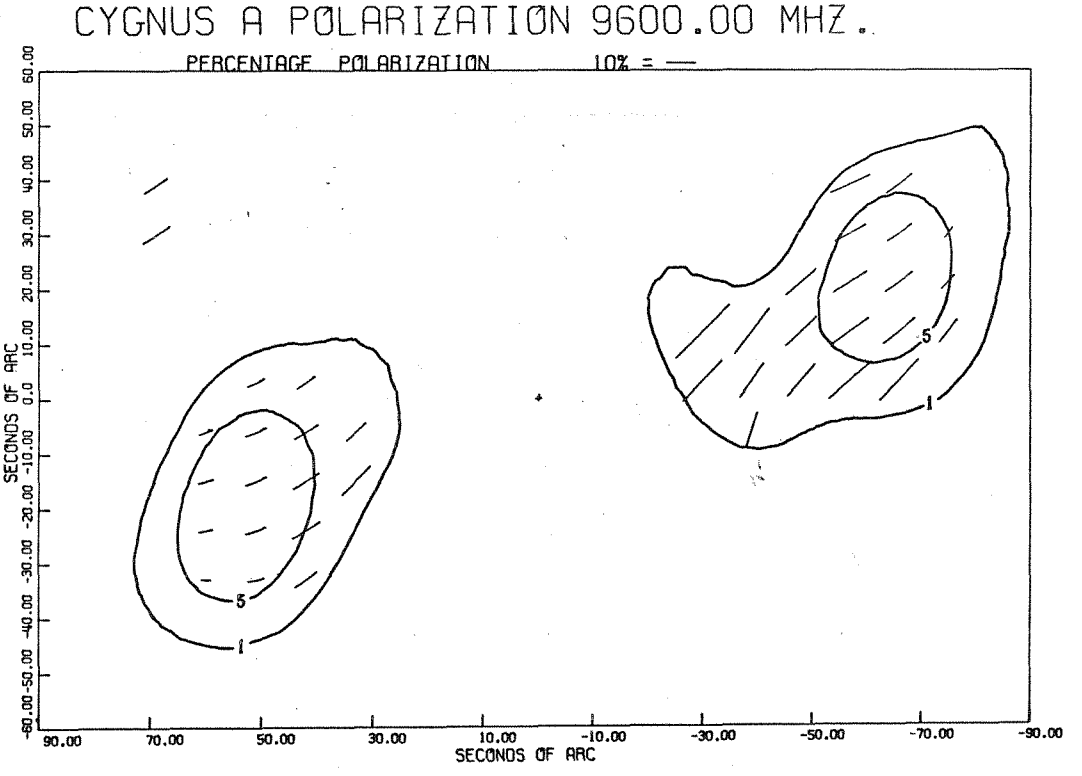
CYGNUS A POLARIZATION 9600.00 MHZ.
PERCENTAGE POLARIZATION 10% = —
SECONDS OF ARC
60.00 50.00 40.00 30.00 20.00 10.00 0.0 -10.00 -20.00 -30.00 -40.00 -50.00 -60.00
5
1
5
1
90.00 70.00 50.00 30.00 10.00 -10.00 -30.00 -50.00 -70.00 -90.00
SECONDS OF ARC

Figure 22

Distribution of polarized intensities in f.u. at 8300 MHz across Cygnus A. Each number covers a 9" x 9" area.

CYGNUS A POLARIZATION 8300MHz
(FLUX UNITS)

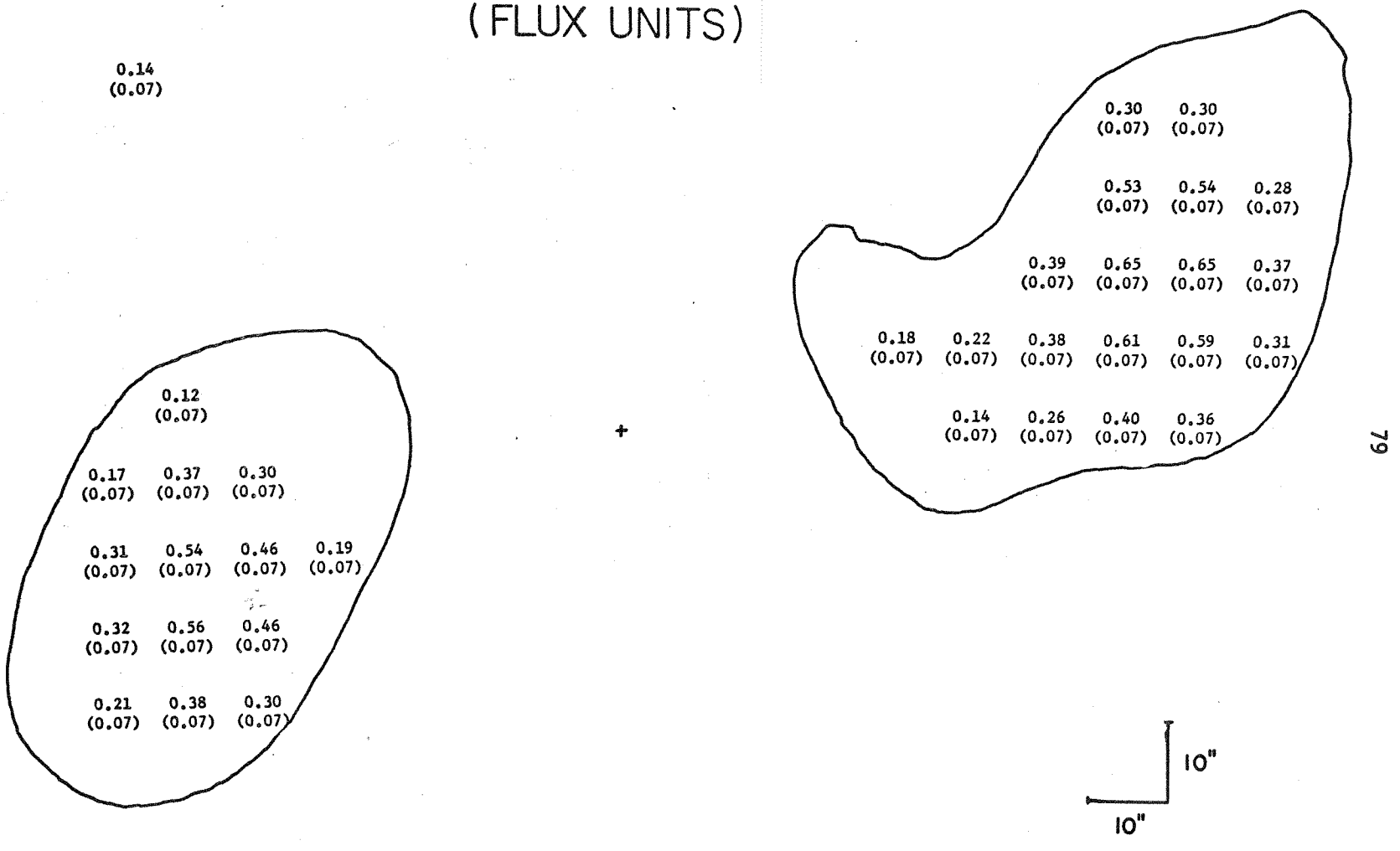

Figure 23

Distribution of polarized intensities in f.u. at 9600 MHz across Cygnus A. Each number covers a 9" x 9" area.

CYGNUS A POLARIZATION 9600 MHz
(FLUX UNITS)

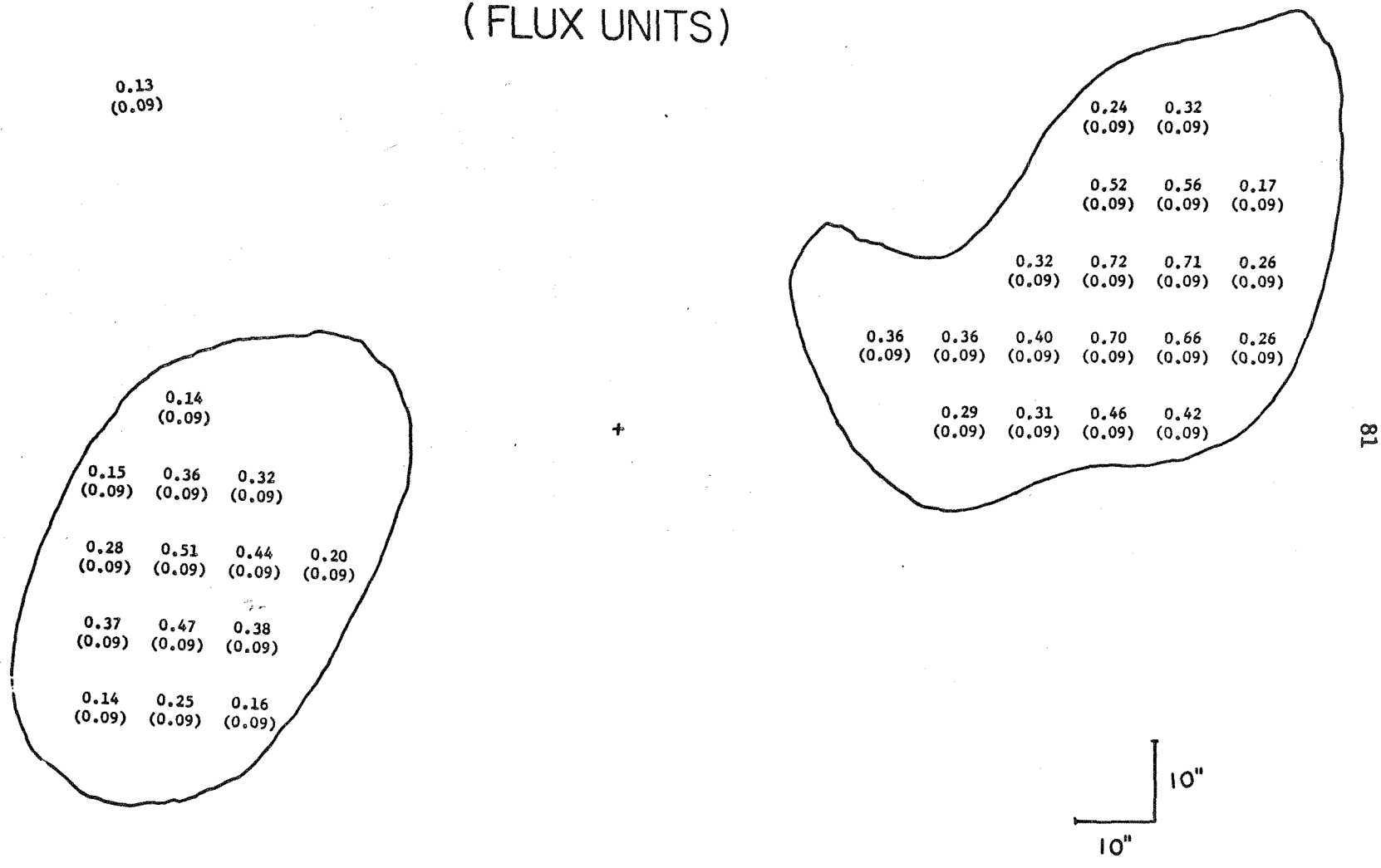

Figure 24

Distribution of polarization in percent at 8300 MHz across Cygnus A. Each number covers a 9" x 9" area.

CYGNUS A POLARIZATION 8300 MHz
(PERCENT)

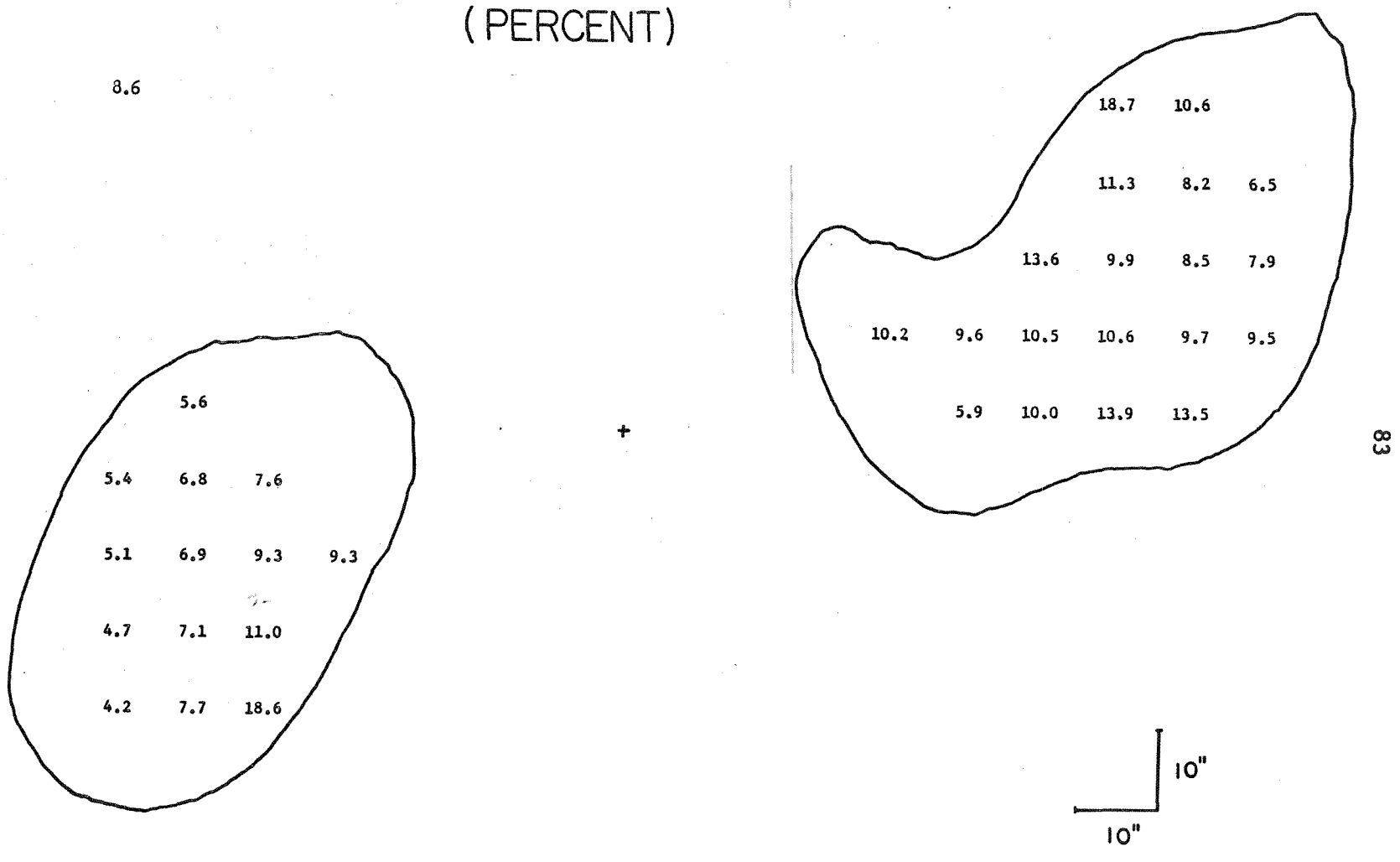

Figure 25

Distribution of polarization in percent at 9600 MHz across Cygnus A. Each number covers a 9" x 9" area.

CYGNUS A POLARIZATION 9600 MHz
(PERCENT)

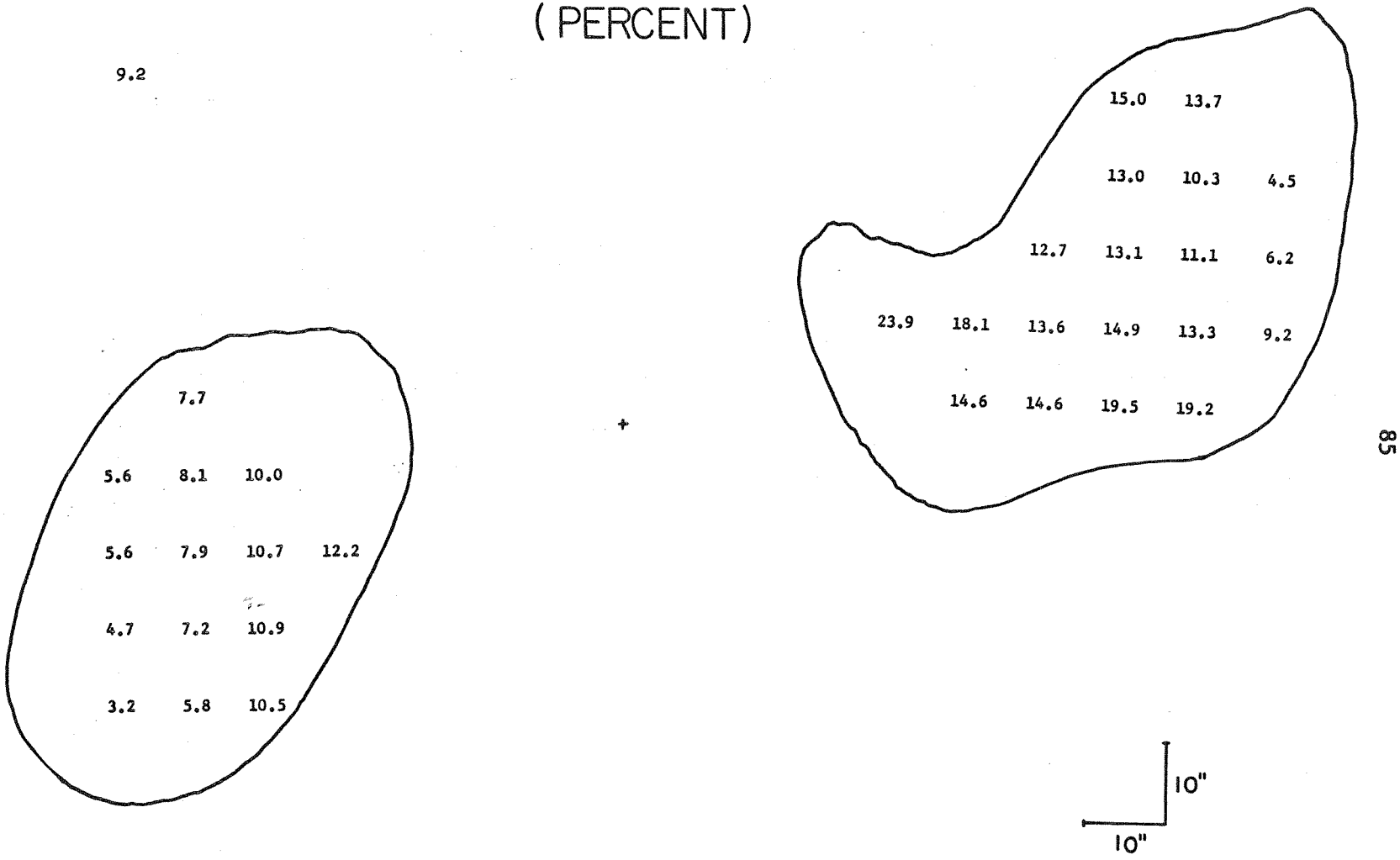

pronounced at 9600 MHz. In the west component, however, a similar increase occurs from the west edge to east (bridge) and is rather pronounced at both frequencies. The polarization distributions agree quite well with the total intensity distribution, varying smoothly across the components and peaking about where the total intensity is maximum. Scans for these distributions along the major axis are shown in figures (26) and (27). Notice also that there is significant polarization in the bridge component.

Figure 26

Total intensity and polarization scans along the major axis of Cygnus A at 8300 MHz. The vectors below the scans give the polarized intensities and position angles.

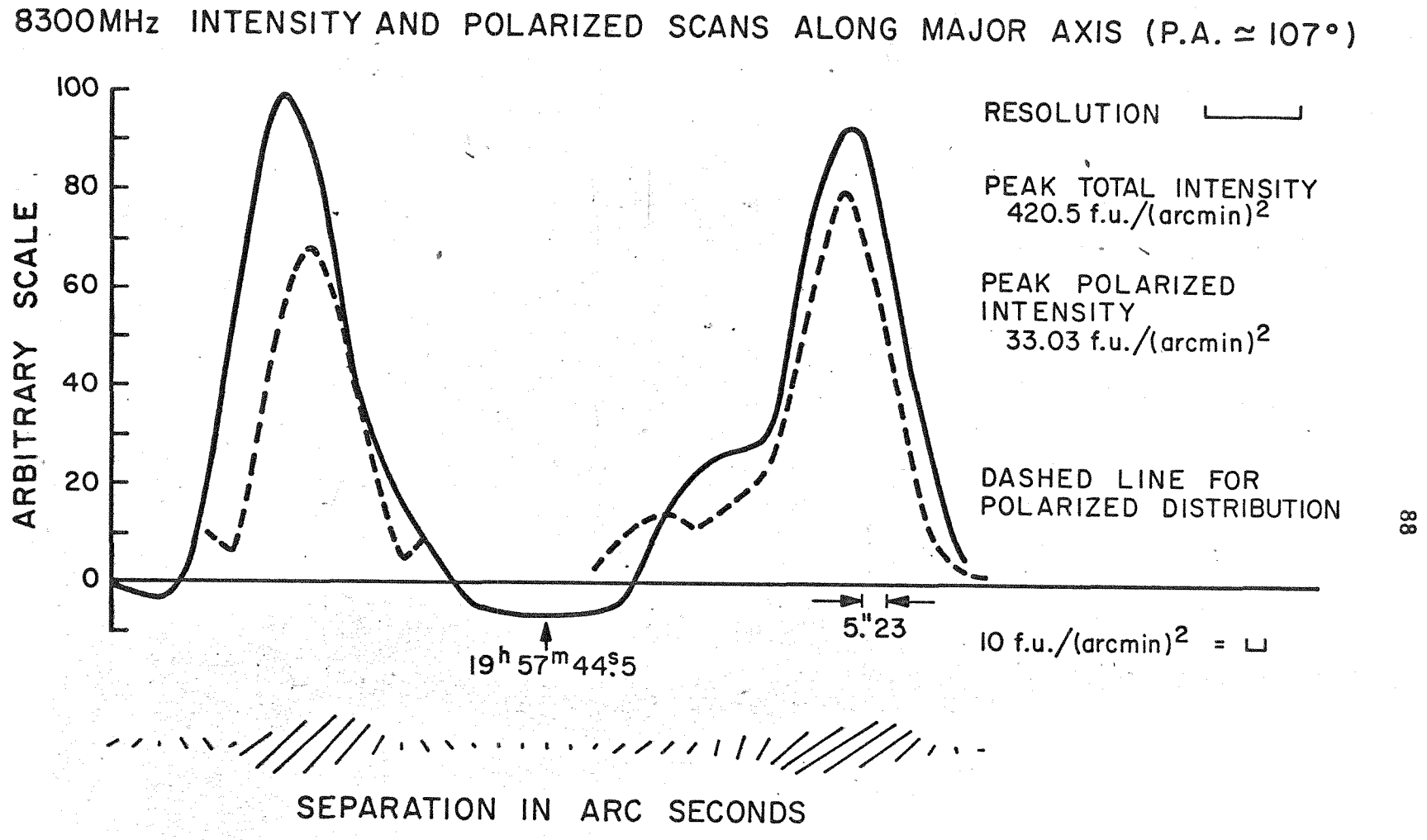
8300MHz INTENSITY AND POLARIZED SCANS ALONG MAJOR AXIS (P.A. ≃ 107°)
ARBITRARY SCALE
100
80
60
40
20
0
RESOLUTION
PEAK TOTAL INTENSITY
420.5 f.u./(arcmin)²
PEAK POLARIZED
INTENSITY
33.03 f.u./(arcmin)²
DASHED LINE FOR
POLARIZED DISTRIBUTION
5."23
10 f.u./(arcmin)² = ⌴
19h 57m 44s.5
SEPARATION IN ARC SECONDS

Figure 27

Total intensity and polarization scans along the major axis of Cygnus A at 9600 MHz. The vectors below the scans give the polarized intensities and position angles.

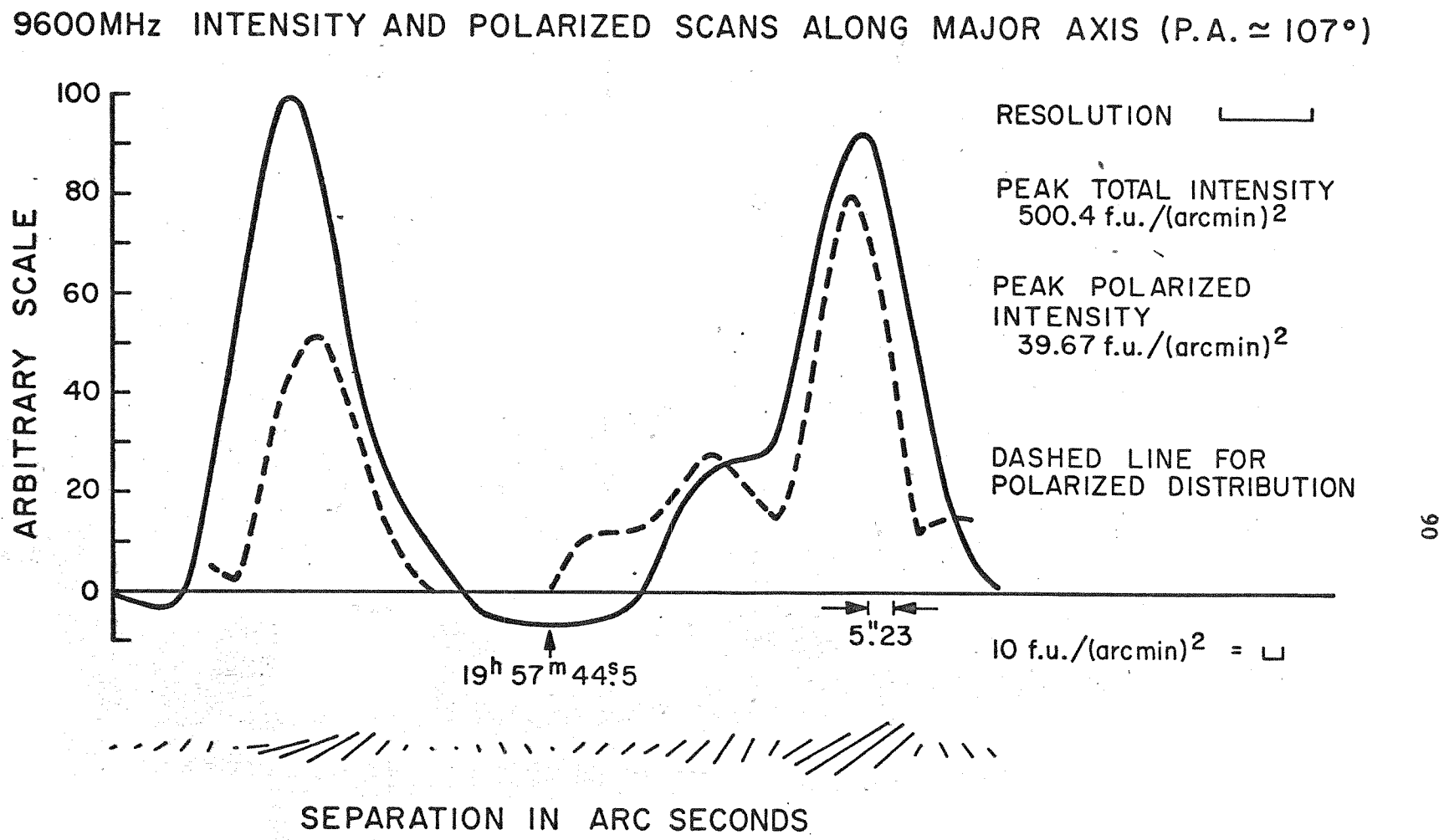
9600MHz INTENSITY AND POLARIZED SCANS ALONG MAJOR AXIS (P.A. ≃ 107°)
ARBITRARY SCALE
100
80
60
40
20
0
RESOLUTION
PEAK TOTAL INTENSITY
500.4 f.u./(arcmin)²
PEAK POLARIZED
INTENSITY
39.67 f.u./(arcmin)²
DASHED LINE FOR
POLARIZED DISTRIBUTION
5".23
10 f.u./(arcmin)² = ⌴
19h 57m 44s.5
SEPARATION IN ARC SECONDS

CHAPTER 6

SECONDARY RESULTS

Further informations can now be deduced from the observational results at these two frequencies. Direct comparisons of these two sets of data are possible because of comparable resolutions and identical instruments used for the observations.

Rotation Measure

The rotation measure R_m as given in equation (23) has been deduced from the position angles of the vectors given in figures (20) and (21). Its variation across the components of the source is shown in figure (28), and the maximum possible error for each number is shown in parenthesis underneath. These numbers have been derived by assuming that there is no $\pm n\pi$ ambiguity associated with the determinations because of the closeness of these two frequencies. In fact, since the rotation meausre in rad/m^2 is given in this case by about $53x(\theta_{8.3}-\theta_{9.6})$ where the angles are in degrees, if we add (or subtract) 180° from the observed rotated position angles of about 20°, we get rotation measures of the order of 10000 rad/m^2, which is very much larger than what is usually expected. Although previous polarization measurements (35, 37) yield rather large rotation measures in the east component, they are about an order of magnitude less than the value obtained if there is a 180° ambiguity.

The large rotation measures quoted by these previous polarization experiments are confirmed by the present observations. Moreover, there is the very interesting discovery that the rotation measure varies by a large amount in this component, from 1400 rad/m^2 on the

Figure 28

Rotation measures across the components of Cygnus A as derived from the 8300 MHz and 9600 MHz observations.

CYGNUS A

ROTATION MEASURE (RAD/M^2)

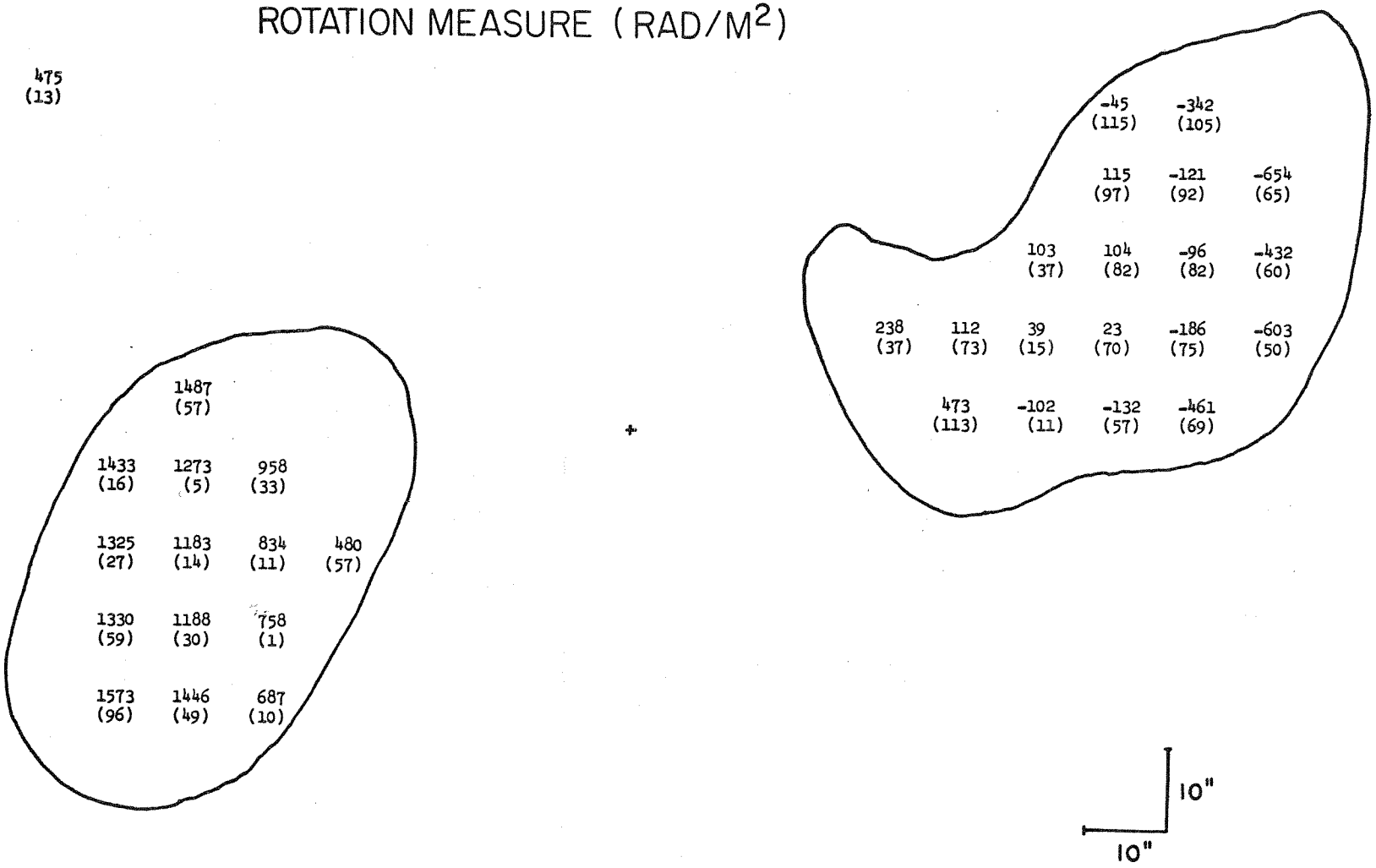

eastern edge to about 500 rad/m^2 on the western side. In contrast to the east component, these polarization measurements (35,37) indicate that the west component has a rather small rotation measure and Schraml and Turlo (37) have obtained a value of -50 rad/m^2. Because of the smallness of this number, and the proximity of the frequencies, the rotation of the position angles involved is rather small and the rotation measure deduced may have larger uncertainties. However, it is apparent that the rotation measures change from negative values at the western edge to positive ones on the eastern side. This implies that there is a change in the direction of the component of the magnetic field along the line of sight somewhere in the direction between the west component and the bridge. The significance of these variations in rotation measure will be discussed later.

The integrated value for the rotation measure of the east component is about 578 rad/m^2 while that for the west component is about 16 rad/m^2. Of course, caution should be exercised in appraising the latter number because of larger uncertainties involved.

Intrinsic Position Angles

These position angles plotted in figure (29) are also derived by applying equation (23) to the position angles of the vectors in figures (20) and (21). The maximum possible error for each number is again shown in parenthesis underneath. The closeness of the two frequencies ensure that no $n\pi$ ambiguity is involved. There is a general trend for the values of the intrinsic angles to increase from the south west to the north east across the components, but the variation on the whole is still rather smooth. The average intrinsic position

Figure 29

Intrinsic position angles for the electric vectors across the components of Cygnus A as derived from the 8300 MHz and 9600 MHz observations.

CYGNUS A

INTRINSIC POSITION ANGLE (DEG)

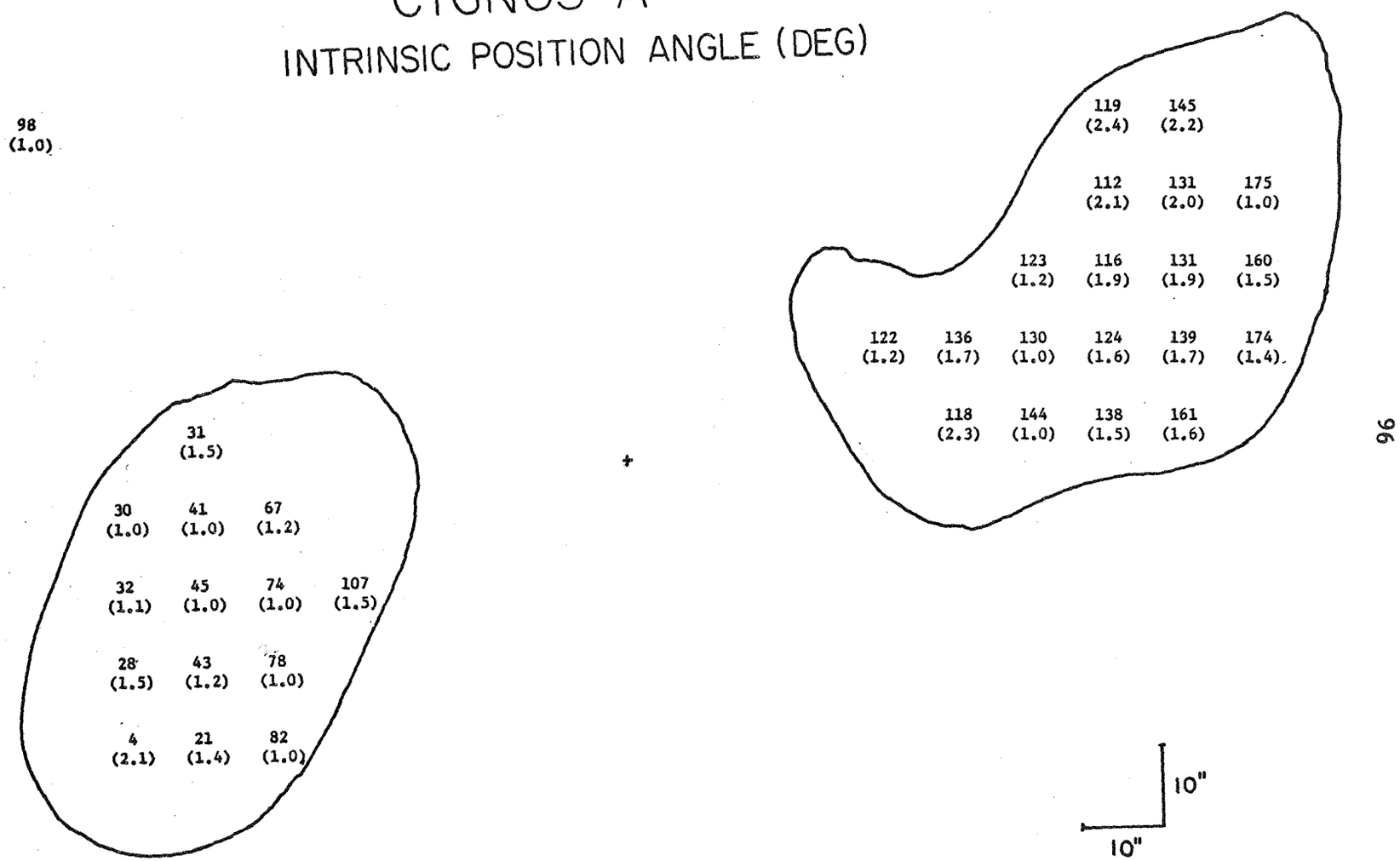

angle for the east component is about 40° or 50° while that for the west component is about 140° or 150°. These agree quite well with the values obtained by Mayer and Hollinger (35).

Since, according to the theory of synchrotron radiation, the component of magnetic field transverse to the line of sight is perpendicular to the intrinsic position angle, figure (29) shows that these transverse field components in the east component are slowly varying at a position angle of about 130°, while those in the west component and the bridge are at position angles of about 230°. In other words, the magnetic field directions in the east component are roughly aligned with the major axis of Cygnus A, while those in the latter are approximately perpendicular to it. This might be significant in the evolution of radio galaxies (91).

Depolarization

A measure of the depolarization across the source components has been obtained by taking the ratio of the polarization observed at 8300 MHz to that observed at 9600 MHz, following the convention of Maltby (92). This is shown in figure (30). Because of the low value of polarized intensity associated with the area covered by each number, the corresponding uncertainty is rather high, as is shown by the number in parenthesis underneath the polarization ratio. Not much therefore can be said about the depolarization for the two components except that this is probably a smooth variation. There is, however, definitely more depolarization in the bridge component. This may be due to the envelope from the optical galaxy covering this part of the west component. This will be discussed later in greater detail.

Figure 30

Cygnus A depolarization distribution $P_{8.3\ GHz}/P_{9.6\ GHz}$.
Each number covers a 9" x 9" area.

CYGNUS A

DEPOLARIZATION $\frac{P_{8.3GHz}}{P_{9.6GHz}}$

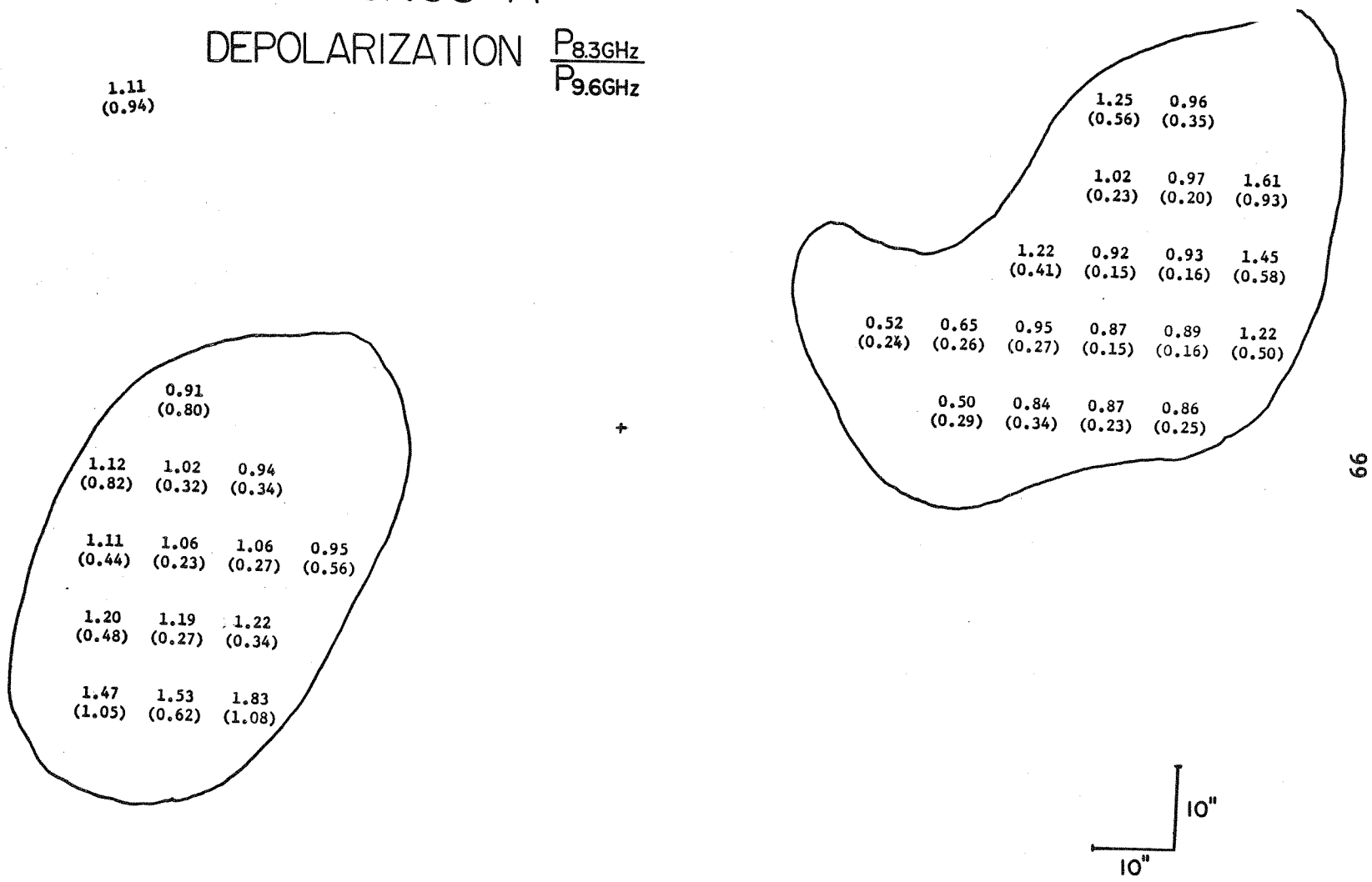

Spectral Index

Since the half width of the synthesized beam is only slightly less than that of the components, it is not too meaningful to attempt for the detection of a variation of the spectral index across each component. However, since the two components are resolved, it is interesting to obtain their respective integrated total intensities so that a comparison with the Cambridge values at 1.4, 2.7 and 5.0 GHz can be made (Table VIII). At this frequency, the integrated intensity of the west component seems to exceed slightly that of the east. This may not be too significant as there is a ten percent uncertainty in the total intensity map.

As suggested by Mitton and Ryle (34), the change in the curvature of the Cygnus spectrum is not likely to be explained exclusively by synchrotron self-absorption. Unfortunately, the resolution of this observation also precludes a detailed comparison of the predictions of the synchrotron self-absorption theory with the observed spectrum because this would require the knowledge of the two dimensional fine structure of the outer edge of each component which is, at present, not available. However, the comparison of the profiles along the major axis of Cygnus A shows that the features observed at 8300 MHz are consistent with those at the lower frequencies. These steep gradients of brightness temperatures are consistent with the predictions derived from the ram pressure confinement model proposed by Mills and Sturrock (93).

TABLE VIII

Spectral Flux Densities of the Components of Cygnus A

Freq (MHz)	East Component (watts m^{-2} Hz^{-1})	West Component (watts m^{-2} Hz^{-1})	
1407	850	750	(34)
2695	370	320	(34)
4995	200	180	(34)
8300	93	101	(*)

*Present Observation

CHAPTER 7

DISCUSSIONS

Rotation Measure

Let us first discuss the implications of the large variation of rotation measure in the east component. It has been known that in the general direction of Cygnus A (galactic coordinates $\ell^{II} = 76°$ and $b^{II} = 6°$), typical rotation measures range from +100 to +200 rad/m^2 (94), and these are caused by faraday rotations in the spiral arms of our galaxy. The high value of $\geq$1000 rad/m^2 obtained for Cygnus A is therefore very unusual, as have been noted before (35,39). To explain this large value, Slysh (42) suggests that the radiation from the east component may have to pass through the extended envelope of the parent optical galaxy before reaching us. However, the direction of this variation and the large change over such a small angular size argue against this possibility. To effect the observed variation with such a model, there would have to be a decrease in the quantity $\langle n_e B_L \rangle$, where n_e is the thermal electron density and B_L is the longitudinal magnetic field, towards the optical galaxy. This seem rather improbable. Moreover, since Cygnus A is a typical double radio source, it is unlikely that this is the only one where the effect of this envelope has been observed. No other double radio source with such a large rotation measure in one of its components has been found.

It is believed that this large faraday rotation is primarily due to the passage of the Cygnus radiation through the spiral arms of our galaxy. Independent investigations by E.W. Greisen (95) on the HI

absorption of the clouds in the Perseus arm in the direction of Cygnus A provide indirect confirmations. It is found that there are several cloudlets of size $\geq$ 1 pc in this direction and that there is a moderately high concentration of hydrogen (average density $\lesssim$ 25 cm^{-3}) toward the eastern edge of the east component of Cygnus A (95). Although the interpretation of Zeeman effect data suggests that high magnetic fields can occur in relatively dense HI clouds (96), the combination of the high density and magnetic fields in a few cloudlets alone cannot produce a rotation measure as large as that observed without assuming a high electron density (up to ~25 cm^{-3}) and a high magnetic field (~50 μG) or a path length much in excess of ~1 pc. This correlation between the large rotation measure and the hydrogen features in the Perseus arm, however, is very interesting. Moreover, the fact that at least two hydrogen features are detected over the west component (95) may be related to the reversal of the longitudinal magnetic field direction.

Figure (31) shows the values of the quantity $\langle n_e B_L \rangle$. A path length of 5 kpc has been assumed.

Depolarization

Although the large depolarization in Cygnus A is well known (35,37,38,39,40) the ratios shown in figure (30) indicate that between these two adjacent frequencies there may be little depolarization in the two components. There is, however, a considerable amount of depolarization in the bridge.

As the following arguments show, if depolarization is occurring in the main components, then it is probably not of the 'slab' type

Figure 31

Distribution of the quantity $\langle n_e B_L \rangle$ in gauss cm^{-3} over Cygnus A.

DISTRIBUTION OF $\langle n_e B_L \rangle$ IN UNITS OF 10^{-7} GAUSS CM^{-3}

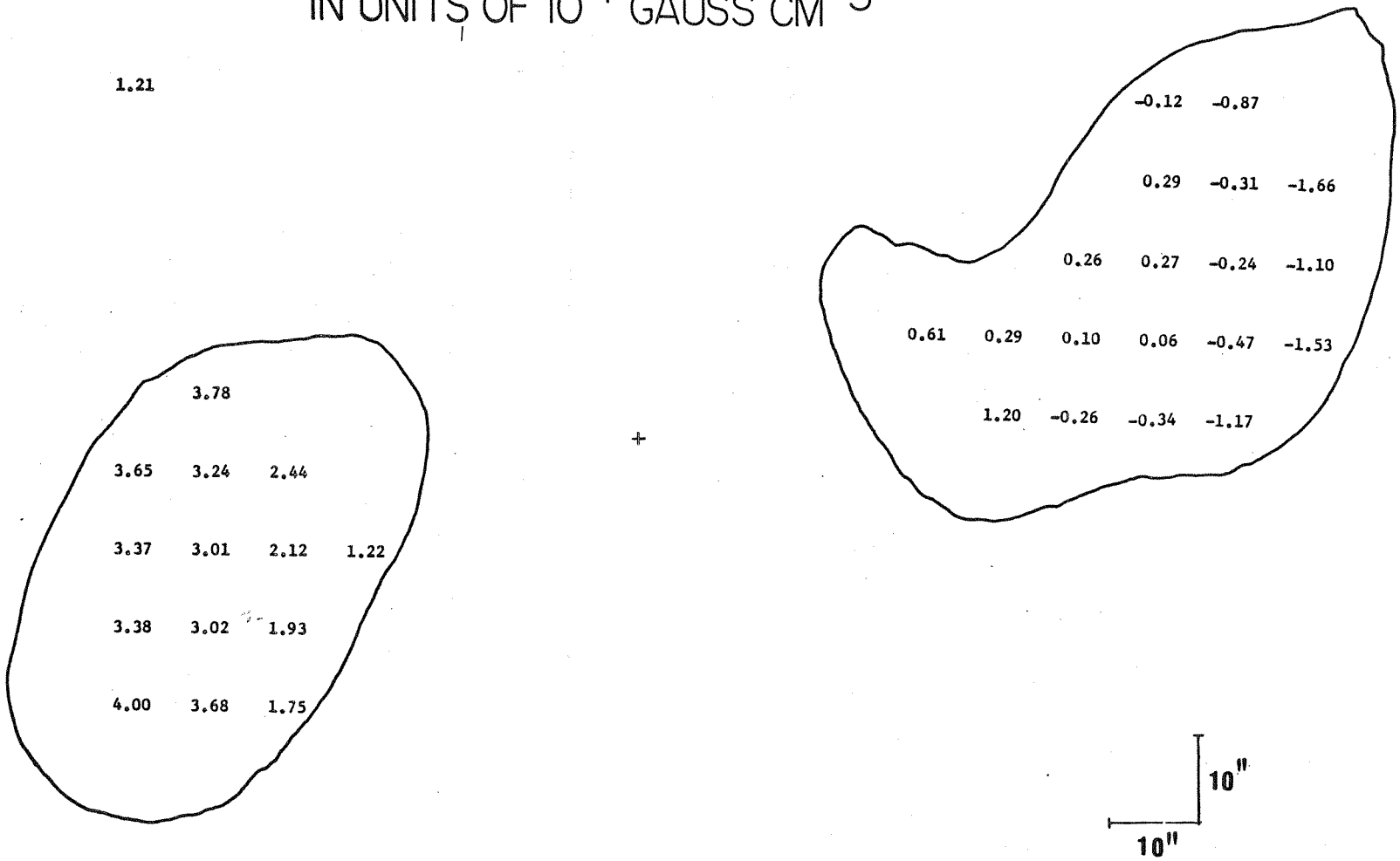

model discussed by Burn (97) and Gardner and Whiteoak (64). Since this is a rather common model whose results are usually applicable, with some modifications, to a variety of cases, it is possible that the depolarization observed is not occurring in the source.

For this discussion, reference will be made to figure (6) from the paper by Gardner and Whiteoak (64). Moreover, for the sake of argument, the average position angles for the individual components will be used. The observed position angles are 135° at 8300 MHz and 124° at 9600 MHz for the east component and 133° for the west component. As mentioned, the intrinsic position angles are about 45° with the east component and 145° with the west. For the east component therefore, we see that the ratio of polarization P(8.3 GHz)/ P(9.6 GHz) ~ 0.1 if the emission and depolarization are occurring throughout a uniform slab in the source. The observed ratio, however, is of the order of unity. It is possible to argue that the theoretical depolarization ratio may not be inconsistent with that observed if one takes the several degrees error into account, but one has to consider the polarization percentages measured at these wavelengths as well. According to the model, there would be a significant difference between the polarization at 1.55 cm (35) and 3 cm. They are nonetheless found to be of comparable magnitudes.

If we take the variation in the intrinsic angles over the surface of this component into account, more difficulties will be encountered since the observed position angles are rather constant across this surface. The different intrinsic angles would then imply different 'tubes' (cross sectional area ~7 kpc x 7 kpc) of different

polarization values across this component surface. Such small scale changes in polarization would be rather unlikely.

Similar arguments can be applied to the west component to show that depolarization is not likely to occur inside the source. It is therefore reasonable to expect the depolarization of the bridge to be occurring in the medium outside. One possible source may be the envelope of the parent optical galaxy, and this will be discussed in the following. It is interesting to note that a similar explanation for the rapid depolarization in the west component of Centaurus A (the central source) has been offered by Cooper, Price and Cole (98). Note also that the association of the bridge with some kind of envelope from the parent galaxy may be independent of whether the west component is in front of or behind this galaxy. The envelope could be matter ejected at the same time with the plasma and loosely associated with it.

Before going into the discussion about the depolarization of the bridge component, it is appropriate to show that the small depolarization between the two frequencies in the east component is not at variance with the significant variation in rotation measure across the component surface. As deduced before, a small change in the observed position angles result in a considerable value in the rotation measure since R.M. $\simeq$ 53 x $(\theta_{8.3} - \theta_{9.6})$ where the θ's are in degrees. However, it is possible for the depolarization ratio to stay rather constant over a considerable range of position angles (c.f. figure (6) in Gardner and Whiteoak). No inconsistency is therefore involved.

If we assume that the fluctuations in the magnetic field and/or

electron density in the envelope is random, then Burn (97) has shown that the degree of depolarization at a wavelength λ is

$$p(\lambda^2) = p_i \exp\left\{-2K^2(n_e B_L)^2 \alpha R^2 \lambda^4\right\} * \qquad (26)$$

where p_i is the polarization before the passage through the envelope, $K = 2.62 \times 10^{-17}$, α is the angular scale of fluctuation and R is the extent of this fluctuation along the line of sight. Taking the angular size of the fluctuation ~ angular size of bridge component ~ 10" and the extent of the envelope in the longitudinal direction ~ the extent perpendicular to the line of sight ~ 3×10^{23} cm, we have the depolarization ratio

$$\frac{P(3.61^2)}{P(3.12^2)} = \exp\left\{-2*(2.62\times10^{-17})^2(n_e B_L)^2 \alpha R^2 (3.61^4 - 3.12^4)\right\}$$

Solving for $\langle n_e B_L \rangle$ with a depolarization ratio of ~0.5, $\langle n_e B_L \rangle \sim 10^{-6}$ gauss cm^{-3}.

Mills Model

Let us now compare our observation with the model proposed by Mills and Sturrock (93). It seems reasonable, as the model suggests, to attribute the confinement of the plasmons to the ram pressure due to the interactions with the intergalactic medium, as the steep brightness gardients have actually been observed. However, the results of this observation on the magnetic field distributions of the components show that while the field lines in the east component do lie in the general direction of the source axis, those in the west component are at right angles to it. It may be speculated that the

*The linear fluctuation scale d is taken to be ~αR.

difference in the magnetic field alignments could be due to the evolution of the components (91), but the informations on their apparent ages and orientations in space are insufficient to permit this calculation.

Besides the magnetic field distributions, it can also be noticed that the broad 'tails' of the two components do not point directly at the parent galaxy. This tilt is also noticed by Mitton and Ryle (34), although the effect is not as pronounced.

CHAPTER EIGHT

CONCLUSIONS

The total intensity and polarization distributions for the double radio source Cygnus A have been observed at 8300 MHz and 9600 MHz. The total intensity maps at the two frequencies have been combined to yield a better map at 8300 MHz. The general features of the source are in agreement with those obtained at lower frequencies and comparable resolutions. Moreover, the bridge component is also present.

The separation along the major axis between the maxima of the two components is found to be about 124" at a position angle of about 107°. The integrated total intensities for the two components are about 93 f.u. for the east and about 101 f.u. for the west. They are consistent with the values obtained by Mitton and Ryle (34) at 1.4, 2.7 and 5.0 GHz. There may be a change in the spectral index of the east component between 5 GHz and 8.3 GHz.

The distribution of polarized intensities over the source has also been obtained. While the east component is brighter in total intensity, the west component has significantly higher polarization percentages at both frequencies. The integrated polarization values are ~5.0% @ 135° at 8300 MHz, ~5.3% @ 124° at 9600 MHz for the east component and ~7.4% @ 133° at 8300 MHz, ~9.5% @ 133° at 9600 MHz for the west component. Although the integrated polarizations are less than 10%, values as high as 24% has been obtained in the partially resolved source.

The existence of an interesting correlation between the large variation in rotation measures over the east component and the detection of

small size clouds (≥1 pc) of moderately high concentration in the corresponding direction in the Perseus spiral arm has been pointed out. If the faraday rotation is to be occurring in these cloudlets in our galaxy, unreasonably large electron density and/or longitudinal magnetic fields have to be present. The presence of these cloudlets is also in accord with the sign reversal of the rotation measures in the west component.

Little or no depolarization has been observed for the main components except in the bridge. It has been shown that this depolarization is probably occurring outside of the emitting region. If it is assumed that the depolarization is due to the extended envelope of the parent galaxy, the values obtained for the product of the average electron density and longitudinal magnetic fields are $\sim 10^{-6}$ gauss cm^{-3}.

BIBLIOGRAPHY

1. Jansky, K., Proc. Inst. Radio Engrs., N.Y. 30, 1920, 1932.

2. Hey, J.S., Parsons, S.J., Phillips, J.W., Nature 158, 234, 1946.

3. Bolton, J., Stanley, G.J., Nature 161, 312, 1948.

4. Ryle, M., Smith, F.G., Nature 162, 462, 1948.

5. Shklovsky, I.S., 'Cosmic Radio Waves', (Harvard Univ. Press, 1960), p. 97 .

6. Shklovsky, I.S., 'Cosmic Radio Waves', (Harvard Univ. Press, 1960), pp. 118, 119 .

7. Ryle, M., Proc. Phys. Soc. Lond. A62, 491, 1949.

8. Smith, F.G., Nature 168, 962, 1951.

9. Baade, W., Minkowski, R., Astrophys. J. 119, 206, 1954.

10. Stanley, G.J., Slee, O.B., Aust. J. Sci. Res. A, 3, 234, 1950.

11. Ryle, M., Smith, F.G., Monthly Notices Roy. Astron. Soc. 110, 508, 1950.

12. Mills, B.Y., Thomas, A.B., Aust. J. Sci. Res. A, 4, 158, 1951.

13. Mills, B.Y., Aust. J. Sci. Res. A, 5, 456, 1952.

14. Hanbury Brown, R., Hazard, C., Monthly Notices Roy. Astron. Soc. 111, 576, 1951.

15. Smith, F.G., Nature 168, 555, 1951.

16. Mills, B.Y., Nature 170, 1063, 1952.

17. Smith, F.G., Nature 170, 1064, 1952.

18. Hanbury Brown, R., Jennison, R.C., Das Gupta, M.K., Nature 170, 1061, 1952.

19. Alfven, H., Herlofson, N., Phys. Rev. 78, 616, 1950.

20. Dombrovsky, V.A., Dokl. Akad. Nauk SSSR 94, 1021, 1954.

21. Oort, J.H., Walraven, T., Bull. Astron. Inst. Neth.12, 285, 1956.

22. Shklovsky, I.S., Dokl. Akad. Nauk SSSR 90, 983, 1953.

23. Mayer, C.H., McCullough, T.P., Sloanaker, R.M., Astrophys. J. 126, 468, 1957.

24. Mayer, C.H., McCullough, T.P., Sloanaker, R.M., paper presented to the XIII th General Assembly U.R.S.I., London, 1960.

25. Kuz'min, A.D., Udal'tsov, V.A., Soviet Astron.-AJ 5, 850, 1962.

26. Morris, D., Radhakrishnan, V., Astrophys. J. 137, 147, 1963.

27. Brown, R.M., Palmer, H.P., Thompson, A.R., Monthly Notices Roy. Astron. Soc. 115, 487, 1955.

28. Mayer, C.H., McCullough, T.P., Sloanaker, R.M., Astrophys. J. 135, 656, 1962.

29. Jennison, R.C., Das Gupta, M.K., Nature 172, 996, 1953.

30. Lequeux, J., Annals d'Astrophys. 25, 221, 1962.

31. Moffet, A.T., Science 146, 764, 1964.

32. Ryle, M., Elsmore, B., Neville, Ann C., Nature 205, 1259, 1965.

33. Hogg, D.E., Macdonald, G.H., Conway, R.G., Wade, C.M., Astron. J. 74, 1206, 1969.

34. Mitton, S., Ryle, M., Monthly Notices Roy. Astron. Soc. 146, 221, 1969.

35. Mayer, C.H., Hollinger, J.P., Astrophys. J. 151, 53, 1968.

36. Allen, R.J., unpublished Ph.D. Thesis, M.I.T., 1967, as quoted in ref. 37.

37. Schraml, J., Turlo, Z., Astrophys. J. Letters 150, 15, 1967.

38. Soboleva, N.S., Timofeva, G.M., Soviet Phys.-Doklady 8, 1037, 1964.

39. Soboleva, N.S., Soviet Astron.-AJ 10, 214, 1966.

40. Gol'nev, V.Ya, Soboleva, N.S., Soviet Astron.-AJ 9, 537, 1966.

41. Hollinger, J.P., Mayer, C.H., Menella, R.A., Astrophys. J. 140, 656, 1964.

42. Slysh, V.I., Soviet Astron.-AJ 9, 533, 1966.

43. Michelson, A.A., Phil. Mag. 30, 1, 1890.

44. Michelson, A.A., Phil. Mag. 31, 256, 1891.

45. Michelson, A.A., Astrophys. J. 51, 257, 1920.

46. Michelson, A.A., Pease, F.G., Astrophys. J. 53, 249, 1921.

47. O'Brien, P.A., Monthly Notices Roy. Astron. Soc. 113, 597, 1953.

48. Ryle, M., Nature 194, 517, 1962.

49. Elsmore, B., Kenderdine, S., Ryle, M., Monthly Notices Roy. Astron. Soc. 134, 87, 1966.

50. Kenderdine, S., Ryle, M., Pooley, G.G., Monthly Notices Roy. Astron. Soc. 134, 189, 1966.

51. Macdonald, G.H., Kenderdine, S., Neville, Ann C., Monthly Notices Roy. Astron. Soc. 138, 259, 1968.

52. Morris, D., Radhakrishnan, V., Seielstad, G.A., Astrophys. J. 139, 560, 1964.

53. Seielstad, G.A., Astrophys. J. 147, 24, 1967.

54. Branson, N.J.B.A., Nature 213, 1211, 1967.

55. Downs, G.S., Thompson, A.R., Astrophys. J. 152, L65, 1968.

56. Morris, D., Whiteoak, J.B., Aust J. Phys. 21, 475, 1968.

57. Seielstad, G.A., Weiler, K.W., Astrophys. J. 154, 817, 1968.

58. Seielstad, G.A., Weiler, K.W., Astrophys. J. Suppl.No.18,158,1969.

59. Weiler, K.W., Ph.D. Thesis, Calif. Inst. of Tech., 1970.

60. Morris, D., Radhakrishnan, V., Seielstad, G.A., Astrophys. J. 139, 551, 1964.

61. Moffet, A.T., Astrophys. J. Suppl. 67, 93, 1962.

62. Read, R.B., Trans. Inst. Radio Engrs. AP-9, 31, 1961.

63. Bracewell, R.N., Proc. of the IRE, 46, 97, 1958.

64. Gardner, F.F., Whiteoak, J.B., Ann. Rev. Astron. & Astrophysics, 4, 245, 1966.

65. Korchak, A.A., Syrovatskii, S.I., Soviet Astron.-AJ, 5, 678, 1962.

66. Ginzburg, V.L., Syrovatskii, S.I., 'The Origin of Cosmic Rays', (New York : The Macmillan Company, 1964), pp. 53-115.

67. Legg, M.P.C., Westfold, K.C., Astrophys. J. 154, 499, 1968.

68. Mayer, C.H., Hollinger, J.P., Allen, P.J., Astrophys. J. 137, 1309, 1963.

69. Biraud, F., Astron. and Astrophys. 1, 156, 1969.

70. Seaquist, E.R., Astrophys. Letters 5, 111, 1969.

71. Gilbert, J.A., Conway, R.G. Nature 227, 585, 1970.

72. Read, R.B., Observations of the Owens Valley Radio Observatory, Caltech, No. 4, 1963.

73. Berge, G.L., Ph.D. Thesis, Calif. Inst. of Tech., 1965.

74. Thompson, A.R., Colvin, R.S., Stanley, G.J., Astrophys. J. 148, 429, 1967.

75. Ryle, M., Windram, M.D., Monthly Notices Roy. Astron. Soc. 138, 1, 1968.

76. Aller, H.D., Astrophys. J. 161, 1, 1970.

77. Berge, G.L., Seielstad, G.A., Astrophys. J., 157, 35, 1969.

78. Kellermann, K.I., Pauliny-Toth, I.I.K., Astrophys. J. 152, 639, 1968.

79. Kellermann, K.I., Pauliny-Toth, I.I.K., Ann. Rev. Astron. and Astrophys. 6, 417, 1968.

80. Medd, W.J., Locke, J.L., Andrew, B.H., van den Bergh, S., Astron. J. 73, 293, 1968.

81. Dent, W.A., Haddock, F.T., Astrophys. J. 144, 568, 1966.

82. Berge, G.L., private communication, 1970.

83. Fomalont, E.B., Astrophys. J. Suppl. 15, No. 138, 1968.

84. Fomalont, E.B., Publ. of the Owens Valley Radio Observatory, Vol. 1, No. 3, 1967.

85. Bracewell, R.N., Riddle, A.C., Astrophys. J. 150, 427, 1967.

86. Baars, J.W.M., Mezger, P.G., Wendker, H., Astrophys. J. 142, 122, 1965.

87. Parker, E.A., Monthly Notices Roy. Astron. Soc. 138, 407, 1968.

88. Hollinger, J.P., Hobbs, R.W., Astrophys. J. 151, 771, 1968.

89. Baars, J.W.M., IEEE Trans. of Ant. and Propag., July, 1967.

90. Hinder, R.A., Nature 225, 614, 1970.

91. Morris, D., Berge, G.L., Astron. J. 69, 641, 1964.

92. Maltby. P., Astrophys. J. 144, 219, 1966.

93. Mills, D.M., Sturrock, P.A., Astrophys. Letters 5, 105, 1970.

94. Seielstad, G.A., Morris, D., Radhakrishnan, V., Astrophys. J. 140, 53, 1964.

95. Greisen, E.W., private communication.

96. Verschuur, G.L., 'Interstellar Gas Dynamics', IAU Symposium No. 39, 1970, p. 150.

97. Burn, B.J., Monthly Notices Roy Astron. Soc. 133, 67, 1966.

98. Cooper, B.F.C., Price, R.M., Cole, D.J., Aust. J. Phys. 18, 589, 1965.

A HIGH-FREQUENCY STUDY OF CYGNUS A

ABSTRACT

We have combined measurements at 8300 and 9600 MHz to map the distribution of total radiation across Cygnus A with a beam of half-power width ~ 20" EW x 30" NS. We note steep brightness contours on the outer edges and more gradual inner extensions towards the optical galaxy. The brightest peaks within each radio component have flatter spectra than the rest of the source.

We have also mapped the distributions of linearly polarized radiation at both 8300 and 9600 MHz. Nearly everywhere in the source the degree of polarization at 9600 MHz exceeds that at 8300 MHz. The rotation measures vary more or less systematically across Cygnus A from a very large negative value at the following edge to a positive value on the preceding edge.

The Sf component of Cygnus A is probably more distant from us than the Np. Magnetic field lines are directed from the optical galaxy toward each radio component. Within each component the density of the thermal plasma and the magnetic field strength are greatest at the outer edges. The observations support the suggestion of ram-pressure deceleration of the radio components by an intergalactic medium.

I. INTRODUCTION

Cygnus A is often regarded as the prototype of the strong double radio galaxies (e.g., Moffet 1966). Consequently it is often used as the classic example for all radio galaxy models, such as that of Mills and Sturrock (1970). However, it has long been known that the linear polarization properties of Cygnus A are unique (most recent summary by Mitton 1971). The degree of polarization integrated over the entire source reaches a maximum near a wavelength of 3 cm, and the integrated position angle does not vary linearly with wavelength squared. The wavelength dependences of the polarization parameters of the two major radio components differ significantly, and the highest resolution polarization study (Mitton 1971) reveals complexity in the polarization of the individual components.

We therefore undertook a high resolution study of the total and linearly polarized radiation from Cygnus A at frequencies of 8300 and 9600 MHz, the results of which are reported herein.

II. OBSERVATIONS AND ANALYSIS

The observations were made with the Owens Valley Radio Observatory's variable spacing interferometer at various times between March 1968 and September 1970. The system has been described by Berge (1968). We used every east-west spacing between 100 and 800 ft, at intervals of 100 ft, and north-south spacings of 200 and 400 ft. At each spacing at both

8300 and 9600 MHz Cygnus A was tracked between hour angles of -4^h and $+4^h$. Thus we adequately covered half the UV-plane, producing synthesized beams of half-widths 21" EW by 30" NS at 9600 MHz and 24" x 35" at 8300 MHz.

Measurements were made alternately with the two linearly polarized feeds parallel at 0° and crossed at 0°/90° and 45°/135°. Thus the system responded alternately to the Fourier transforms of the Stokes parameters $\tilde{I} + \tilde{Q}$, $\tilde{U}$, and $-\tilde{Q}$, respectively, assuming, as we have, that V = 0 (see Weiler and Seielstad 1971 for most recent discussion of technique). An upper limit of 2 per cent has been set to the integrated degree of circular polarization of Cygnus A at λ 3.15 cm (Mayer, Hollinger and Allen 1963). Integration times were 6^m and 10^m for the parallel and crossed-feed measurements, respectively.

The flux density and phase were calibrated about once each hour, using the small diameter sources listed in Table 1. The rms deviations for the calibrators were approximately ±0.4 f.u.† and ±0.04 lobes. Perhaps as much as half of the phase fluctuation has an atmospheric origin (Hinder 1970).

†1 f.u. = 10^{-26} W m^{-2} Hz^{-1}

TABLE 1

Calibrators

Source	Flux Density		α_{1950}	δ_{1950}
	8.3GHz	9.6GHz		
3C48	3.36f.u.†	2.97f.u.†	$01^h\ 34^m\ 49^s.81$	32°54'20".2
3C84			03 16 29.60	41 19 52.0
3C147	5.19	4.84	05 38 43.58	49 49 43.1
3C196	2.63	2.33	08 09 59.43	48 22 08.0
3C286	5.71	5.39	13 28 49.67	30 45 59.3
3C295	3.67	3.14	14 09 33.75	52 26 13.6
3C345			16 41 17.67	39 54 11.1
3C380			18 28 13.41	48 42 39.3
NGC7027	6.49	7.27	21 05 09.4	42 02 03.1

†1 f.u. = 10^{-26} W m^{-2} Hz^{-1}

The instrumental polarization was calibrated by observing NGC7027 and 3C84. The former source is a thermal emitter (Wynn-Williams 1971) and therefore presumed to be unpolarized, whereas 3C84 is either unpolarized or extremely weakly polarized at all wavelengths (summary of several measurements in Seielstad and Weiler 1969; 8-GHz measurements in Aller 1970). Both sources are within 1°.5 in declination of Cygnus A. No instrumental circular polarization correction at either frequency exceeded 0.8 per cent, and each correction was known to within 0.5 per cent.

Our primary objective was to obtain distributions of the linearly polarized radiation at both frequencies. Consequently at either frequency our sampling with parallel-feed measurements was inadequate to determine the distribution of the total radiation. However, the parallel-feed measurements at both frequencies were interleaved such that the sampling on the Fourier transform plane was sufficient. The foregoing procedure is correct if,

as we believe, the differences in spectral index across Cygnus A between 8300 and 9600 MHz are less than the uncertainties of our measurements.

From the parallel feed measurement (α $\underset{\sim}{I}+\underset{\sim}{Q}$) at each frequency the appropriate value of $\underset{\sim}{Q}$, as determined from the 45°/135° combination, was vectorially subtracted. The resulting values of $\underset{\sim}{I}$ at 9600 MHz were multiplied by $(9.6/8.3)^{1.19}$, where the spectral index of -1.19 is from Baars, Mezger, and Wendker (1965), and combined with the 8300 MHz $\underset{\sim}{I}$ data. These combined data were Fourier inverted, using a Gaussian taper of halfwidth 15", to obtain the distribution of total radiation. At each frequency the measurements of $\underset{\sim}{U}$ and $\underset{\sim}{Q}$, tapered as above, were inverted separately and then combined into maps of the linearly polarized flux density, $\sqrt{Q^2+U^2}$, and the position angle of the plane of polarization, $0.5 \tan^{-1} (U/Q)$. All positions were referred to an origin at $\alpha_{1950}=19^h57^m44^s.5$, $\delta_{1950}=40°35'46".0$.

III. RESULTS

a) Distribution of total radiation

In Figure 1 we show the structure of Cygnus A revealed by a beam of halfwidth ~20" x 30". In accord with our assumption, this is the structure at any frequency between 8300 and 9600 MHz. We have scaled the contours to values appropriate for a frequency of 8950 MHz.

The radio source consists of two well separated components

with steep brightness gradients on the outer edges and more gradual inner extensions, particularly on the north - preceding (Np) component. This is the same basic structure revealed by other high-resolution observations at lower frequencies (Ryle, Elsmore, and Neville 1965; Mitton and Ryle 1969; Hogg, Macdonald, Conway, and Wade 1969).

The flux densities of the two components near 9 GHz are equal to within 7 per cent, although the peak brightnesses are in the ratio Sf:Np = 1.1:1. The peaks of the components are separated by 124"±4" in position angle 109°.5±1°.5. The 1950.0 positions of the peaks are $19^h57^m49^s.1\pm0^s.2$, 40°35'26"±2" and $19^h57^m38^s.9\pm0^s.2$, 40°36'08"±2".

There seems a suggestion that in each component successively greater brightness contours are elongated in ever increasing position angles. We note this same suggestion in the higher resolution studies of Hogg et al. (1969) at 2.7 GHz and of Mitton and Ryle (1969) at 2.7 and, particularly, 5 GHz. The very high resolution study by Miley and Wade (1971), again at 2.7 GHz, confirms the trend by revealing a double structure in the Np core separated in position angle 130°. Perhaps these radio observations indicate that the central optical object has a clockwise rotation. Baade and Minkowski (1954) point out that the two bright central optical condensations are separated in position angle 115°, whereas the fainter outer envelope is elongated in position angle 150°, a pattern consistent with clockwise rotation.

Furthermore, the optical emission lines indicate rotation with the Sf side receding, but of course they contain no information concerning motions in the plane of the sky.

b) Spectral index distribution

Mitton and Ryle (1969) have compared profiles of Cygnus A along its major axis obtained at frequencies of 1.4, 2.7, and 5.0 GHz. In Figure 2 we add our ~9 GHz data, convolved to the Cambridge beam at 1.4 GHz. We also normalized the intensities to the peak of the Sf component.

The trend evident in the three Cambridge measurements for the peak of the Np component to move westward with increasing frequency is definitely confirmed by our profile. For example, at 1.4 GHz the separation of the major peaks is 108"±5" (Ryle et al. 1965), while we find 124"±4" with comparable resolution near 9 GHz. Also, with the exception of the 5-GHz profile, we note that the ratio Np/Sf of the peak brightnesses increases with increasing frequency. We conclude, as did Mitton and Ryle, that the small-diameter cores in each component have flatter spectra than the inner extensions, and that possibly the spectrum of the Sf core is steeper than that of the Np. Miley and Wade (1971) have likewise concluded that "the spectrum of the fine structure in Cygnus A is very much flatter than that of the whole source."

c) Distributions of linearly polarized radiation

Figure 3 displays the distributions of the linearly

polarized flux density, $\sqrt{Q^2+U^2}$, at 9600 MHz in part (a) and at 8300 MHz in part (b). In Figure 4 we have superposed on some I contours vectors representing, by their length, percentage polarization and, by their orientation, position angle of the E vector at various points in Cygnus A. Vectors are shown for both frequencies. Finally, since we barely resolve Cygnus A along its minor axis, we present in Figure 5 cuts along the major axis of the distributions in Figures 1 and 3 (a and b). Each of the one-dimensional linearly polarized distributions has been multiplied by 10 and then assigned the same brightness scale as the distribution of total radiation at that frequency. These two brightness scales are then plotted in the ratio $(8.3/9.6)^{-1.19}$ so that the I curve refers to either frequency. Direct comparisons of the percentage polarizations are therefore possible. Figure 5 also displays the distributions of position angle at the two frequencies.

Table 2 summarizes the linear polarization parameters of the individual components and of the entire source at both 8.3 and 9.6 GHz. These values are all in excellent agreement with those compiled by Mitton (1971).

The linearly polarized distributions agree generally with the distribution of total radiation. Hence all portions of the source are linearly polarized. The peaks of the linearly polarized distributions of both components at both frequencies are displaced slightly inwards (~3" each) from the peaks of the

total radiation. It follows that the inner portions of the components are more highly polarized than the outer. The inner extension of the Np component especially is very highly polarized. The ratio Np:Sf of peak brightnesses is <1 for the total radiation, but >1 for both linearly polarized distributions. This is reflected in the higher percentage polarizations for the Np component listed in Table 2. The same ratio is greater for the 9.6 GHz polarization distribution than for that at 8.3 GHz; consequently the depolarization of the Np component is more rapid.

TABLE 2

Linear Polarization of Cygnus A

Frequency	Sf Component		Np Component		Entire Source	
	Per Cent	P.A.	Per Cent	P.A.	Per Cent	P.A.
9.6 GHz	6.5±2.0	160°±9	10.4±2.2	143°±6	8.2±3.1	149°±10°
8.3 GHz	5.6±1.6	136 ±6	8.0±1.2	142 ±5	6.8±2.0	140 ±7

The position angles measured at both frequencies vary across the source. They decrease as the source is scanned from east to west across the Sf component and the inner extension of the Np component; there is then a significant increase in position angle and the trend across the peak of the Np component is less systematic.

The polarization distributions, including the position angle information, as well as the cut along the major axis of the total radiation indicate that the inner extension of the Np component does not merge smoothly with the brighter outer peak. In fact, Ryle et al. (1965) have suggested the existence of a third component at λ 21.3 cm.

d) Depolarization, rotation measures, and intrinsic position angles.

Both Figures 4 and 5 display the fact that nearly everywhere in the source the percentage polarization at 9.6 GHz exceeds that at 8.3 GHz. The ratio $P_{8.3}/P_{9.6}$ is ~0.8 over the entire Sf component, but varies considerably over the Np component. The most rapid depolarization occurs in the inner extension of the Np component, where $P_{8.3}/P_{9.6} \leq 0.5$. Near the peak of the Np component this ratio is ~0.7. Of course any change in the degrees of polarization measured at such closely spaced high frequencies is most unusual, and the large changes detected in Cygnus A make it unique in this respect among all known extragalactic objects.

We purposely chose two frequencies sufficiently close that no $n\pi$ ambiguities in position-angle differences could occur. However, determining rotation measures and intrinsic position angles from only two closely spaced values of wavelength squared is obviously difficult. An uncertainty in the position-angle difference of only 1°, for example, produces an

uncertainty in rotation measure of 53 rad m^{-2} and in intrinsic position angle of 3°. We note, however, that using only the position angles integrated over the individual components from Table 2 we obtain rotation measures of -1277 rad m^{-2} for the Sf component and -42 rad m^{-2} for the Np. These can be compared with the values of -1350 rad m^{-2} and -35 rad m^{-2} calculated by Mitton (1971), or -1250 rad m^{-2} and +50 rad m^{-2} calculated by Schraml and Turlo (1967), from data at several frequencies. We therefore feel justified in presenting rotation measures and intrinsic position angles calculated from our data alone, especially near the peak brightness where most of the polarized flux density originates, although the uncertainties could be $\sim\pm300$ rad m^{-2} and $\sim\pm15°$-20°.

Both Figures 4 and 5 illustrate that the position angles of the Sf component at the two frequencies differ greatly, whereas the difference is smaller, but probably nonzero, over much of the Np component. The two components therefore have vastly different rotation measures, that of the Sf component being the larger, as has been noted several times previously. The position-angle differences are not constant in either component. Consequently the rotation measures vary across the source. This variation appears to be systematic: the rotation measure has its largest negative value at the following edge of the source, then increases steadily across Cygnus A until it assumes a positive value at the preceding edge. The only anomalies to this trend occur at the innermost portion of the

Np component. The gradient is especially smooth over the Sf component.

Quantitative estimates of the rotation measure are available in Figure 5, where we have indicated the position angle difference corresponding to a rotation measure of 1000 rad m^{-2}. Also we present in Figure 6 the rotation measures, polarization ratios, and intrinsic polarization angles at a few spots in Cygnus A.

The intrinsic position angles for the individual components are 52° (Sf) and 145° (Np), nearly exactly orthogonal. At the peak brightnesses in total radiation the intrinsic position angles are nearly the same as the above, viz., 47° and 148°. Since the line joining these two peaks is in position angle 109°.5, the differences between the intrinsic polarization angles of the components and the position angle of the major axis are not near 0° nor 90°. In this respect Cygnus A is unusual among radio galaxies (Seielstad and Weiler 1971). However, we have already noted that the high brightness contours in total radiation of both components are elongated in larger position angles than that of the major axis. Thus the intrinsic polarization angle of the Np component is very roughly parallel to its elongation, whereas in the Sf it is very roughly perpendicular. In the inner extensions of both components the intrinsic position angles are possibly perpendicular to the axis of the extensions.

In summary, if ridge lines are drawn within each component, the intrinsic position angle is everywhere approximately perpendicular to the ridge in the Sf component, but swings from being perpendicular to the ridge along the inner extension to parallel farther from the center in the Np component. According to the theory of synchrotron radiation, the component of the magnetic field perpendicular to the line of sight is orthogonal to the intrinsic polarization angle.

IV. A THREE-DIMENSIONAL MODEL OF CYGNUS A

The rapid decrease in degree of polarization with increasing wavelength, the great difference in rotation measures of the two components, and the enormous rotation measure of the Sf component in Cygnus A have long been known. Nearly every previous author has argued that these properties are not imposed by the galactic medium (see, e.g., Woltjer 1962, Schraml and Turlo 1967, and Mitton 1971). We agree with this conclusion.

Mitton has pointed out that there must be some galactic contribution to the rotation measure and adopts a value of -250 rad m^{-2} at the location of Cygnus A, $\ell=76°$, $b=6°$. Unfortunately the evidence for the sign of the galactic rotation measure is not clear-cut. The signs of rotation measures of extragalactic radio sources near Cygnus A alternate, and, in fact, presumably reverse at or near the galactic plane (Berge and Seielstad 1967). The closest source, 3C410 at $\ell=69°$, $b=-4°$, does indeed have a large negative rotation measure,

-216 rad m^{-2} (Berge and Seielstad 1967). In addition, the rotation measures of all nearby pulsars, are negative (Manchester 1972). Finally, the rotation measure of the polarized galactic background radiation implies though not unambiguously, a field directed toward $\ell=60°$ (Berkhuijsen 1971), which would produce a negative rotation measure in the direction of Cygnus A. We therefore agree that the galaxy imposes a negative rotation measure on the polarized radiation from Cygnus A whose magnitude is probably a few hundred rad m^{-2}.

When this galactic contribution is subtracted, the rotation measure of the Sf component is negative and that of the Np component positive. In each component the magnitudes of the remaining rotation measures increase toward the outer edges. We interpret this as strong evidence that the rotation measures are produced by plasma embedded in the radio components themselves. If most of the magneto-plasma were instead associated with the optical galaxy, as suggested by Slysh (1966), the magnitudes of the rotation measures would probably be greatest near the center of the source.

The line-of-sight components of the magnetic fields are away from the observer in the Sf component and toward him in the Np. The density of the thermal plasma and/or the strength of the longitudinal field increase toward the outer edges of the radio components.

The rotation measure of the Sf component is still probably greater in magnitude than that of the Np even after subtraction

of the galactic contribution (see also Mitton 1971). The brightness distributions indicate that most of the radiation is produced near the outer edges. From these facts we infer that the outer edge of the Np component is nearer to us. The radiation from the bright peak of the Sf source traverses the length of that component and also possibly through any halo of the optical galaxy, and thereby receives its additional Faraday rotation. In addition, the radiation from the inner extension of the Np component passes through the dense Faraday plasma concentrated toward the outer boundary of that component, and is consequently rapidly depolarized. This interpretation is consistent with the model of source evolution proposed by Ryle and Longair (1967). Mitton and Ryle (1969) have shown that this model explains the observed differences in flux densities and angular distances from the central galaxy of the two components of Cygnus A if the Sf is receding and the Np approaching. We have noted previously that the optical galaxy is rotating with the Sf side receding (Baade and Minkowski 1954).

Since we believe we are viewing the brightest spot of the Np component relatively unobscured, we are not surprised that the intrinsic polarization angle of that spot differs from the angles measured elsewhere in Cygnus A. If, for instance, the magnetic field of each component is compressed at the contact surface between source and surrounding medium, then seemingly any relation between field orientation and major axis of the source may appear if the source is seen nearly end-on.

In summary, we present a model of Cygnus A in which the two components have been ejected in opposite directions probably making a considerable angle with the plane of the sky. The Sf component is beyond this plane while the Np is in front of it. The magnetic field threading each radio component is directed predominantly along the axis of ejection away from the central optical galaxy. The field is probably compressed into a plane normal to the ejection axis at the leading edge of each component. The field strength and the densities of both thermal and relativistic particles are greatest near the leading edges.

V. COMPARISON WITH THEORETICAL MODELS

The structure of the magnetic field proposed in the preceding section closely corresponds with the expectations of Mills and Sturrock (1970) and of Piddington (1970). Whether the axis from optical galaxy to radio component can have field directions of both senses, as both sets of authors predict, and still produce the large rotation measures observed seems uncertain. Mitton (1971) produced some evidence supporting opposite rotation measures on each side of the major axis of Cygnus A. However, his two-vector model for the Sf component predicts a second maximum in its degree of polarization near 8.3 GHz which we do not detect.

Mills and Sturrock (1970) and Mills (1972) have made further predictions which our observations support. For one, deceleration by the ram pressure of the intergalactic medium (De Young

and Axford 1967) produces steep total brightness contours at the outer edges of the radio components. We confirm their existence, already noted several times previously. The thermal gas is predicted to concentrate at the outer edges, and we have presented strong evidence that this is so. The turbulent field is presumably coupled to the thermal plasma, and therefore greatest turbulence, hence lowest degree of polarization, should be observed near the outer edges of the components. In contrast, the field lines trailing the components back along the axis of ejection are expected to be highly ordered, and therefore high degrees of polarization are predicted. Our observations support these predictions.

Rees (1971) has proposed a radio-source model in which low-frequency electromagnetic waves evacuate an expanding cavity by accelerating electrons to relativistic energies, which then radiate "synchro-Compton" radiation. No thermal plasma would be left within the radio components, which definitely contradicts our interpretation of the Cygnus A observations.

Research in radio astronomy at the California Institute of Technology is supported by the National Science Foundation under grant GP30400-X and by the Office of Naval Research under Contract N00014-67-A-0094-0019.

We wish to thank G. L. Berge, E. B. Fomalont, and K. W. Weiler for informative discussions. We also gratefully acknowledge the assistance of the Observatory staff in making the observations possible.

REFERENCES

Aller, H. D. 1970, Ap. J., 161, 1.

Baade, W., and Minkowski, R. 1954, Ap. J., 119, 206.

Baars, J. W. M., Mezger, P. G., and Wendker, H. 1965, Ap. J., 142, 122.

Berge, G. L. 1968, Astrophys. Letters, 2, 127.

Berge, G. L, and Seielstad, G. A. 1967, Ap. J., 148, 367.

Berkhuijsen, E. M. 1971, Astron. and Astrophys., 14, 359.

De Young, D. S., and Axford, W. I. 1967, Nature, 216, 129.

Hinder, R. A. 1970, Nature, 225, 614.

Hogg, D. E., Macdonald, G. H., Conway, R. G., and Wade, C. M. 1969, A. J., 74, 1206.

Manchester, R. N. 1972, Ap. J., 172, 43.

Mayer, C. H., Hollinger, J. P., and Allen, P. J. 1963, Ap. J., 137, 1309.

Miley, G. K., and Wade, C. M. 1971, Astrophys. Letters, 8, 11.

Mills, D. M. 1972, in press.

Mills, D. M., and Sturrock, P. A. 1970, Astrophys. Letters, 5, 105.

Mitton, S. 1971, M.N.R.A.S., 153, 133.

Mitton, S., and Ryle, M. 1969, M.N.R.A.S., 146, 221.

Moffet, A. T. 1966, Ann. Rev. Astron. and Astrophys., 4, 145.

Piddington, J. H. 1970, M.N.R.A.S., 148, 131.

Rees, M. J. 1971, Nature, 229, 312.

Ryle, M., Elsmore, B., and Neville, A. C. 1965, Nature, 205, 1259

Ryle, M., and Longair, M. S. 1967, M.N.R.A.S., 136, 123.

Schraml, J., and Turlo, Z. 1967, Ap. J. (Letters), 150, L15.

Seielstad, G. A., and Weiler, K. W. 1969, Ap. J. Suppl., No. 158.

Seielstad, G. A., and Weiler, K. W. 1971, Astron. J., 76, 211.

Slysh, V. I. 1966, Sov. Astron. --A. J., 9, 533.

Weiler, K. W., and Seielstad, G. A. 1971, Ap. J., 163, 455.

Woltjer, L. 1962, Ap. J., 136, 1152.

Wynn-Williams, C. G. 1971, M.N.R.A.S., 151, 397.

FIGURE CAPTIONS

Figure 1: Distribution of total radiation from Cygnus A at frequencies near 8950 MHz. North is at top and east at left. The origin of coordinates is $\alpha_{1950}=19^h57^m44^s.5$, $\delta_{1950}=40°35'46''.0$. The half-power beamwidth is shown at lower right. Contours are presented at 10 per cent intervals. The peak brightness is 4.55×10^{-17} W m^{-2} Hz^{-1} ster^{-1}, or 1845°K, the values appropriate for 8950 MHz.

Figure 2: Profiles along the major axis of Cygnus A convolved to a common resolution. All profiles are normalized to equalize the peaks of the Sf component. The data at 1.4, 2.7, and 5.0 GHz are summarized in Mitton and Ryle (1969). Measurements from this paper are shown by open circles.

Figure 3: Distributions of linearly polarized radiation, $\sqrt{Q^2+U^2}$. North at top and east at left. Origin of coordinates is $\alpha_{1950}=19^h57^m44^s.5$, $\delta_{1950}=40°35'46''.0$. Ten per cent contours shown. (a) 9600 MHz. Peak brightness 5.06×10^{-18} W m^{-2} Hz^{-1} ster^{-1}, or 179°K. (b) 8300 MHz. Peak brightness 4.16×10^{-18} W m^{-2} Hz^{-1} ster^{-1}, or 197°K.

Figure 4: Distributions of percentage polarization and position angle. The 10, 50, and 90 per cent contours of the distribution of total radiation from Figure 1 are reproduced, as is the origin of coordinates. Dashed lines refer to 8.3 GHz data; solid lines to 9.6 GHz data. Because of their near coincidence in position angle, the 8.3 GHz vectors in the Np component are

slightly displaced to the west from the 9.6 GHz vectors. Vectors whose lengths represent 10 per cent polarization are at lower right.

Figure 5: Cuts along the major axis of the distributions of total radiation (solid curve) and of ten times the linearly polarized radiation at 9.6 GHz (dashed curve) and at 8.3 GHz (dotted curve). The Np component is at right. The two ordinate scales are in the ratio $(8.3/9.6)^{-1.19}$, which normalizes the total intensity distributions at the two frequencies. The scale on the right is for the 9.6 GHz polarization distribution; on the left for the 8.3 GHz polarization distribution. The ratio of either linearly polarized curve to the total curve is therefore ten times the percentage polarization. At the bottom of the figure are the distributions of position angles at the two frequencies. Also shown is the magnitude of the difference in position angles, $|\chi_{8.3}-\chi_{9.6}|$, corresponding to a rotation measure of 1000 rad m^{-2}.

Figure 6: Distribution of intrinsic position angles (E vectors) superposed on 10, 50, and 90 per cent contours of distribution of total radiation from Figure 1. The two numbers with each vector represent the ratio of percentage polarizations, $P_{8.3}/P_{9.6}$ (upper number), and the rotation measure in rad m^{-2} (lower number).

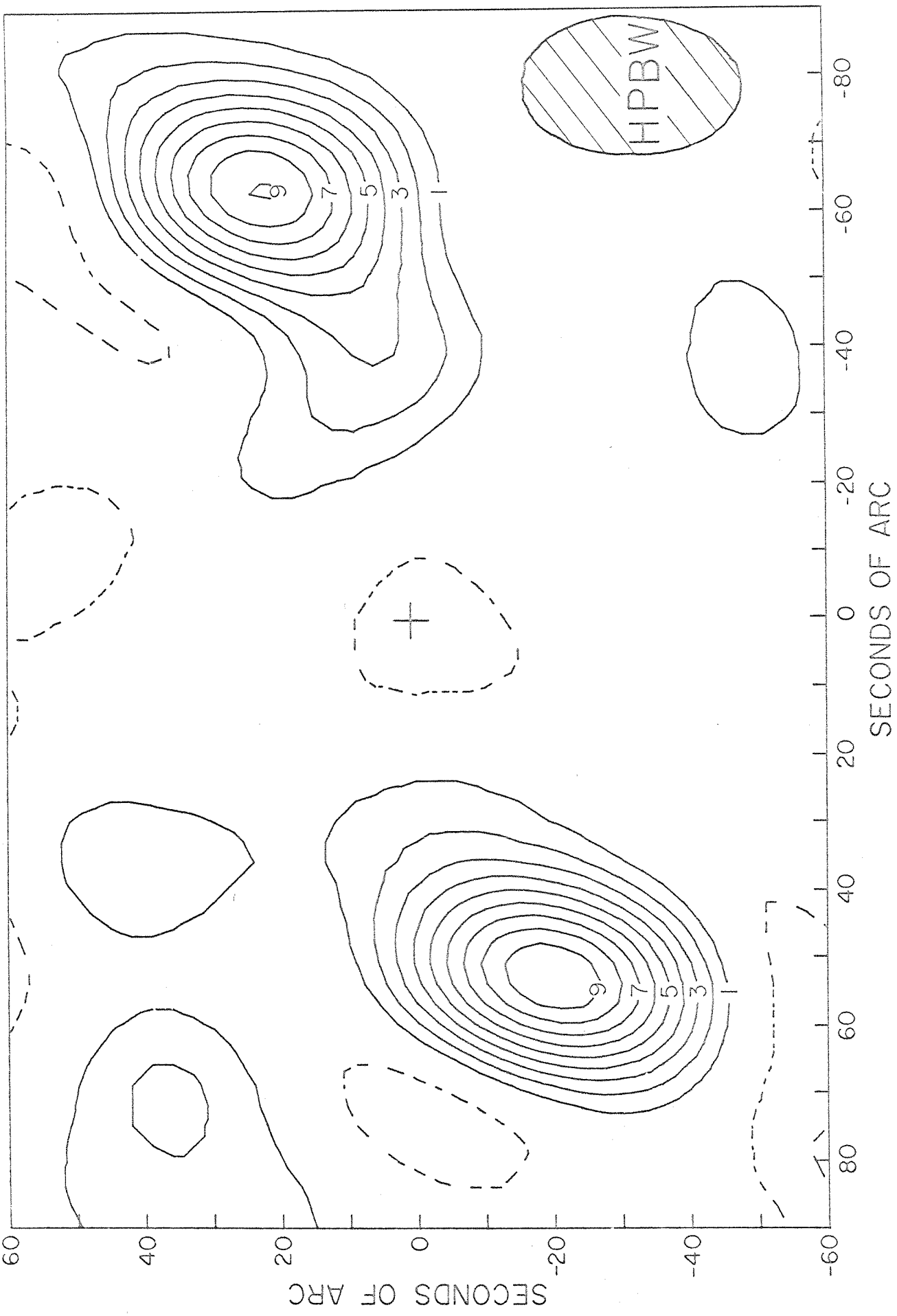
HPBW
9
7
5
3
1
SECONDS OF ARC
60
40
20
0
-20
-40
-60
-80
-60
-40
-20
0
20
40
60
80
SECONDS OF ARC

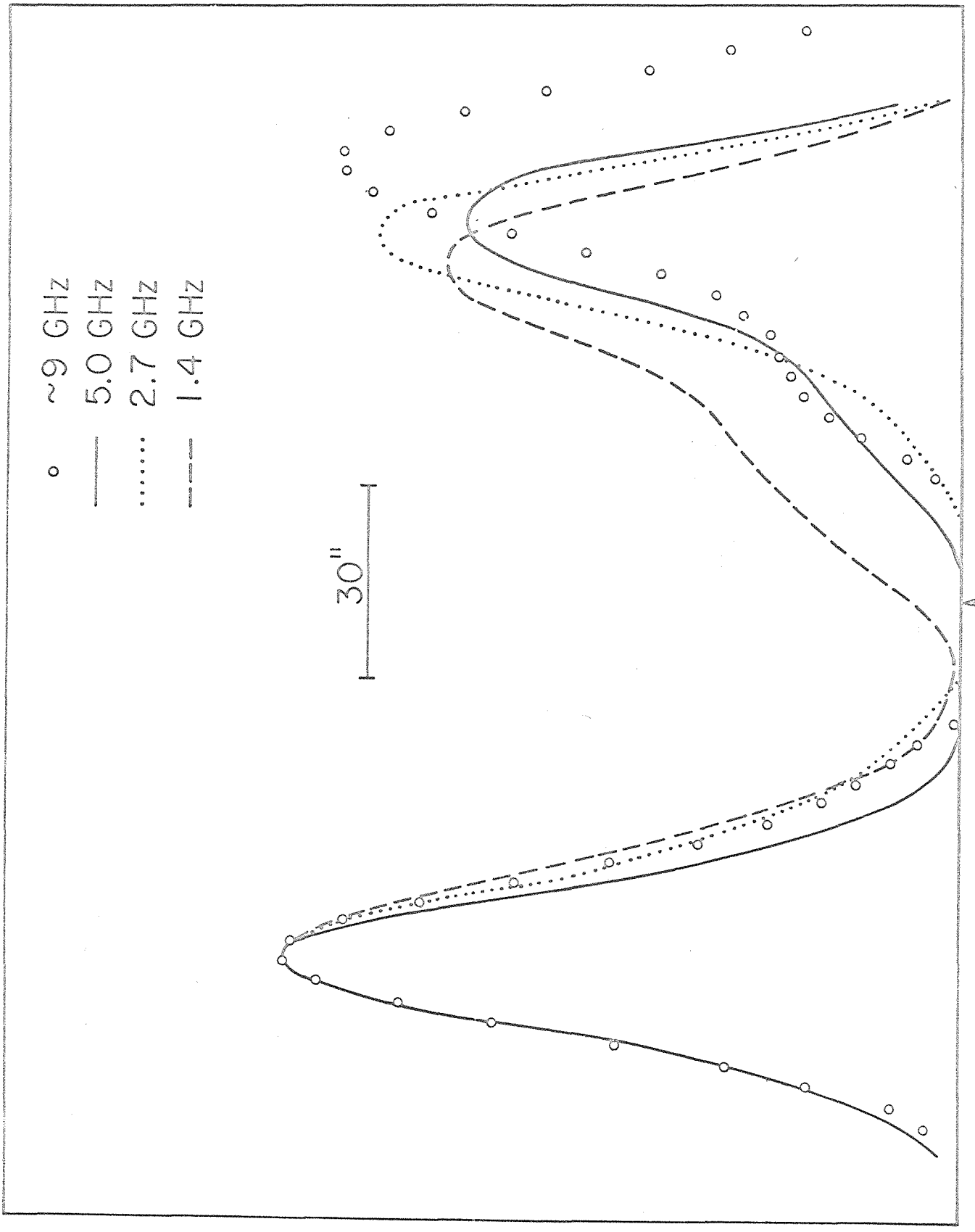
~9 GHz
5.0 GHz
2.7 GHz
1.4 GHz
30"
19h 57m 44s.5

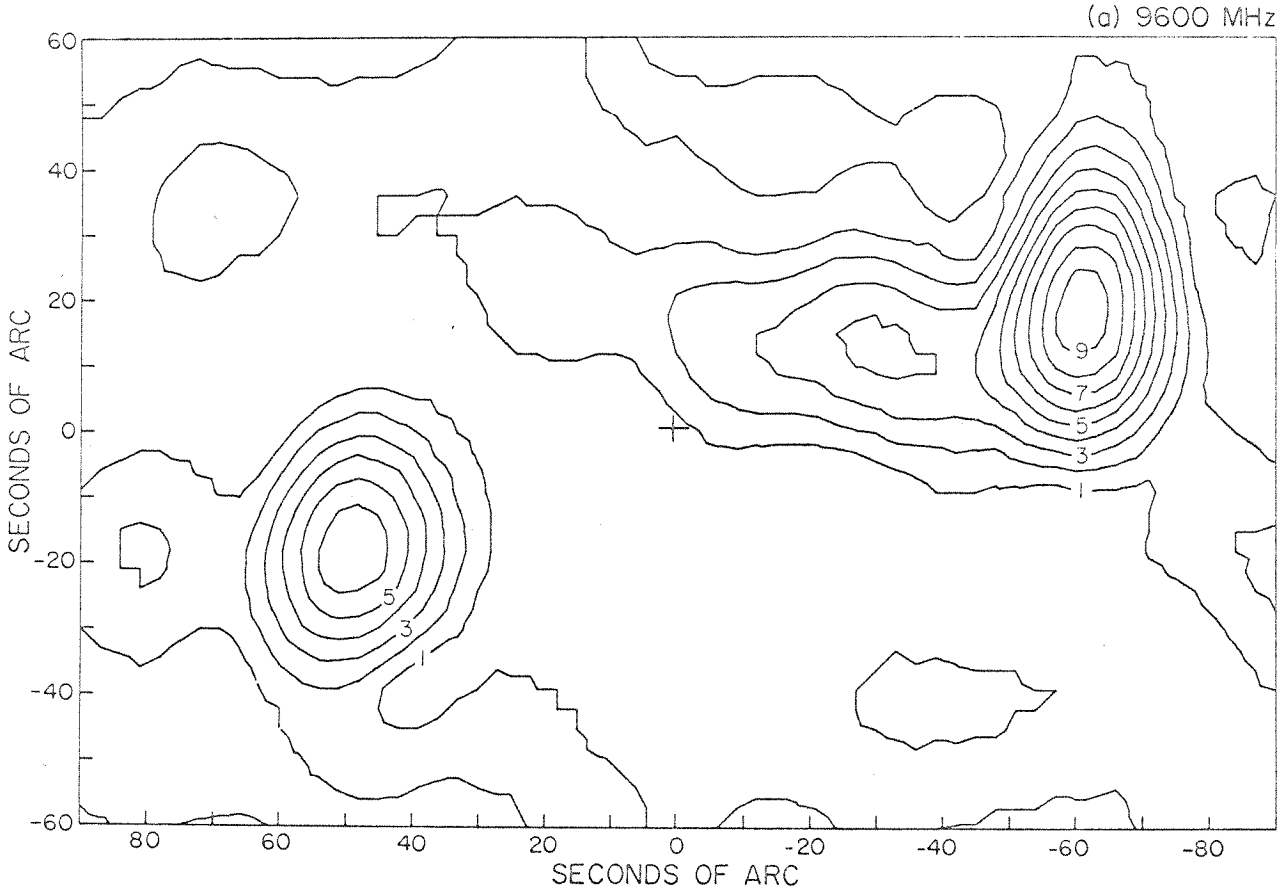
(a) 9600 MHz
SECONDS OF ARC
SECONDS OF ARC
60
40
20
0
-20
-40
-60
80
60
40
20
0
-20
-40
-60
-80
9
7
5
3
1
5
3
1

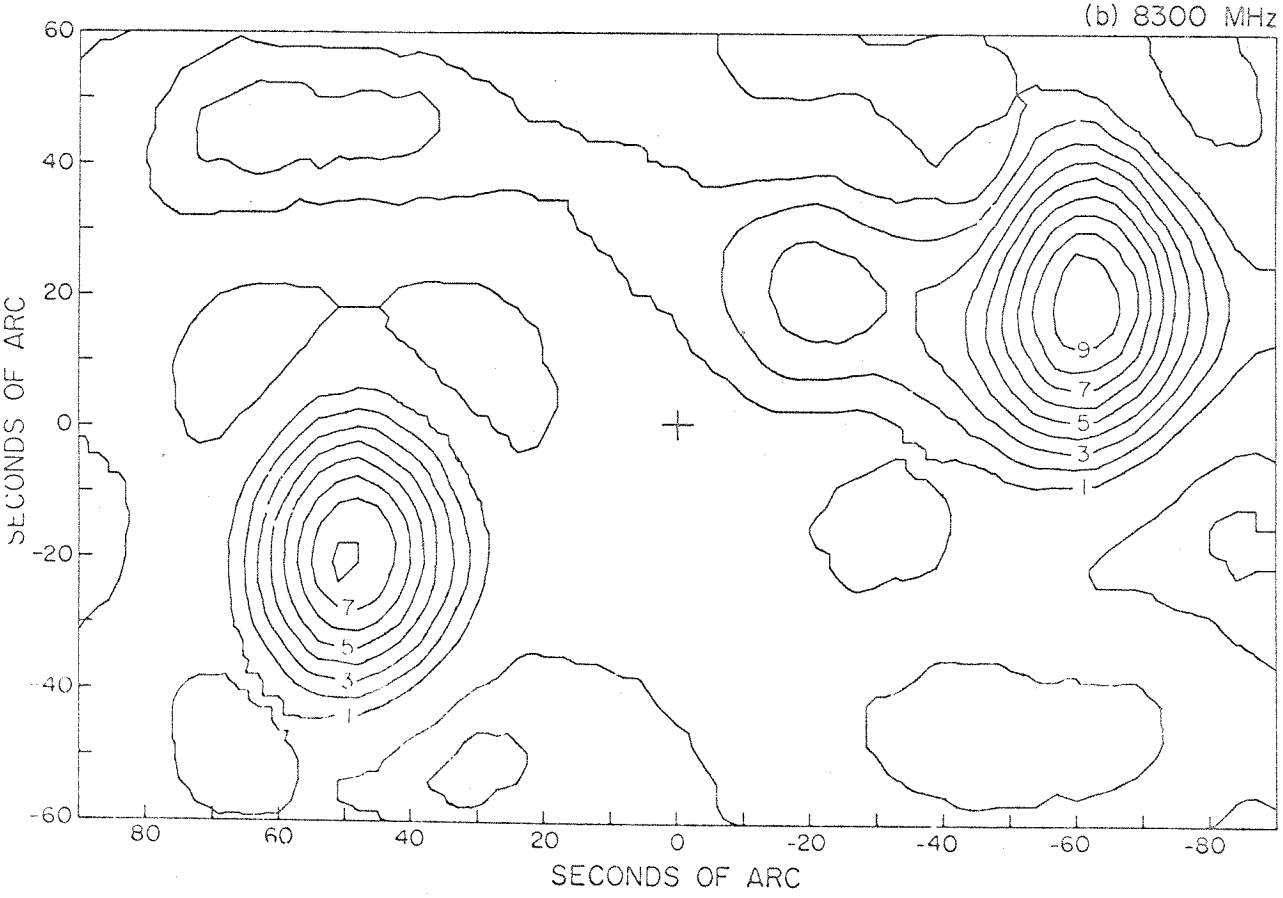
(b) 8300 MHz
SECONDS OF ARC
SECONDS OF ARC
60
40
20
0
-20
-40
-60
80
60
40
20
0
-20
-40
-60
-80
9
7
5
3
1
7
5
3
1

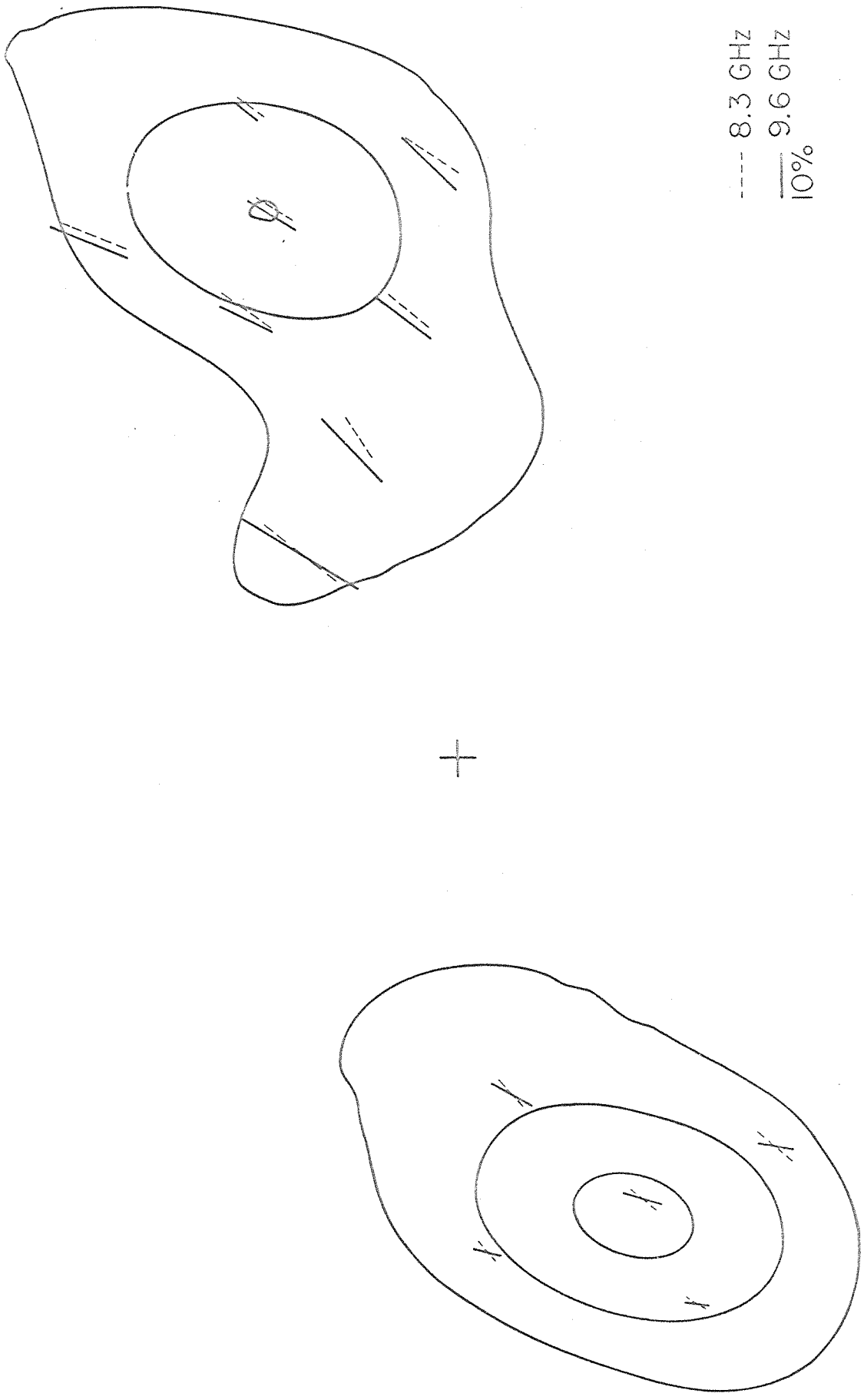
8.3 GHz
9.6 GHz
10%

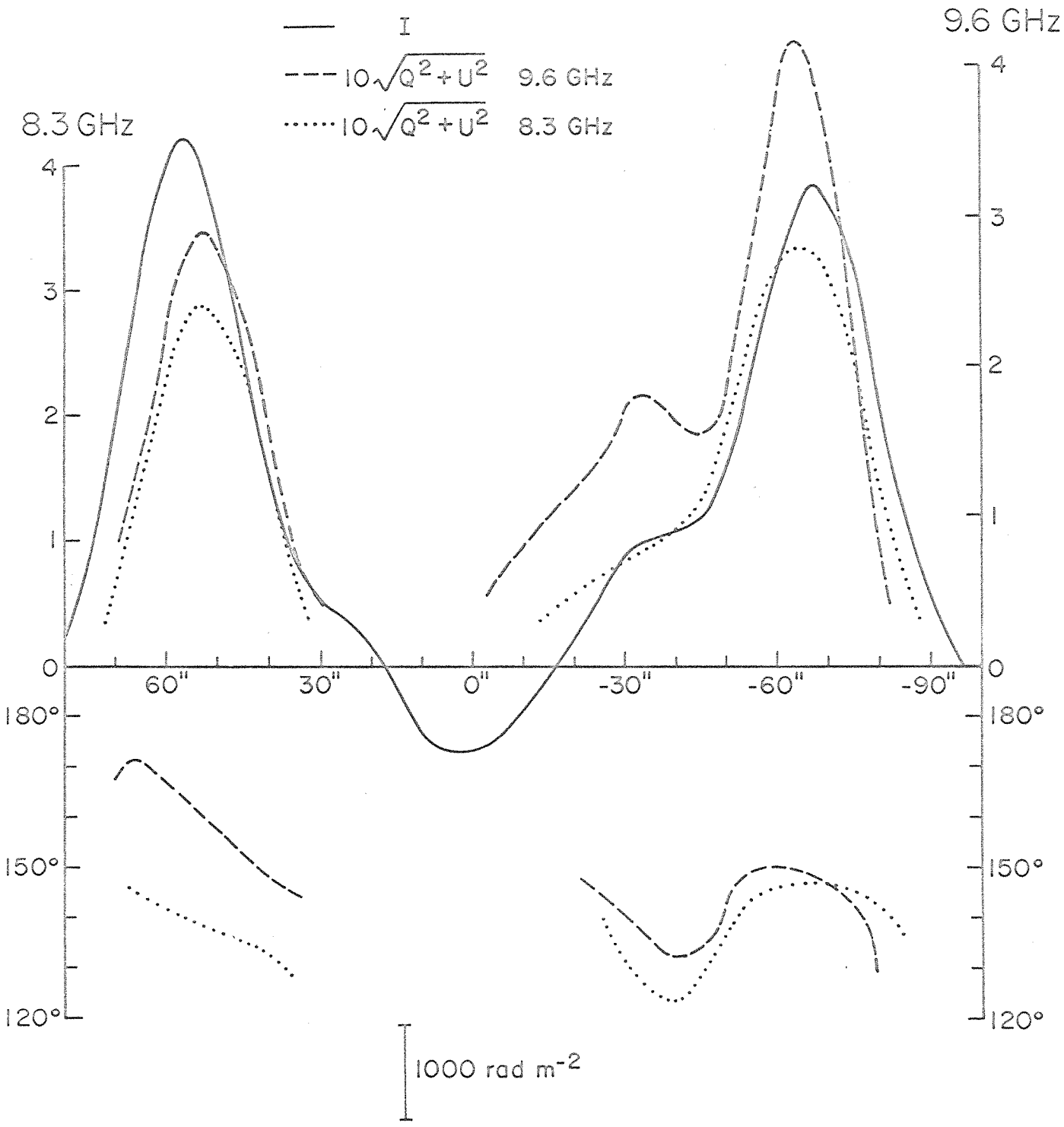
I
$10\sqrt{Q^2+U^2}$ 9.6 GHz
$10\sqrt{Q^2+U^2}$ 8.3 GHz
8.3 GHz
9.6 GHz
4
3
2
1
0
60"
30"
0"
-30"
-60"
-90"
180°
150°
120°
1000 rad m^{-2}

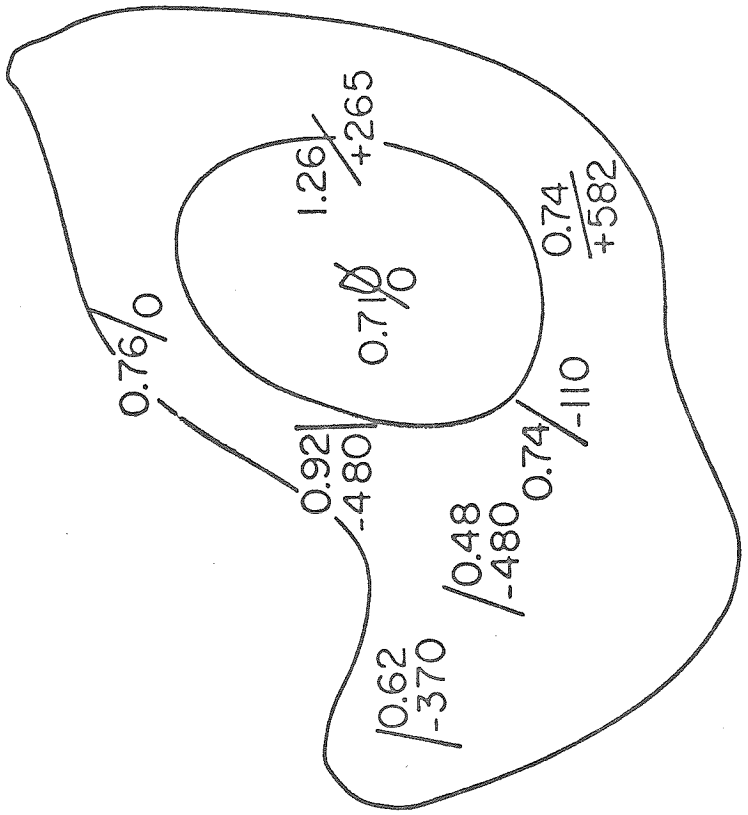
0.76/0
1.26/+265
0.74/+582
0.71/0
0.92/-480
0.74/-110
0.48/-480
0.62/-370

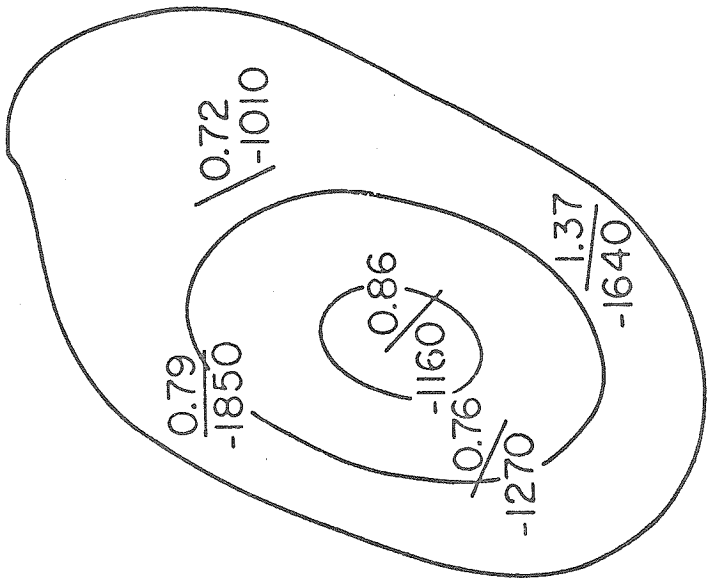
0.72/-1010
0.79/-1850
0.86/-1160
1.37/-1640
0.76/-1270